

ISTANBUL TECHNICAL UNIVERSITY ★ GRADUATE SCHOOL OF SCIENCE
ENGINEERING AND TECHNOLOGY

**AXIAL BEHAVIOR OF HIGH PERFORMANCE FIBER REINFORCED
CEMENTITIOUS COMPOSITES WRAPPED BY FRP SHEETS**

M.Sc. THESIS

Ugur DEMIR

Department of Civil Engineering

Structural Engineering Programme

JANUARY 2013

ISTANBUL TECHNICAL UNIVERSITY ★ GRADUATE SCHOOL OF SCIENCE
ENGINEERING AND TECHNOLOGY

**AXIAL BEHAVIOR OF HIGH PERFORMANCE FIBER REINFORCED
CEMENTITIOUS COMPOSITES WRAPPED BY FRP SHEETS**

M.Sc. THESIS

**Ugur DEMIR
(501101074)**

Department of Civil Engineering

Structural Engineering Programme

Thesis Advisor: Prof. Dr. Alper ILKI

JANUARY 2013

İSTANBUL TEKNİK ÜNİVERSİTESİ ★ FEN BİLİMLERİ ENSTİTÜSÜ

**YÜKSEK PERFORMANSLI, ÇELİK LİF TAKVİYELİ, LİFLİ POLİMERLER
İLE SARGILANMIŞ, CİMENTO ESASLI KOMPOZİTLERİN EKSENEL
YÜKLER ALTINDA DAVRANIŞI**

YÜKSEK LİSANS TEZİ

**Ugur DEMİR
(501101074)**

İnşaat Mühendisliği Anabilim Dalı

Yapı Mühendisliği Programı

Tez Danışmanı: Prof. Dr. Alper İLKİ

OCAK 2013

Ugur DEMIR, a **M.Sc.** student of ITU **Graduate School of Science Engineering and Technology** student ID **501101074**, successfully defended the **thesis** entitled “**AXIAL BEHAVIOR OF HIGH PERFORMANCE FIBER REINFORCED CEMENTITIOUS COMPOSITES WRAPPED BY FRP SHEETS**”, which he prepared after fulfilling the requirements specified in the associated legislations, before the jury whose signatures are below

Thesis Advisor : **Prof. Dr. Alper ILKI**
İstanbul Technical University

Co-advisor : **Dr. Medine ISPIR ARSLAN**
İstanbul Technical University

Jury Members : **Prof. Dr. Mustafa ZORBOZAN**
Yıldız Technical University

Assoc. Prof. Dr. Kutlu DARILMAZ.....
İstanbul Technical University

Asst. Prof. Dr. Kutay ORAKCAL
Bogazici University

Date of Submission : 17 December 2012
Date of Defense : 16 January 2013

To my family and wife,

FOREWORD

First, I would like to thank my parents and my wife who were giving me support all the time I need.

I would like to thank my thesis advisor Prof. Dr. Alper ILKI for giving me his valuable times and guiding me throughout this study. His working discipline will be a norm and his lessons will form a fundamental basis of me.

I would like to thank my Co-advisor Dr. Medine ISPIR ARSLAN for her self-sacrificing help at the all stages of this work.

I would like to thank Research Assistant Yusuf SAHINKAYA for his help.

I would also like to surely thank to BASF-YKS Construction Chemicals, Ak-Kim Chemistry, Art-Yol Engineering and Giray ARSLAN from ISTON, Istanbul Concrete Elements and Ready Mixed Concrete Factories Corporation for their manufacturing.

December 2012

Ugur DEMIR
(Civil Engineer)

TABLE OF CONTENTS

	<u>Page</u>
FOREWORD	ix
TABLE OF CONTENTS	xi
ABBREVIATIONS	xiii
LIST OF TABLES	xv
LIST OF FIGURES	xvii
SUMMARY	xxi
OZET	xxiii
1. INTRODUCTION	1
2. HIGH PERFORMANCE CEMENTITIOUS COMPOSITES	5
2.1 Cementitious Composites	5
2.2 Key Features of High Performance Cementitious Composite	8
3. COMPARISON OF AVAILABLE COMMERCIAL CFRP SHEETS	11
3.1 Preparation and Retrofit of the Specimens for Comparison	11
3.2 Test Results for Comparison	12
3.2.1 Specimens confined by 2 plies of CFRP	13
3.2.2 Specimens confined by 4 plies of CFRP	15
4. EXPERIMENTAL PROGRAM	17
4.1. Preparation and Retrofit of the Specimens	17
4.2. Test Set-up	20
4.3. Test Results for Circular Members	21
4.3.1 Unconfined circular specimens	22
4.3.2 Circular specimens confined by 2 plies of CFRP	26
4.3.3 Circular specimens confined by 4 plies of CFRP	34
4.3.4 Circular specimens confined by 6 plies of CFRP	37
4.3.5 Circular specimens confined by 8 plies of CFRP	41
4.3.6 Circular specimens confined by 10 plies of CFRP	45
4.4. Test Results for Non-circular Members	51
4.4.1 Unconfined non-circular specimens	53
4.4.2 Non-circular specimens confined by 2 plies of CFRP	58
4.4.3 Non-circular specimens confined by 8 plies of CFRP	62
4.4.4 Non-circular specimens confined by 10 plies of CFRP	67
5. ANALYTICAL WORK	75
6. CONCLUSION AND RECOMMANDATIONS	77
REFERENCES	79
CURRICULUM VITAE	83

ABBREVIATIONS

FRP	: Fiber Reinforced Concrete
HPC	: High Performance Concrete
HPFRCC	: High Performance Fiber Reinforced Cementitious Composite
CFRP	: Carbon Fiber Reinforced Polymer
NSC	: Normal Strength Concrete
CC-C-0-1	: Unconfined Circular Shape Cement Composite, Specimen 1
CC-C-0-2	: Unconfined Circular Shape Cement Composite, Specimen 2
CC-C-0-3	: Unconfined Circular Shape Cement Composite, Specimen 3
CC-C-0-4	: Unconfined Circular Shape Cement Composite, Specimen 4
CC-C-0-5	: Unconfined Circular Shape Cement Composite, Specimen 5
CC-C-0-6	: Unconfined Circular Shape Cement Composite, Specimen 6
CC-C-2-1	: 2 Plies of CFRP Confined Circular Shaped Cement Composite, Specimen 1
CC-C-2-2	: 2 Plies of CFRP Confined Circular Shaped Cement Composite, Specimen 1
CC-C-2-3	: 2 Plies of CFRP Confined Circular Shaped Cement Composite, Specimen 1
CC-C-2-4	: 2 Plies of CFRP Confined Circular Shaped Cement Composite, Specimen 1
CC-C-4-1	: 2 Plies of CFRP Confined Circular Shaped Cement Composite, Specimen 1
CC-C-4-2	: 2 Plies of CFRP Confined Circular Shaped Cement Composite, Specimen 1
CC-C-4-3	: 2 Plies of CFRP Confined Circular Shaped Cement Composite, Specimen 1
CC-C-8-1	: 2 Plies of CFRP Confined Circular Shaped Cement Composite, Specimen 1
CC-C-8-2	: 2 Plies of CFRP Confined Circular Shaped Cement Composite, Specimen 1
CC-C-8-3	: 2 Plies of CFRP Confined Circular Shaped Cement Composite, Specimen 1
CC-C-8-4	: 2 Plies of CFRP Confined Circular Shaped Cement Composite, Specimen 1
CC-C-10-1	: 2 Plies of CFRP Confined Circular Shaped Cement Composite, Specimen 1
CC-C-10-2	: 2 Plies of CFRP Confined Circular Shaped Cement Composite, Specimen 1
CC-C-10-3	: 2 Plies of CFRP Confined Circular Shaped Cement Composite, Specimen 1

CC-C-10-4	: 2 Plies of CFRP Confined Circular Shaped Cement Composite, Specimen 1
CC-S-0-1	: Unconfined Square Shaped Cement Composite, Specimen 1
CC-S-0-2	: Unconfined Square Shaped Cement Composite, Specimen 2
CC-S-0-3	: Unconfined Square Shaped Cement Composite, Specimen 3
CC-S-0-4	: Unconfined Square Shaped Cement Composite, Specimen 4
CC-S-2-1	: 2 Plies of CFRP Confined Square Shaped Cement Composite, Specimen 1
CC-S-2-2	: 2 Plies of CFRP Confined Square Shaped Cement Composite, Specimen 2
CC-S-2-3	: 2 Plies of CFRP Confined Square Shaped Cement Composite, Specimen 3
CC-S-8-1	: 8 Plies of CFRP Confined Square Shaped Cement Composite, Specimen 1
CC-S-8-2	: 8 Plies of CFRP Confined Square Shaped Cement Composite, Specimen 2
CC-S-8-3	: 8 Plies of CFRP Confined Square Shaped Cement Composite, Specimen 3
CC-S-8-4	: 8 Plies of CFRP Confined Square Shaped Cement Composite, Specimen 4
CC-S-10-1	: 10 Plies of CFRP Confined Square Shaped Cement Composite, Specimen 1
CC-S-10-2	: 10 Plies of CFRP Confined Square Shaped Cement Composite, Specimen 2
CC-S-10-3	: 10 Plies of CFRP Confined Square Shaped Cement Composite, Specimen 3
CC-S-10-4	: 10 Plies of CFRP Confined Square Shaped Cement Composite, Specimen 4

LIST OF TABLES

	<u>Page</u>
Table 3.1: Properties of Composite Sheets Wrapped	12
Table 3.2: Peak Loads during the Comparison Test	16
Table 4.1: Mix Proportion for Cementitious Composite (kg/m ³)	17
Table 4.2: Properties of Measurement Equipments	20
Table 4.3: Details of the Circular Specimens	21
Table 4.4: Reference Cylinder Test Results	23
Table 4.5: Experimental Test Results for Circular Specimens	50
Table 4.6: Details of the Square Specimens	53
Table 4.7: Experimental Test Results for Square Cross Section Specimens	72
Table 4.8: After Test Enhancement Ratios for all Specimens	73
Table 5.1: Experimental and Analytical Comparison for Circular Specimens	75
Table 5.2: Experimental and Analytical Comparison for Non-Circular Specimens	76

LIST OF FIGURES

	<u>Page</u>
Figure 2.1 : Examples of deformed steel fibers	6
Figure 2.2 : Crack pattern in reinforced concrete (RC) and fiber reinforced concrete (FRC) elements subjected to tension	7
Figure 2.3 : Structures of long and short fibers controlling the crack propagation; after Betterman et al.....	7
Figure 2.4 : Comparison of typical stress–strain response in tension of HPFRCC with conventional FRCC, after Naaman [8].	8
Figure 3.1 : Casting the specimens for comparison	11
Figure 3.2 : Stress-strain curves of the unconfined specimens	11
Figure 3.3 : Preparation of specimens	12
Figure 3.4 : Stress – lateral strain relationship between specimens confined by 2 plies of CFRP	13
Figure 3.5 : A_2C_1 damage	13
Figure 3.6 : A_2C_2 damage	14
Figure 3.7 : B_2C_1 damage	14
Figure 3.8 : B_2C_1 damage	15
Figure 3.9 : Stress - lateral strain relationship between specimens confined by 4 plies of CFRP	15
Figure 3.10 : A_4C_1 damage	15
Figure 3.11 : A_4C_2 damage	15
Figure 3.12 : B_4C_1 damage	15
Figure 3.13 : B_4C_2 damage	15
Figure 4.1 : Casting mixer at ISTON	17
Figure 4.2 : Moulds at casting step	18
Figure 4.3 : All specimens after taking moulds	18
Figure 4.4 : Caps performing	19
Figure 4.5 : Primer performed specimens before confining	19
Figure 4.6 : Confining the specimens	19
Figure 4.7 : End zones retrofit	19
Figure 4.8 : 5000 kN capacity Instron test machine	20
Figure 4.9 : Stress -strain relationship for C-CC-0-4	23
Figure 4.10 : Stress - strain relationship for C-CC-0-5	24
Figure 4.11 : Stress -strain relationship for C-CC-0-6	25
Figure 4.12 : Stress - strain relationship comparison for unconfined circular specimens	25
Figure 4.13a : CC-C-0-1	26
Figure 4.13b : CC-C-0-2	26
Figure 4.13c : CC-C-0-3	26
Figure 4.14 : CC-C-0-4	26

Figure 4.15 : CC-C-0-5	26
Figure 4.16 : CC-C-0-6	26
Figure 4.17 : Stress - strain relationship for C-CC-2-1	27
Figure 4.18 : Stress - strain relationship for C-CC-2-2	27
Figure 4.19 : Stress - strain relationship for C-CC-2-3	29
Figure 4.20 : Stress - strain relationship for CC-C-2-4	29
Figure 4.21 : Stress - strain relationship for CC-C-2-5	30
Figure 4.22 : Stress - strain relationship for CC-C-2-6	31
Figure 4.23 : Stress - strain relationship for CC-C-2-7	31
Figure 4.24 : A comparison for specimens that confined by 2 plies of CFRP	32
Figure 4.25 : CC-C-2-1	33
Figure 4.26 : CC-C-2-2	33
Figure 4.27 : CC-C-2-3	33
Figure 4.28 : CC-C-2-4	33
Figure 4.29 : CC-C-2-5	33
Figure 4.30 : CC-C-2-6	33
Figure 4.31 : CC-C-2-7	33
Figure 4.32 : Stress - strain relationship for CC-C-4-1	34
Figure 4.33 : Stress - strain relationship for CC-C-4-2	35
Figure 4.34 : Stress - strain relationship for CC-C-4-3	36
Figure 4.35: A comparison for the specimens that confined by 4 plies of CFRP	36
Figure 4.36 : CC-C-4-1	37
Figure 4.37 : CC-C-4-2	37
Figure 4.38 : CC-C-4-3	37
Figure 4.39 : Stress - strain relationship for CC-C-6-1	38
Figure 4.40 : Stress - strain relationship for CC-C-6-2	38
Figure 4.41 : Stress - strain relationship for CC-C-6-3	39
Figure 4.42: A comparison for the specimens that confined by 6 plies of CFRP	39
Figure 4.43 : CC-C-6-1	40
Figure 4.44 : CC-C-6-2	40
Figure 4.45 : CC-C-6-3	40
Figure 4.46 : Stress - strain relationship for CC-C-8-1	41
Figure 4.47 : Stress - strain relationship for CC-C-8-2	42
Figure 4.48 : Stress - strain relationship for CC-C-8-3	43
Figure 4.49 : Stress - strain relationship for CC-C-8-4	44
Figure 4.50: A comparison for the specimens that confined by 8 plies of CFRP	44
Figure 4.51 : CC-C-8-1	45
Figure 4.52 : CC-C-8-2	45
Figure 4.53 : CC-C-8-3	45
Figure 4.54 : CC-C-8-4	45
Figure 4.55 : Stress - strain relationship for C-CC-10-1	46
Figure 4.56 : Stress - strain relationship for C-CC-10-2	47
Figure 4.57 : Stress - strain relationship for CC-C-10-3	47
Figure 4.58 : Stress - strain relationship for C-CC-10-4	48
Figure 4.59: A comparison for the specimens that confined by 10 plies of CFRP	49
Figure 4.60 : C-CC-10-1	49
Figure 4.61 : C-CC-10-2	49
Figure 4.62 : C-CC-10-3	49
Figure 4.63 : C-CC-10-4	49
Figure 4.64 : Lateral, axial stress and strain increments,due to the FRP layer	51

Figure 4.65 :	Test set-up for square specimens	53
Figure 4.66 :	Stress - strain relationship for CC-S-0-1	54
Figure 4.67 :	Stress - strain relationship for CC-S-0-2	55
Figure 4.68 :	Stress - strain relationship for CC-S-0-3	56
Figure 4.69 :	Stress - strain relationship for CC-S-0-4	56
Figure 4.70 :	A comparison for the unconfined square specimens	57
Figure 4.71 :	CC-S-0-1	58
Figure 4.72 :	CC-S-0-2	58
Figure 4.73 :	CC-S-0-3	58
Figure 4.74 :	CC-S-0-4	58
Figure 4.75 :	Stress - strain relationship for CC-S-2-1	59
Figure 4.76 :	Stress - strain relationship for CC-S-2-2	60
Figure 4.77 :	Stress - strain relationship for CC-S-2-3	61
Figure 4.78 :	A comparison for the specimens that confined by 2 plies of CFRP	61
Figure 4.79 :	CC-S-2-1	62
Figure 4.80 :	CC-S-2-2	62
Figure 4.81 :	CC-S-2-3	62
Figure 4.82 :	Stress - strain relationship for CC-S-8-1	63
Figure 4.83 :	Stress - strain relationship for CC-S-8-2	63
Figure 4.84 :	Stress - strain relationship for CC-S-8-3	64
Figure 4.85 :	Stress - strain relationship for CC-S-8-4	64
Figure 4.86 :	A comparison for the specimens that confined by 8 plies of CFRP	65
Figure 4.87 :	CC-S-8-1	67
Figure 4.88 :	CC-S-8-2	67
Figure 4.89 :	CC-S-8-3	67
Figure 4.90 :	CC-S-8-4	67
Figure 4.91 :	Stress - strain relationship for CC-S-10-1	68
Figure 4.92 :	Stress - strain relationship for CC-S-10-2	69
Figure 4.93 :	Stress - strain relationship for CC-S-10-3	69
Figure 4.94 :	Stress - strain relationship for CC-S-10-4	70
Figure 4.95 :	A comparison for the specimens that confined by 10 plies of CFRP	70
Figure 4.96 :	CC-S-10-1	71
Figure 4.97 :	CC-S-10-2	71
Figure 4.98 :	CC-S-10-3	71
Figure 4.99 :	CC-S-10-4	71
Figure 4.100 :	Lateral, axial stress and strain increments,due to the FRP layer	73

AXIAL BEHAVIOR OF HIGH PERFORMANCE FIBER REINFORCED CEMENTITIOUS COMPOSITES WRAPPED BY FRP SHEETS

SUMMARY

It is well established that external confinement of concrete with fiber reinforced polymer (FRP) jackets results in significant improvements of the axial and dilation performance of concrete. To reduce the brittleness of the concrete we can change both the mixture and confinement type. The aim of this study is to make it clear that if the use of HPFRCC confined by Carbon Fiber Reinforced Polymer (CFRP) sheets can exhibit a strain-hardening character versus the plain concrete or not. Therefore, to research this behavior, an experimental study has been carried out. Circular and square cross-sectional specimens were cast at once. In this study, experimental results, obtained for the concrete specimens wrapped by various thicknesses of CFRP jackets, are presented. Thicknesses of the CFRP sheets were 2-4-6-8 and 10 plies for circular specimens and 2-8-10 for non-circular. All confinements had an overlap of 150 mm. Thirty specimens with circular cross-section, 19 specimens with square cross-section were included into the testing program. Concentric compression tests were carried out on specimens with circular, square cross-sections wrapped by CFRP jackets. After a while, end zones of the specimens were retrofitted by 5 cm width and three plies of CFRP bands to move the damage to the mid-height of the specimens. All confinements were done by hand. All of the specimens during the study had the same height of 300 mm and different aspect ratios. The sizes of the cross-sections were; 150*300 mm for the circulars and 150*150*300 mm for the squares with a rounding radius of 25 mm on the edges of the each specimen. Concentric compressive loads were applied on the specimens by using an Instron universal testing machine with the capacity of 5000 kN. Lateral strains were measured at mid-height by surface strain gauges with the gauge length of about 150 mm for all specimens. For measuring the vertical strains, LVDTs were used. Load was applied 0.6 mm per minute (TS EN 12390-3) and test was displacement controlled. For measurements of average axial strains for different gauge lengths, displacement transducers were used. For specimens with circular cross-section, two strain gauges with the gauge length of 60 mm (PL60) and two transducers with the gauge length of 25 mm (LVDT25) were used. For non-circular specimens, four transducers with the gauge length of 25 mm (LVDT25) were used to measure the vertical strains that were placed to the corners of the specimens.

YÜKSEK PERFORMANSLI, ÇELİK LİF TAKVİYELİ, LİFLİ POLİMERLER İLE SARGILANMIŞ, ÇİMENTO ESASLI KOMPOZİTLERİN EKSENEL YÜKLER ALTINDA DAVRANIŞI

ÖZET

Geçmişte 1960'lı yıllarda erişilebilen en yüksek beton basınç dayanımı 15–25 MPa arasında iken 1970'li yıllarda yüksek katlı yapılarda kolon yüklerinin temele aktarılabilmesi için 40–50 MPa beton basınç dayanımlarına ulaşılmıştır. Zaman içerisinde dayanımları artan bu betonlara yüksek dayanımlı beton adı verilmiş ve yol, köprü, liman yapısı vb. uygulamalarda kullanılmaya başlanmıştır. Betondaki dayanım artışına paralel olarak zaman içerisinde su/çimento oranında da düşüş gerçekleşmiştir. 1950'li yıllarda su/çimento oranı 0.60–0.70 aralığında değişirken 1970'li yıllarda akışkanlaştırıcıların devreye girmesi ile bu aralık 0.40–0.55'e düşmüş, 1980 ve 1990'lı yıllarda ise süper akışkanlaştırıcılar sayesinde söz konusu su/çimento oranı 0.25–0.35 aralığına inmiştir. Tüm bunlarla birlikte 1980'li yıllardan sonra ultra ince mineral katkı olan silis dumanının beton içerisinde kullanımının yaygınlaşması ile dayanımlarda çok yüksek artışlar sağlanmıştır. Daha sonra su/çimento oranının 0.20'nin altına düşürülmesi ile yeni kuşak süperakışkanlaştırıcılar, kısa kesilmiş yüksek dayanımlı çelik teller ve sıcak su kürü ve basınçlı su buharı kullanarak beton basınç dayanımları 200 MPa'nın üzerine çıkarılmıştır. Tüm bunlarla birlikte yeni beton teknolojileri gündeme gelmeye başlamıştır.

Daha yüksek yapıların, daha uzun açıklıklı köprülerin yapılmaya ihtiyaç duyulması nedeniyle Yüksek Dayanımlı Betonlar (YDB) tasarlanarak kesitler küçültülmeye ve ekonomi sağlanmaya çalışılmıştır. Betonlarda sadece dayanımın yeterli olmayacağı düşüncesi, performansla bağlı tasarımı ve buna uyumlu olarak durabilite koşulunu da sağlayan Yüksek Performanslı Betonların (YPB) üretilmesine yol açmıştır. Dayanım artışına neden olan düşük su/çimento oranı sünekliğin azalmasına neden olmuş ve betondaki en önemli sorun olan gevrekliği arttırmıştır. Birçok araştırmacı tarafından yapılan çalışmalarda, bu olumsuzluk, beton karışımının içine lifler katılarak giderilmeye çalışılmıştır. Böylece; Lif Donatılı Çimento Esaslı Kompozit (FRCC), Lif Donatılı Beton (FRC), Lif Donatılı Harç (FRM), Sünek Lif Donatılı Çimento Esaslı Kompozit (DFRCC), Yüksek Performanslı Lif Donatılı Çimento Esaslı Kompozit (HPFRCC), Yüksek Oranda Ağ Şeklinde Çelik Tel İçeren Çimento Bulamacı (SIMCON), Yüksek Oranda Kısa Kesilmiş Çelik Tel İçeren Çimento Bulamacı (SIFCON), Reaktif Pudra Betonu (RPC) ve Tasarlanmış Çimento Esaslı Kompozit (ECC) gibi yeni malzemeler geliştirilmiştir (Taşdemir vd., 2004). Bu sorunu çözmek üzere çatlakları kontrol edip, betonun deformasyon özelliğini arttırmak üzere betonlara çekme dayanımını almak üzere fiberler eklenmeye

başlanmıştır. Bu da Çimento Esaslı Kompozitler kavramını ortaya çıkarmıştır. Su/çimento oranı 0.35 ten küçük, hacimce %3'ün altında çelik tel içeren ve dayanımı 70 MPa 'ı geçen kompozitlere Yüksek Performanslı Çimento Esaslı Kompozitler denir. Hacimce düşük oranda çelik lif içermesi nedeniyle, normal betona yakın bir gevrek davranış gösterdiği kaydedilmiştir. Çalışmada kullanılan kompozit, hacimce %1 oranında çelik lif içerdiğinden yeterince sünek davranış göstermediği gözlenmiş ve gerekli bu süneklik artışının, CFRP sargılama ile yapılıp yapılamayacağı araştırılmıştır. Yapı teknolojisi konusunda çok ileri gidilen günümüzde; emniyet, estetik ve ekonomi ile birlikte yeni bir kavram ortaya çıkmıştır, hız! Birbirleriyle ve kendileriyle yarış içinde olan günümüz mühendisleri, yapım hızına oldukça önem vermek durumundadır. Pratik çözümler üretmek, işçilik hataları ve malzeme kusurlarını minimuma indirmek ve bu şekilde yapım hızını arttırmak, ön-dökümlü elemanlar kullanılarak gerçekleştirilebilir. Bu teknoloji; birçok avantajının yanı sıra, taşıma ve döküm konusunda dezavantaja sahip olan HPFRCC elemanların ön-dökümlü üretilerek kullanılmasına olanak sağlamaktadır. Betonun dayanımla birlikte deformasyonunu da arttırmak üzere geliştirilmiş Lifli Polimerlerle Güçlendirme tekniği günümüz inşaat dünyasının popüler çalışma konularındandır. Bu anlamda İTÜ Yapı ve Deprem Laboratuvarında birçok çalışma yapılmış, uluslararası camiada kabul görmüş birçok olumlu sonuca ulaşılmıştır. Yüksek performanslı çimento esaslı kompozit numuneler deneylerde hiç kullanılmamıştır. Bu öngörüler ışığında, ortalama 116 MPa basınç dayanımına sahip Yüksek Performanslı Çimento Esaslı Kompozitler, İSTON tesislerinde imal edilmiştir. Silindir ve kare kesitli numunelerde sağlanan dayanım ve süneklik artışları kıyaslanmak suretiyle bir sonuca varılmaya çalışılmıştır. Bu anlamda toplam 30 silindir ve 19 kare kesitli numuneden meydana gelen bir deney seti oluşturulmuştur. Kullanılan LP kat sayısı bir parametre olarak seçilmiş ve her kesit için değiştirilerek göz önünde bulundurulmuştur. Silindir kesitli numuneler 2-4-6-8 ve 10 kat sargılanırken, kare kesitli numuneler 2-8 ve 10 kat sargılanmıştır. Her numune türü için sargılanmamış beton numuneler hazırlanmış ve basınç deneyleri yapılarak sargısız beton davranışı tespit edilmiştir. Elde edilen referans deney sonuçları ışığında, sargılama sonrası davranış gözlenmiştir. Her numune türü için, numune kenarlarında 25 mm yarıçapında köşe yuvarlatması teşkil edilerek bu bölgelerde gerilme yığılmaları engellenmeye çalışılmıştır. Sıyrılmayı engellemek amacıyla her sargılama için 150 mm bindirme boyu teşkil edilmiştir. Tüm sargılamalar elle yapılmış, mekanik bir sargılama yöntemi kullanılmamıştır. Çalışma sonucunda, Yüksek Performanslı Kompozitler için LP ile sargılama yoluyla süneklik artışı kaydedilmiştir. Silindir ve kare kesitli numunelerde, CFRP sargılama sonucunda, dayanım ve süneklik anlamında farklı artışlar kaydedilmiştir. Silindir kesitli numunelerde artış oranı daha fazlayken, kare kesitli numunelerde bu artış oranının daha az olduğu gözlenmiştir. Her iki kesit türü için, şekildeğiştirmeye kıyasla, dayanımda ciddi bir artış olmadığı gözlenmiştir. Birbirinden farklı sargılı beton modelleri için bir analitik çalışma hazırlanmış ve neticesinde öngörüldüğü gibi, normal beton için isabetli tahminler yapan modellerin, çalışma konusunda yeterince başarı kaydedemedikleri gözlenmiştir. Yüksek performanslı çimento esaslı kompozitlerin, sargılama sonucu kaydettiği dayanım ve şekildeğiştirme artışlarını tahmin etmek üzere yeni bir model geliştirilmesinin gereği ortaya konmuştur. Yapılan çalışma ile LP sargılı yüksek performanslı çimento esaslı kompozitlerin deprem durumundaki davranışının anlaşılması ve tasarım için yeni modeller geliştirilmesinde yardımcı olunacağı düşünülmektedir.

1. INTRODUCTION

Concrete is by far the most important building material and its consumption is increasing in all countries and regions in our globe. The reasons are multiple: its components are available everywhere and relatively inexpensive, its production may be relatively simple, its application covers large variety of building and civil infrastructure works. Moreover, since around 30 years, its development has gone in new directions: high performance concretes (HPC) and high performance cementitious composites. This new kind of building materials are defined as a concrete in which certain characteristics are developed for a particular application and environment; these characteristics are not only strength, but also improved durability, increased resistance to various external agents, high rate of hardening, better aspect, etc. The only disadvantage of concrete is its brittleness, i.e. relatively low tensile strength and poor resistance to crack opening and propagation. In the development of concrete-like materials, the reinforcement with dispersed fibers plays an important role. Since Biblical times, approximately 3500 years ago, brittle building materials, e.g. clay sun baked bricks, were reinforced with horsehair, straw and other vegetable fibers. The concept of fiber reinforcement was developed in modern times and brittle cement-based paste was reinforced with asbestos fibers when in about 1900 the so-called Hatschek technology was invented for production of plates for roofing, pipes, etc. Later, glass fibers were proposed for reinforcement of cement paste and mortar by Biryukovichs [1]. The ordinary E-glass fibers are not resistant and durable in highly alkaline Portland cement paste and Majumdar and Ryder [2] invented the alkali-resistant (AR) glass fibers with addition of zircon oxide ZrO_2 . Important influences of the development of steel fiber reinforced cements (SFRC) are papers published by Romualdi and his co-authors [3, 4] for the first times on this subject. It is not surprising that in such an excellent material as concrete, after many recent improvements of additions and admixtures, with considerable development of technology in precast factories and in situ, and with exploitation of highly sophisticated test methods, the application of dispersed fiber reinforcement results after three decades in a large variety of excellent building. As it is shown at

the next title, because of the necessity, the studies went on the High Performance Fiber Reinforced Cementitious Composites (HPFRCC). Such types of composites can be called as “Structural Concretes”. That is why we use structural concretes for high-rise buildings, long-span bridges, highway and airfield pavements, and many other kinds of outstanding structures. In earthquake prone countries, many existing reinforced concrete structures suffer from low quality of concrete and lack of adequate confinement reinforcement. In such cases, axial capacity and the deformability of the vertical structural members may need to be enhanced to exhibit satisfactory seismic performance. Wrapping these members by high strength fiber reinforced polymer (FRP) composite jackets can enhance the axial strength and deformability of the members significantly. Compared to conventional retrofit techniques, lower density, higher tensile strength and modulus, durability and excellent constructional workability are the advantages of composite retrofit system. Particularly, when there is a time limitation and/or access to the members to be strengthened is limited, composite retrofit system may be more preferable. These and many other studies proved that significant enhancement in compressive strength and deformability of concrete is possible by adequate confinement of concrete by lateral reinforcement. Similar enhancement is possible when the concrete is confined by high strength FRP composites. According to Fukuyama and Sugano [2000], the repair and seismic strengthening by continuous fiber sheet wrapping method was first developed in Japan, where research was first carried out in [1979]. Fardis and Khalili [1982] stated that excellent strength and ductility characteristics were obtained during the experimental study on the FRP encased concrete cylinders in axial compression and of rectangular FRP encased beams in bending. Saadatmanesh et al. [1994] examined the behavior of concrete columns externally reinforced with fiber composite straps. They proposed an analytical model to quantify the gain in strength and ductility by adopting the Mander’s model [1988b] to the fiber composite straps case. Fyfe [1996] summarized the going on experimental studies on the behavior of high strength FRP wrapped concrete members. Mirmiran and Shahawy [1997] reported that the available models in literature that were originally developed for conventional reinforced concrete columns generally did not give accurate results for the FRP wrapped concrete members. Karbhari and Gao [1997] developed experimental data for cylinder specimens based on a variety of fiber types, orientations and jacket thicknesses. Toutanji [1999] investigated the effect of type of

wrapping material on the behavior of FRP jacketed concrete cylinder specimens. Saafi et al. [1999] investigated the behavior of concrete filled GFRP and CFRP tubes under uniaxial compressive load. They indicated that the available models generally overestimate the strength of concrete confined by FRP tubes, resulting in unsafe design. Rochette and Labossiere [2000] conducted axial loading tests on CFRP and AFRP jacketed specimens with circular, square and rectangular cross-sections. They analyzed the effect of corner radius on the behavior of specimens with non-circular cross-sections. Wang et al. [2000], and Wang and Restrepo [2001], tested square and rectangular concrete columns confined by glass fiber composites. In their study, Mander's model [1988b] is adopted for the stress-strain behavior of FRP wrapped concrete. Fukuyama and Sugano [2000] presented the outline of the continuous fiber wrapping technique by comparing the experimental data obtained for various rehabilitation techniques with a special emphasis on performance based engineering and effective rehabilitation techniques without hindrance of building operation. Xiao and Wu [2000] investigated the effect of concrete compressive strength and thickness of CFRP jacket wrapped around cylinder specimens. They also proposed a simple bilinear stress-strain model for the CFRP jacketed concrete. To reduce the brittleness of the concrete we can change both the mixture and confinement type. The aim of this study is to make it clear that the use of HPFRCC confined by CFRP sheets can exhibit a strain-hardening character versus the plain concrete. Therefore, to research this behavior, an experimental study has been carried out. Circular and square cross-sectional specimens were cast at once. In this study, experimental results, obtained for the concrete specimens wrapped by various thicknesses of CFRP jackets, are presented. Thirty specimens with circular cross-section, 19 specimens with square cross-section were included into the testing program. Concentric compression tests were carried out on specimens with circular and square specimens that were wrapped by CFRP jackets. The loading was applied monotonically. A pre-study has been carried out to clarify a manufacturer. All of the specimens during the study had the same height of 300 mm and different aspect ratios. The sizes of the cross-sections were; 150*300 mm for the circulars, 150*150*300 mm for the squares.

2. HIGH PERFORMANCE CEMENTITIOUS COMPOSITES

2.1 Cementitious Composites

Cement-based matrices have developed considerably during last 40 years. The main components are still Portland Cement and coarse and fine aggregate of different origin, and there are several other components: superplasticizers, admixtures and microfillers. In addition, proportions between these components have changed. There are many kinds of Portland Cements that may be selected for particular purposes. The national and international companies may furnish cements that are characterized by high or low strength, high-early strength or low heat of hydration, high sulfate resistance, low content of C3A, and large variety of blended cements, i.e. with addition up to 70% by weight of fly ash and ground blast furnace slag. The next groups of concrete components are additions and admixtures that create special properties of fresh mix and hardened concrete; these are superplasticizers, air-entraining agents, micro fillers and secondary cementing materials: fly ash, natural pozzolans, rice husk ash, metakaolin, etc. In fact, often binary, ternary or quarternary concretes are distinguished i.e. based on compositions of different binders. As aggregate, not only crushed stone and natural gravel with sand are used, but also various artificial materials, carefully selected and inserted into fresh mix in well-determined proportions. In concrete, many kinds of waste materials are used, including recycled aggregate, in order to decrease cost and to satisfy increasing demands of sustainability and ecology. As a result, concretes and particularly concretes that have to satisfy special requirements, became rather complicated materials and are 'tailor-made' to provide the precise properties necessary for a particular project. The design of such a concrete is based on deep knowledge and substantial experience; with the same concerns regarding the selected applications of technology. At all stages, high competence of the personnel is needed. In general, modern concretes are more brittle than those in the first half of 20th century, with higher rates of strength and higher heat of hydration, and often less durable, i.e. less

resistant against intensive corrosive attacks from environment if not specially designed. As remedies, there are special kinds of concretes called high performance concretes, described hereafter, frequently with application of dispersed reinforcement in different forms. The main role of short dispersed fibers is to control the crack opening and propagation. Basic groups of fibers applied for structural concretes and classified according to their material by Brandt [2]:

- Steel fibers of different shapes and dimensions, also microfibers;
- Glass fibers, in cement matrices used only as alkali-resistant (AR) fibers;
- Synthetic fibers made with different materials: polypropylene,
- Polyethylene and polyolefin, polyvinyl alcohol (PVA), etc.;
- Carbon, pitch and polyacrylonitrile (PAN) fibers.

Natural vegetable fibers are not suitable for high performance structural concrete, but are applied in ordinary concretes. Asbestos fibers are completely abandoned in construction because of their detrimental influence on human health and are replaced by other kinds of fibers, e.g. polymeric. Certainly, the most important for structural concrete are steel fibers; a few examples are shown in Figure 2.1; hooks at the ends and various modifications of shape improve fiber-matrix bond and increase efficiency of the fibers.

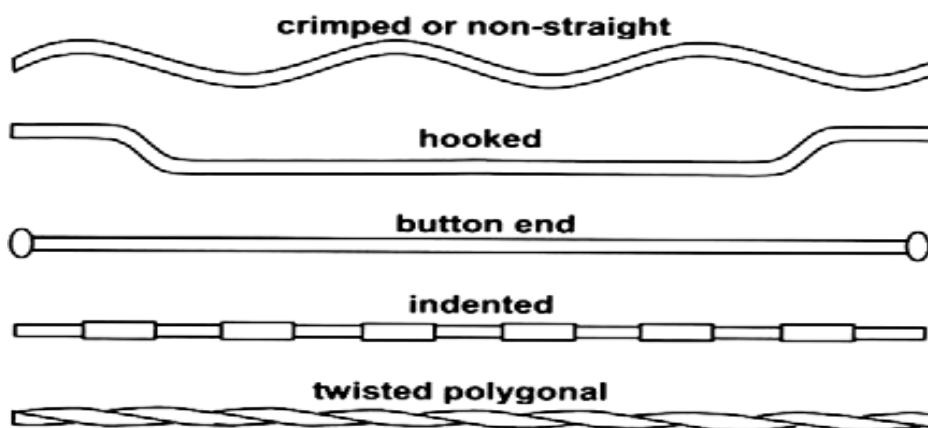


Figure 2.1: Examples of Deformed Steel Fibers [6]

The influence of the fibers on cracking of cement-based matrix is explained in Figure 2.2: thanks to the fibers, large single cracks are replaced with dense systems of microcracks, which may be acceptable from both safety and durability viewpoints.

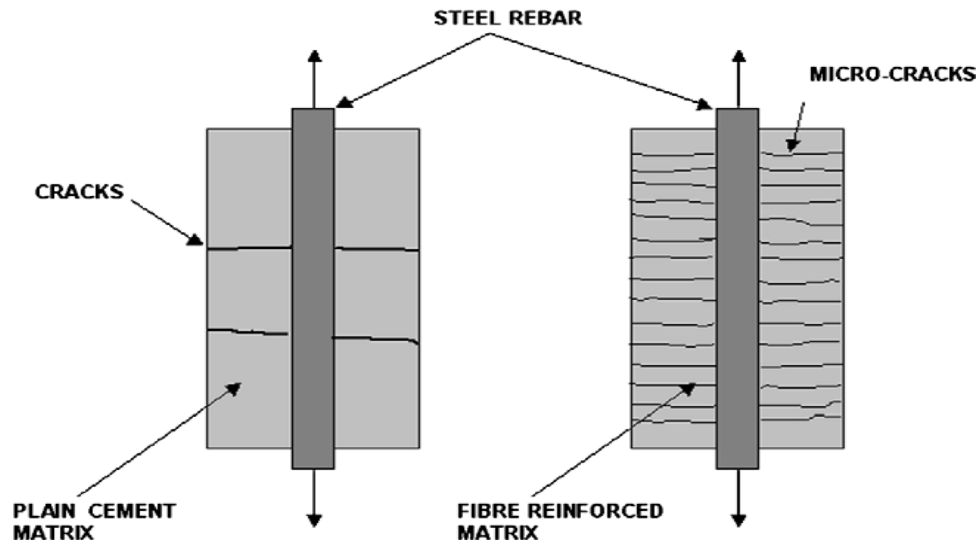


Figure 2.2: Crack Pattern in Reinforced Concrete (RC) and Fiber Reinforced Composite Elements Subjected to Tension [3].

Fine fibers control opening and propagation of micro-cracks as they are densely dispersed in cement matrix. Longer fibers up to 50 or 80 mm control larger cracks and contribute to increase the final strength of FRC, as it is shown in Figure 2.3.

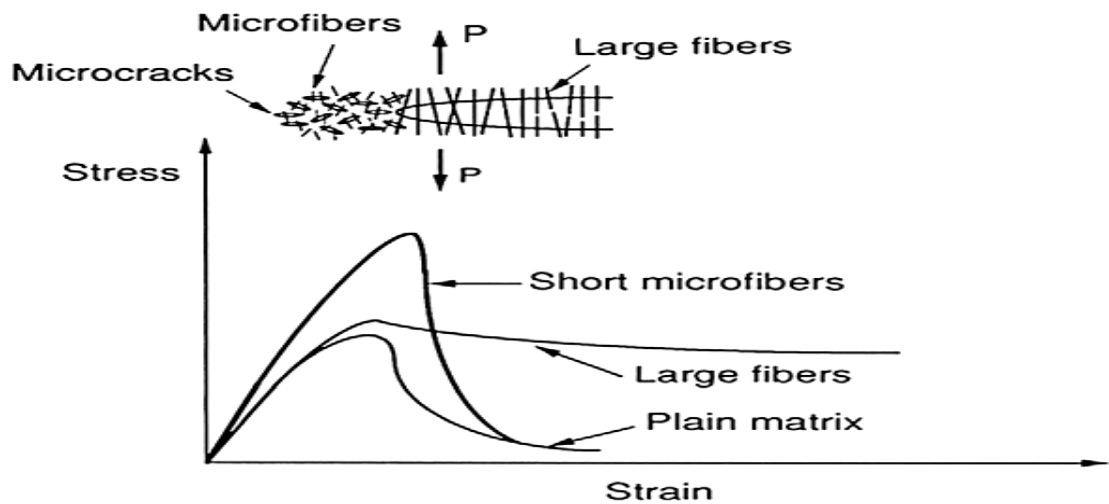


Figure 2.3: Structures of Long and Short Fibers Controlling the Crack Propagation; after Betterman et al. [3]

With the increase of fiber volume and efficiency, their influence on behavior of a SFRC element modifies completely its behavior under load, as it is described in Figure 2.4 with strain–stress diagrams. The conventional SFRC element is characterized by initial linear increase of stress and after the first crack opening there is a slow decrease, the so-called softening branch. In contrast, where the

reinforcement is sufficient, after the first crack, there is a strain hardening stage, which accompanies multiple cracking and considerable amount of energy is absorbed that is proportional to the area under the curve. The softening branch follows that stage. In Figure 2.4, the main difference between conventional FRC and high performance fiber reinforced cement composites (HPFRCC) is defined.

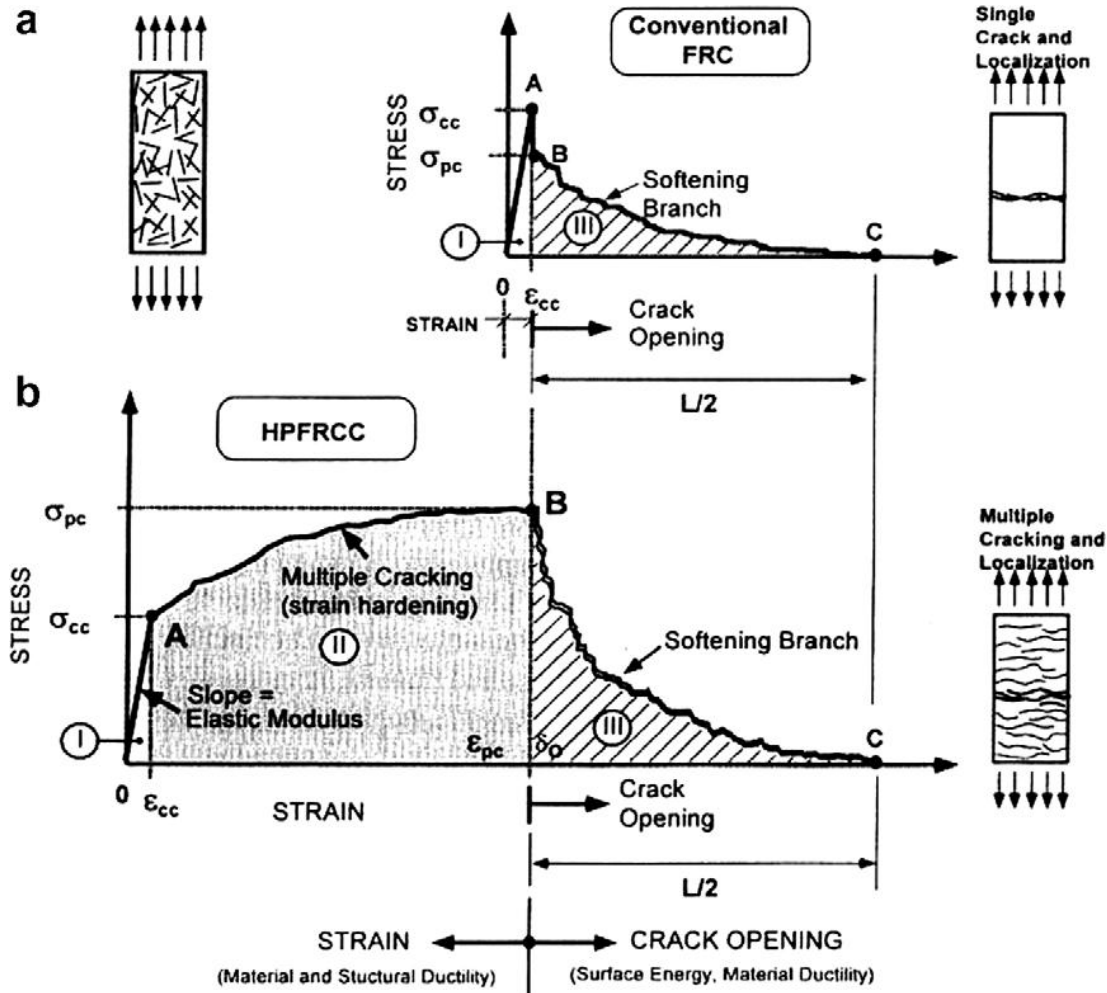


Figure 2.4: Comparison of Typical Stress–Strain Response in Tension of HPFRCC with Conventional FRCC, after Naaman [8].

2.2 Key Features of High Performance Cementitious Composites

The demand has never been greater for tougher, more ductile materials to improve the behavior of civil engineering structures under rapid and severe loading, such as blast, impact and earthquakes. A particularly promising class of materials for such

applications is high performance fiber reinforced cementitious composites (HPFRCCs), which exhibit a 'high performance' response in tension, i.e. Strain Hardening response after first cracking, tensile ductility, both of which lead to improved durability and high-energy absorption capacity. HPFRCCs, as first defined and developed by Naaman [9], can now achieve high performance behavior using a relatively low volume fraction (usually 2% or less) of short, randomly oriented steel or polymeric fibers. At the present time, HPFRCCs are classified as strain-hardening fiber reinforced cementitious composites.

In order to achieve strain-hardening behavior, various approaches have been tried and used by many researchers. One well established example is SIFCON (slurry infiltrated fiber concrete) and its similar derivative SIMCON (slurry infiltrated mat concrete) which were developed during the late 1970s and 1980s . Engineered Cementitious Composites (ECC) is also one family of HPFRCC. ECC utilize about 2% PVA fiber to produce strain-hardening behavior with 3–4 MPa tensile strength; their strain capacity may be relatively high but is dependent on the size of the specimen and the method of testing. Value as high as 3–4% were reported newer forms of HPFRCC include Ultra High Performance Fiber Reinforced Cement Composites [UHPFRC] which are characterized at the mechanical level by a very high compressive strength (practically in the range of 150–200 MPa). However, to develop strain-hardening behavior in tension, they require 5–11% fiber contents by volume, mostly smooth steel fibers. Very little information is available to describe the entire stress–strain response of UHPFRCC in direct tension using reasonably large size specimens. As of this writing, the tensile strength achieved by UHPFRCC using 2% high strength steel fibers by volume, is around 11 MPa and its strain capacity at maximum stress is close to 0.5%. In this research, high strength deformed hooked-up steel fibers, which show slip hardening behavior under single fiber Pullout testing are used to obtain tensile strain hardening behavior of the composite. It was shown earlier that the slip hardening behavior, which leads to high pullout energy (or work), is a critical condition for the strain hardening behavior of FRC composites. The promise of HPFRCCs for dynamic loading application stems from their observed good response under static loading.

3. COMPARISON OF AVAILABLE COMMERCIAL CFRP SHEETS

3.1 Preparation and Retrofit of the Specimens for Comparison

The specimens were cast at once ready-mixed at the Structural and Earthquake Engineering Laboratory (STEEL). Casting process and moulds used for study can be seen on Figure 3.1. 150*300 mm circular cross-sections were used as moulds. All of the moulds required for the study, were provided from STEEL. At the 28th day of casting, two reference cylinder tests were performed to obtain the compressive stress of the concrete at 28 days. Results of the tests can be seen at Figure 3.2.



Figure 3.1: Casting the Specimens for Comparison

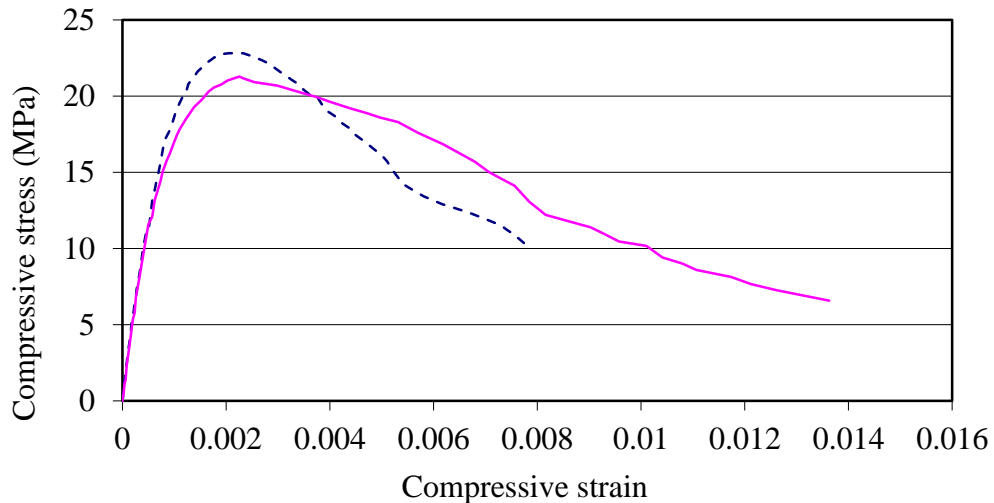


Figure 3.2: Stress-Strain Curves of the Unconfined Specimens

All of the specimens were prepared to be performed under uni-axial loading. As seen, the average compressive stresses of the specimens at 28th day can be approved as 20 MPa. The only parameter of the study was compressive stress to clarify the comparison between two products. Product A is manufactured by Akkim and

Product B by BASF and preparation of the specimens can be seen on Figure 3.3. The black colored specimens are CFRP of Product A used specimens since the epoxy of Product A is crystalline. Product B epoxy is blue colored, so the colors of the specimens are also blue. Mechanical properties of the composite sheets are given for both Product A and B on Table 3.1.

Table 3.1: Properties of Composite Sheets Wrapped

	Product A	Product B
Tensile strength (MPa)	4200	3430
Tensile elasticity modulus (MPa)	240000	230000
Ultimate tensile deformation (%)	1.8	1.5
Effective area per unit width (mm ² /mm)	0.0166	0.0165



Figure 3.3: Preparation of Specimens

3.2 Test Results for Comparison

Eight specimens were exposed to a uniaxial loading on an Amsler universal testing machine with the capacity of 5000 kN. Lateral strains were measured at midheight by surface strain gauges with the gauge length of about 150 mm for all specimens. Load was applied 0,6 mm per minute (TS EN 12390-3) and test was displacement controlled. For measurements of average axial strains for different gauge lengths, displacement transducers were used. For specimens with circular cross-section, two transducers with the gauge length of 60 mm (PL60) and two transducers with the gauge length of 250 mm (LVDT25) were used for circular specimens. The only parameters were Peak Stresses and Peak Lateral Strains to compare two manufacturers CFRPs.

3.2.1 Specimens confined by 2 plies of CFRP

These specimens were confined by two plies of Product A and Product B CFRP. The epoxies impregnated on the surfaces of the specimens also belong to manufacturer A or B. End zones' retrofit was not applied to these specimens. Stress-Strain relationships those were obtained by average of two specimens 2 plies of Product A and B can be seen on Figure 3.4.

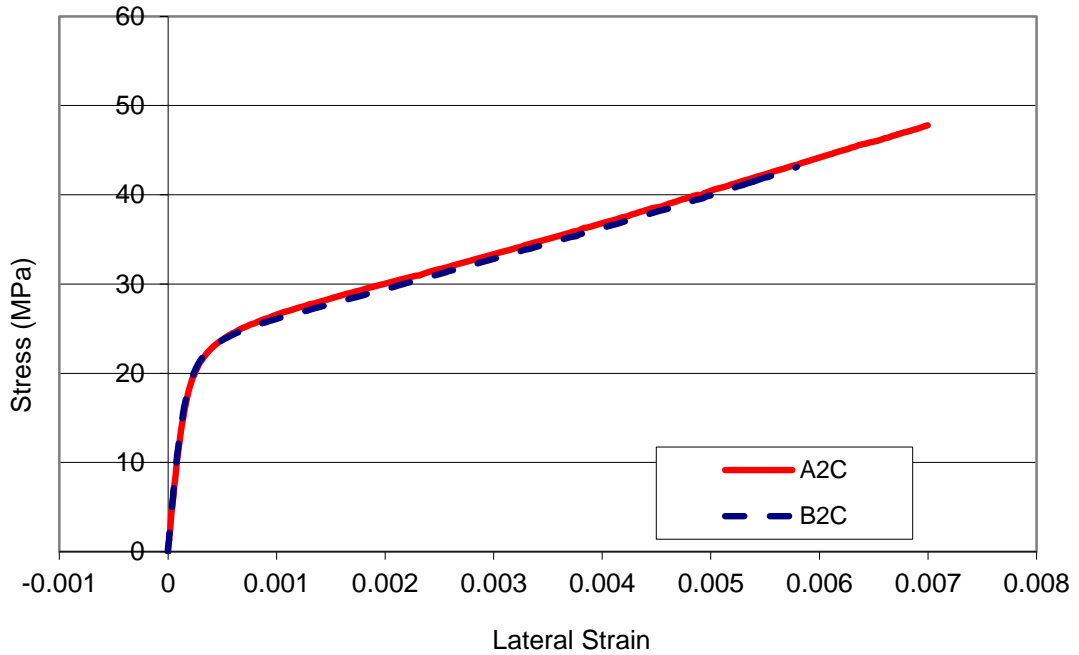


Figure 3.4: Stress – Lateral Strain Relationship Between Specimens Confined by 2 Plies of CFRP

Peak Lateral Strain is objected to the Peak Stress. These datas was acquired by strain gauges. As seen above, an enhancement for compressive stress from 20MPa to 48MPa (%140) and for lateral strain from 0.002 to 0.007 (%250) was observed by confining 2 plies of CFRP by Product A and for Product B. A compressive stress enhancement was about %110 and lateral strain enhancement was about %200. Peak Stress-Peak Strain Load datas are summarized at the end of the chapter on a chart. On Figures 3.5, 3.6, 3.7, 3.8 after test photos (damaged) for specimens can be seen.



Figure 3.5: A_2C_1 Damage



Figure 3.6: A_2C_2 Damage



Figure 3.7: B_2C_1 Damage



Figure 3.8: B_2C_2 Damage

3.2.2 Specimens confined by 4 plies of CFRP

Similarly, we have totally four of four plies of CFRP confined specimens. Two for Product A and 2 for Product B. Given values on the Figure 3.9, include the average of two specimens both for Product A and two for Product B. A compressive stress enhancement was about %275 and lateral strain enhancement was about %450 for 4 plies of CFRP confined by using Product A specimens and %240 stress enhancement and %300 strain enhancement was observed for Product B specimens.

On Figures 3.10, 3.11, 3.12, 3.13 after test photos (damaged) for specimens can be seen.

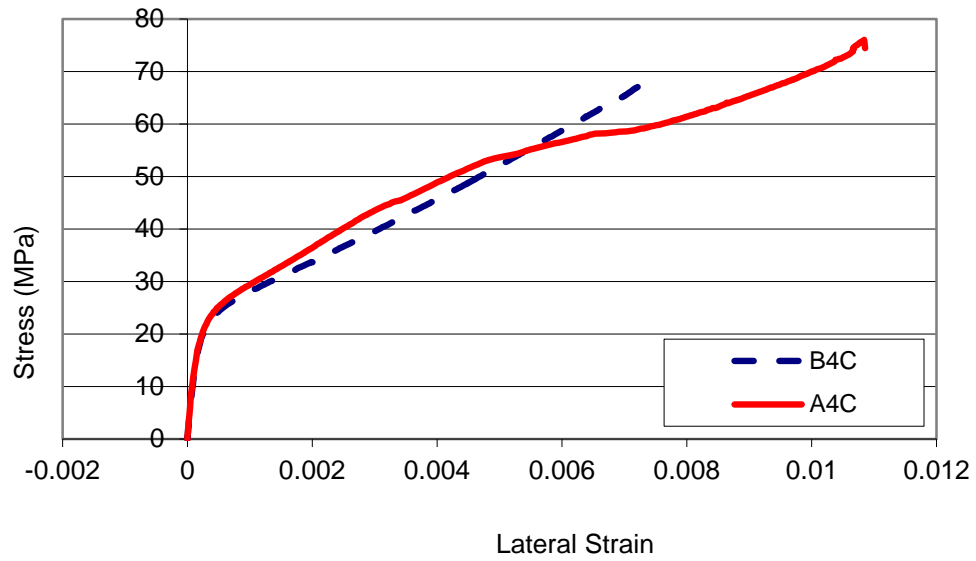


Figure 3.9: Stress - Lateral Strain Relationship between Specimens Confined by 4 Plies of CFRP



Figure 3.10: A_4C_1 Damage



Figure 3.11: A_4C_2 Damage



Figure 3.12: B_4C_1 Damage



Figure 3.13: B_4C_2 Damage

Table 3.2: Peak Loads during the Comparison Test

Specimen Name	Peak Load (kN)
A_2C_1	845
A_2C_2 (*)	998.2
A_4C_1	902.4
A_4C_2	1346
B_2C_1	762
B_2C_2 (*)	989.5
B_4C_1	1198
B_4C_2 (*)	1357

The (*) statements clarify end zones retrofit by 5cm width and three plies of CFRP bands after confinement. As seen at table above, two plies Product A CFRP confined and then retrofitted specimens have about % 18 much more compressive stresses with respect to unconfined. This ratio is about % 29 at 2 plies Product B CFRP confined retrofitted and unconfined specimens. At four plies, Product B CFRP confined specimens; this ratio is about % 13. Since Product A and B have very close results, Product A was used on the study as confining material.

4. EXPERIMENTAL WORK

4.1 Preparation and Retrofit of the Specimens

For casting the composite, a computer controlled ready mix concrete company was used. Casting equipment can be seen on Figure 4.1. The composition of composite was literated and researched by the researcher. The goal strength of the proportion was about 100-110 MPa compressive. To acquire this strength, steel fibers should be used. 6 cm length hooked-up steel fibers were used. Details of the composite compounds can be seen under Table 4.1.



Figure 4.1: Casting Mixer at ISTON

Table 4.1: Mix Proportion for Cementitious Composite (kg/m³)

C	SF	FA	CA	STF	W	SP	TOTAL
1000	250	489	326	78,5	124	125	2392

C:Cement (Aslan CEM I 42,5R) SF:Silica Fume (Norchem) FA: Fine Aggregate (0-0,5mm)
CA: Coarse Aggregate (0-0,5mm) STF: Steel Fiber (Dramix 6cm-hooked-up) SP: Superplasticizer (Chryso Optima 208) W:Water

All specimens were casted at once. Moulds were taken at the following day of casting. 3 days of cure was performed to make them early strengthen. After curing and then a week, all specimens were carried to laboratory for cap performing. On

Figure 4.2, moulds for circular and non-circular specimens can be seen and on Figure 4.3, specimens after taking moulds are shown.



Figure 4.2: Moulds at Casting Step



Figure 4.3: All Specimens after Taking Moulds

A cap preparation was performed for all specimens to take local stresses over the end zones. On Figure 4.4, process can be seen. All specimens were impregnated by AKRESİN AS 400 A resins and AKRESİN AS 400 B the hardener of it, to create a smooth surface over the specimen. Applied primer can be seen on Figure 4.5.



Figure 4.4: Caps Performing



Figure 4.5: Primer Performed Specimens before Confining

AKRESİN EP 250 B and AKRESİN 250 A are two components of resin to be mixed and applied during confining. Components were mixed about 3 minutes and then applied to surfaces of specimens. After preparing the epoxy and applying over the specimens, previous day cut CFRPs were confined over the specimens. Confining process can be seen on Figure 4.6. After body confining, CFRP sheet bands to carry the damage on the mid-height of the specimens of those retrofitted both end zones. Retrofit of the end zones can be seen on Figure 4.7.



Figure 4.6: Confining the Specimens



Figure 4.7: End Zones Retrofit

4.2 Test Set-Up

Prepared specimens were tested on an Instron Test Machine with the capacity of 5000 kN as seen on Figure 4.8. The software Bluehill 2 performed loading steps of machine. All the data was taken from the surface of the specimens by strain gauges and transducers. Lateral and vertical strains and the loads defiant these strains were measured.



Figure 4.8 : 5000 kN Capacity Instron Test Machine

Properties of measurement equipment can be seen on Table 4.2. PL-60-11-3L refers to 60mm measurement capacity of strain gauge, used to measure the lateral strain. Strain gauges were used two for cylinder specimens and four for square specimens. CDP-25 refers to 25 mm measurement capacity of transducer (LVDT) to measure the axial strain. LVDTs were used two for along all height of specimens and four for middle of four surfaces of specimens.

Table 4.2: Properties of Measurement Equipments

Equipment	Reaction	Measurement Capacity
PL-60-11-3L	20 Hz	60 mm
CDP-25	8 Hz	25 mm

4.3 Test Results for Circular Members

There are 30 circular cross-sectional specimens to perform. All specimens have the same sizes as 150*300 mm. Loading rate during the test was 0.6 mm/min for confined specimens and 0.4 mm/min for unconfined with respect to TS EN 12390-3. A pre-load applied before test to consider either the space between cap of specimen and test machine or the crush of the cap under test start and calculated as 95 kN. All confinements are lateral and all made by hand. An overlap of 150 mm was applied to all specimens. A radius of rounding with 25 mm on the edges was also performed. Loads applied during tests are monotonic and displacement controlled.. Stress-

Lateral Strain and Stress-Axial Strain relationships after tests are mentioned and photos are over the graphics.

There is a comparison at the end with the unconfined and confined specimens. Stress, lateral and axial strains are the parameters. Average stress and strain enhancements subjected to CFRP confinement thickness are summarized as a result at the end of the part. At the 28th day of the casting, 3 standard cylinder specimens were tested to determine compressive strength and strains under uni-axial loading.

The goal was, to start the main study and to research the enhancement on strength, lateral and axial strains by FRP on HPFRCCs. The after test results are summarized below on a table. The aim of literated composite proportion was in a rank of 100-110 MPa at 28 days and the average compressive strength of the circular cross sectional specimens after 28 days was 116.03. Details of the specimens are mentioned on a chart below on Table 4.3;

Table 4.3: Details of the Circular Specimens

Specimen Code	Number of CFRP Sheet Plies
CC-C-0-1	0
CC-C-0-2	0
CC-C-0-3	0
CC-C-0-4	0
CC-C-0-5	0
CC-C-0-6	0
CC-C-2-1	2
CC-C-2-2	2
CC-C-2-3	2
CC-C-2-4	2
CC-C-2-5	2
CC-C-2-6	2
CC-C-2-7	2
CC-C-4-1	4
CC-C-4-2	4
CC-C-4-3	4
CC-C-6-1	6
CC-C-6-2	6
CC-C-6-3	6
CC-C-8-1	8
CC-C-8-2	8
CC-C-8-3	8
CC-C-8-4	8
CC-C-10-1	10
CC-C-10-2	10
CC-C-10-3	10
CC-C-10-4	10

4.3.1 Unconfined circular specimens

CC-C-0-1, CC-C-0-2 and CC-C-0-3

These three specimens are unconfined reference circular cross sectional specimens. Compressive tests were carried out at 28th day of casting. On Figure 4.13a, 4.13b, 4.13c failures of the specimens can be seen. On Table 4.4, test results are summarized for these three unconfined specimens.

Table 4.4: Reference Cylinder Test Results

Specimen Name	Specimen Age	f'_{co} (MPa)	f'_{co} (MPa) (Average)
CC-C-0-1	28	104.69	116.03
CC-C-0-2	28	118.84	
CC-C-0-3	28	124.55	

CC-C-0-4

This specimen is an unconfined reference specimen. After the test, observed failure behavior is as seen on Figure 4.14. Some concrete pieces spilled before crush and longitudinal cracks occurred after the test. The failure was concentrated at the middle and the top of the specimen. Stress – Axial Strain behavior of the specimen can be seen on Figure 4.9.

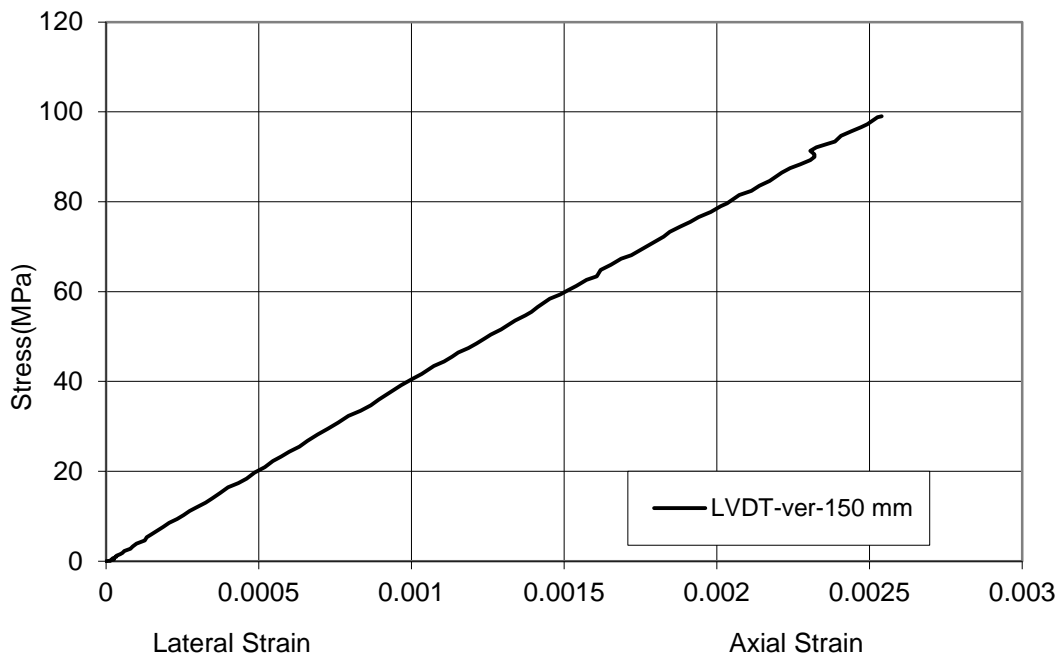


Figure 4.9: Stress - Strain Relationship for C-CC-0-4

Branch represents the measurement of transducers along 150 mm gage length over the middle of the surfaces. Two LVDTs we have and this branch represents average values of these. Since the parameter was just to obtain the compressive ultimate stress, strain gauges were not used to evaluate the lateral strains. A value of axial strain was observed as approximately 0.0025 at a stress of 103.22 MPa at 90th day/compressive.

CC-C-0-5

This specimen is an unconfined reference specimen. After the test, observed failure behavior is as seen on Figure 4.15. Stress - Axial Strain relationship for C-CC-0-5 can be seen on Figure 4.10.

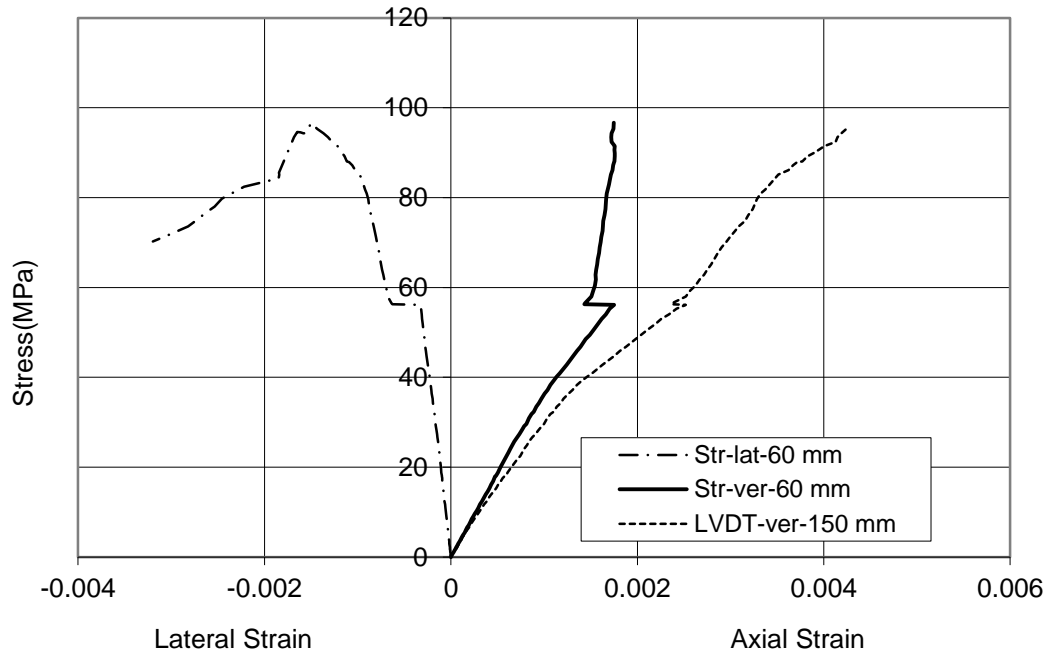


Figure 4.10: Stress - Strain Relationship for C-CC-0-5

Two strain gauges we have and this branch represents average values of these. A value of approximately 0.005 axial strain was observed from LVDTs. Peak axial stresses are close to each other for vertical strain gauges and laterals at a level of 96.65 MPa compressive at 120th day. A lateral strain of a 0.002 was observed under ultimate stress. Rupture occurred at a lateral strain of 0.006.

CC-C-0-6

This specimen is an unconfined reference specimen. After the test, observed failure behavior is as seen on Figure 4.16. Stress – Strain behavior of the specimen can be seen on Figure 4.11.

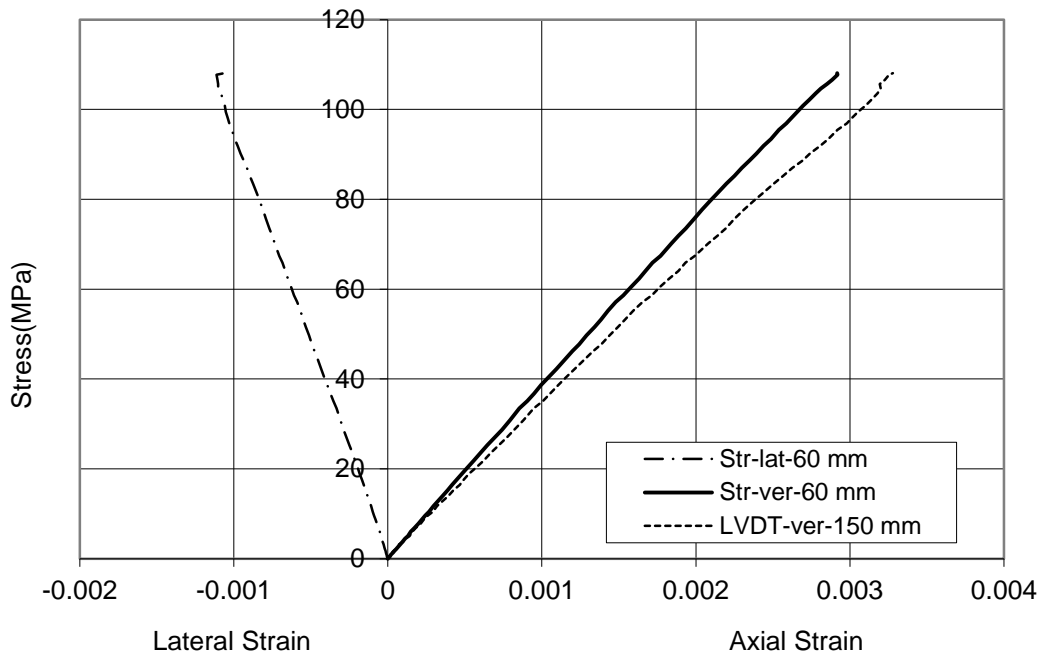


Figure 4.11: Stress - Strain Relationship for C-CC-0-6

While value of axial strain was approximately 0.003, a lateral rupture strain could not be observed since strain gauges did not work. Peak axial stresses are close to each other for vertical strain gauges and transducers at level of 108.08 MPa compressive at 120th day. Obtained average axial stress was 103 MPa. Strain obtained from tests was 0.0033 average. Comparison for all unconfined circular specimens can be seen on Figure 4.12.

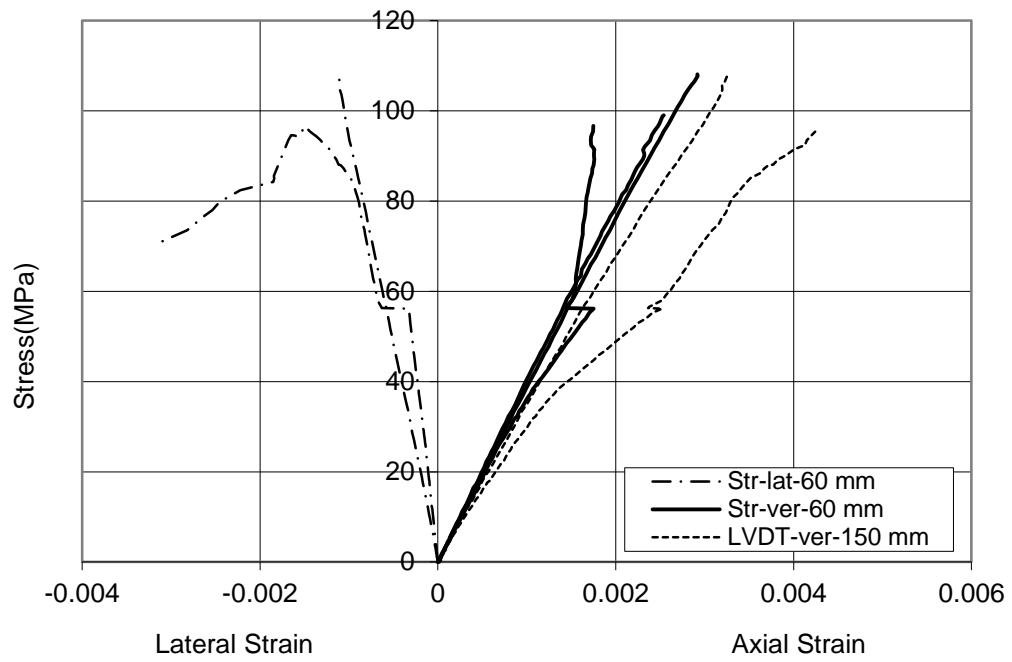


Figure 4.12: Stress - Strain Relationship Comparison for Unconfined Circular Specimens



Figure 4.13a: CC-C-0-1



Figure 4.13b: CC-C-0-2



Figure 4.13c: CC-C-0-3



Figure 4.14: CC-C-0-4



Figure 4.15: CC-C-0-5



Figure 4.16: CC-C-0-6

4.3.2 Circular specimens confined by 2 plies of CFRP

CC-C-2-1

This specimen was confined by two plies of CFRP. Test was carried out after 90 days of casting the composite. Rupture of FRP was seen along the surface laterally. 3cm width and two plies of CFRP sheets with an overlapping of 15 cm was applied. End zones retrofit both ruptured during the test. After the test, observed failure behavior is as seen on Figure 4.25. Stress – strain behavior of the specimen can be seen on Figure 4.17.

A value of axial strain was observed as approximately 0.003 at about 116 MPa at 90th day/compressive. Specimen reached a peak axial load of 2050 kN and then concrete crush was observed. FRP kept on load carrying until a strain of 0.009. For the evaluated axial stress was about 103 MPa and strain was 0.0033, a stress enhancement ratio of 1.126 was obtained. Since strain gauges did not work strain enhancement ratio could not be obtained.

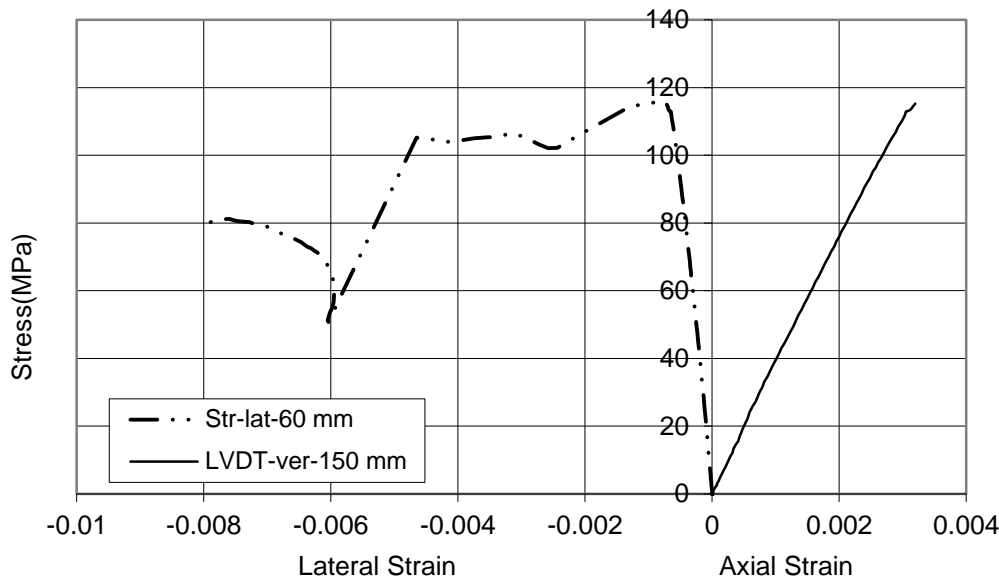


Figure 4.17: Stress - Strain relationship for C-CC-2-1

CC-C-2-2

This specimen was confined by two plies of CFRP. Test was carried out after 195 days of casting the composite. After the test, observed failure behavior is as seen on Figure 4.26. Rupture of FRP was seen along the surface laterally. End zones retrofit

were both occurred by 5 cm width and five plies of CFRP sheets with an overlapping of 15cm. End zone retrofit ruptured during the test.

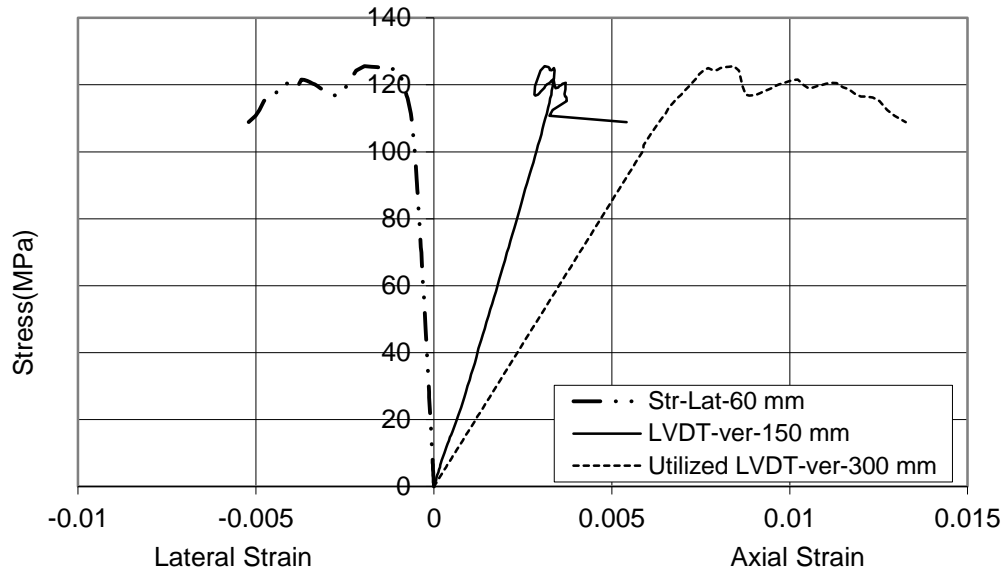


Figure 4.18: Stress - Strain Relationship for CC-C-2-2

A value of axial strain was observed as approximately 0.005. We have two LVDTs to measure the axial strain along 300 mm gage length over the height of specimen similarly. Also two stress values, read by along middle and all surfaces LVDTs are close to each other at about 125.6 MPa at 195th day / compressive. Approximately, at a lateral strain of 0.005 cementitious composite crushes under a stress of about 125.6 MPa. Maximum load, reached during the test was 2219 kN. There are two strain gauges to measure the lateral strains over all surfaces of the specimen. Lateral strain seen on figure is the average of those two strain gauges. Enhancement ratio for stress is 1.219 and for strain it is 1.515.

CC-C-2-3

This specimen was confined by two plies of CFRP. Test was carried out after 195 days of casting the composite. After the test, observed failure behavior is as seen on Figure 4.27. Rupture of FRP was seen along the surface laterally. End zones retrofit were both occurred by 5cm width and five plies of CFRP sheets with an overlapping of 15 cm. end zones retrofit both ruptured during the test. A value of axial strain was observed as approximately 0.004. We have two LVDTs to measure the axial strain along 300 mm gage length over the height of specimen similarly. Also two stress

values, read by along middle and all surfaces LVDTs are close to each other at about 134.7 MPa at 195th day compressive.

Approximately, at a lateral strain of 0.008 cementitious composite crushes under a stress of about 134.7 MPa as seen on figure. Maximum lateral strain for rupture was 0.0011. Maximum load reached during the test was 2380kN. There are two strain gauges to measure the lateral strains over all surfaces of the specimen. Lateral strain seen on figure is the average of those two strain gauges. Enhancement ratios for this specimen is 1.307 as stress and 1.212 for strain.

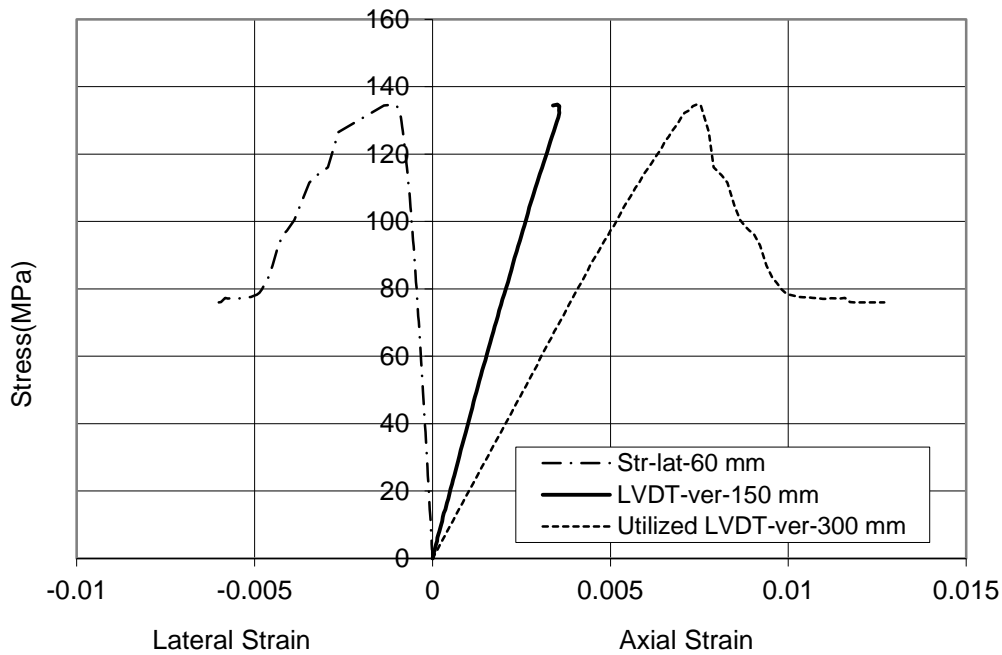


Figure 4.19: Stress - Strain Relationship for CC-C-2-3

CC-C-2-4

After the test, observed failure behavior is as seen on Figure 28. Rupture of FRP was seen along the surface both laterally and vertically. End zones retrofit were both occurred by 5 cm width and 5 Plies of CFRP sheets with an overlapping of 15 cm. End zones retrofit both were ruptured during the test.

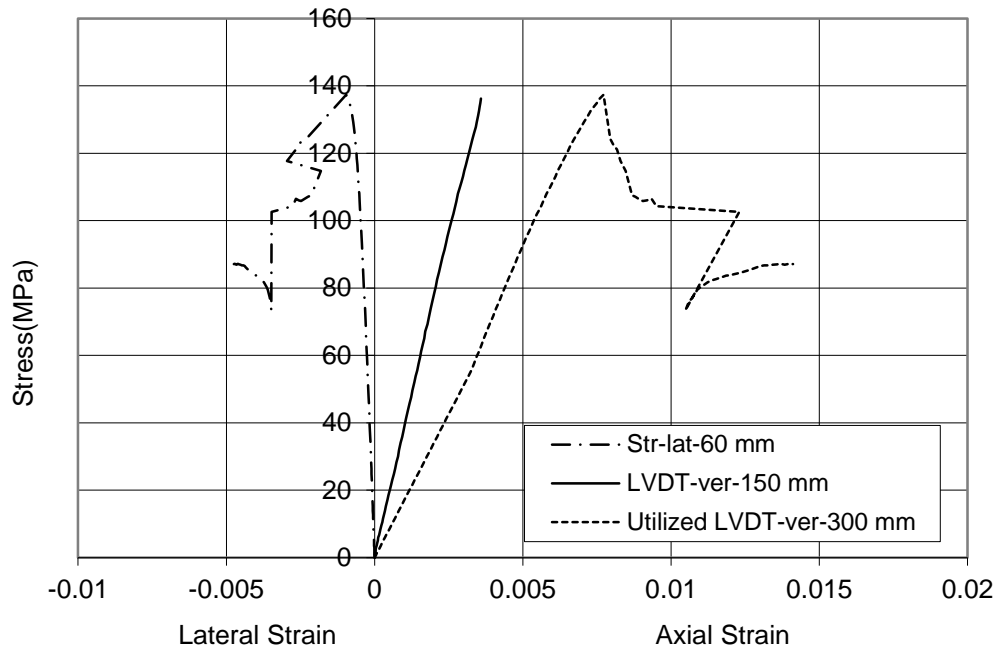


Figure 4.20: Stress - Strain Relationship for CC-C-2-4

A value of axial strain was observed as approximately 0.004. We have two LVDTs to measure the axial strain along 300 mm gage length over the height of specimen similarly. Also two stress values, read by along middle and all surfaces LVDTs are close to each other at about 137.4 MPa at 195th day compressive. Approximately, at a lateral strain of 0.0009 cementitious composite crushes under a stress of about 137.4 MPa as seen on figure. Maximum load reached during the test was 2428 kN. Enhancement ratios for stress and strain are 1.334 and 1.091.

CC-C-2-5

This specimen was confined by two plies of CFRP. Test was carried out after 195 days of casting the composite. After the test, observed failure behavior is as seen on Figure 29. Rupture of FRP was seen along the surface laterally. End zone retrofit were both occurred by 5cm width and 5 Plies of CFRP sheets with an overlapping of 15 cm. End zone retrofit both ruptured during the test. A value of axial strain was observed as approximately 0.004. Also two stress values, read by along middle and all surfaces LVDTs are close to each other at about 147.6 MPa at 225th day compressive. Approximately, at a lateral strain of 0.0009 cementitious composite crushes under a stress of about 147.6 MPa as seen on figure. Maximum load reached during the test was 2608 kN. Enhancement ratios for stress and strain are 1.433 and

1.121.

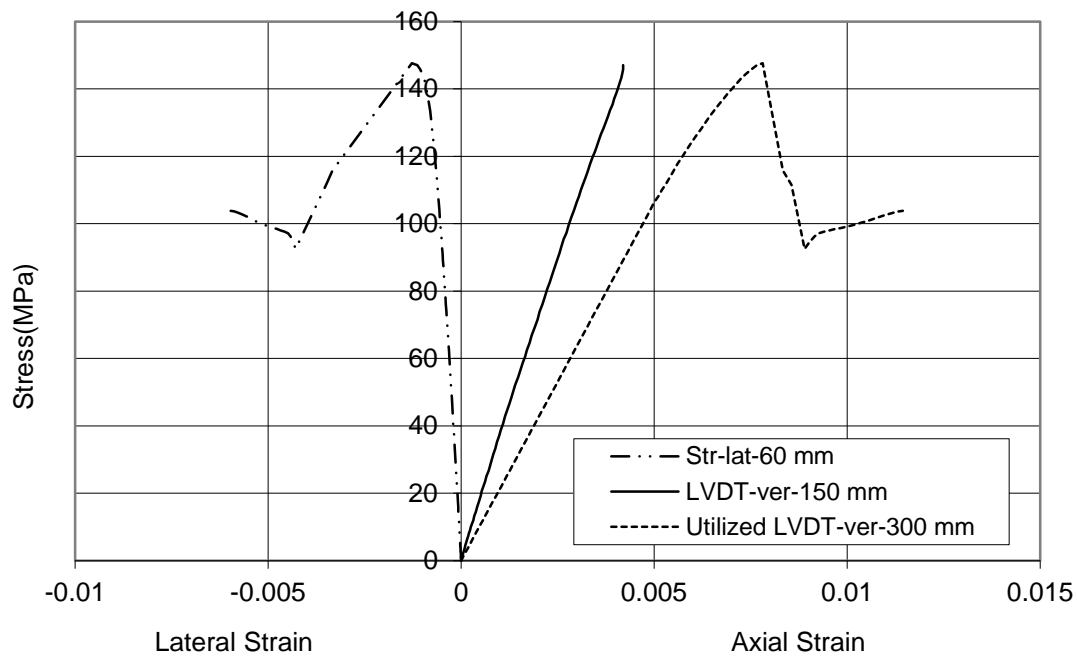


Figure 4.21: Stress - Strain Relationship for CC-C-2-5

CC-C-2-6

This specimen was confined by two plies of CFRP. Test was carried out after 195 days of casting the composite. After the test, observed failure behavior is as seen on Figure 30. Rupture of FRP was seen along the surface laterally. End zone retrofit were both occurred by 5cm width and 5 plies of CFRP sheets with an overlapping of 15cm. End zones retrofit both were ruptured during the test.

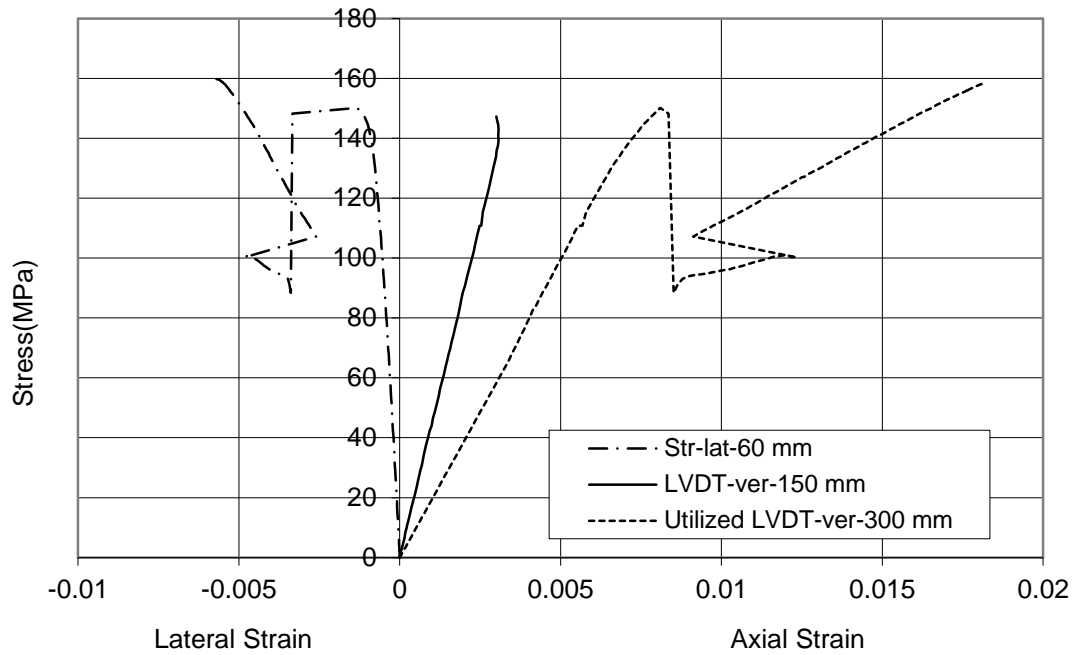


Figure 4.22: Stress - Strain Relationship for CC-C-2-6

A value of axial strain was observed as approximately 0.003. Also two stress values, read by along middle and all surfaces LVDTs are close to each other at about 160.1 MPa at 195th day compressive. Approximately, at a lateral strain of 0.003 cementitious composite crushes under a stress of about 160.1 MPa as seen on figure. Maximum load reached during the test was 2829 kN. Enhancement ratios are 1.55 for stress and 0.909.

CC-C-2-7

This specimen was confined by two plies of CFRP. Test was carried out after 195 days of casting the composite. After the test, observed failure behavior is as seen on Figure 31. End zones retrofit was both occurred by 5 cm width and 5 Plies of CFRP sheets with an overlapping of 15 cm.

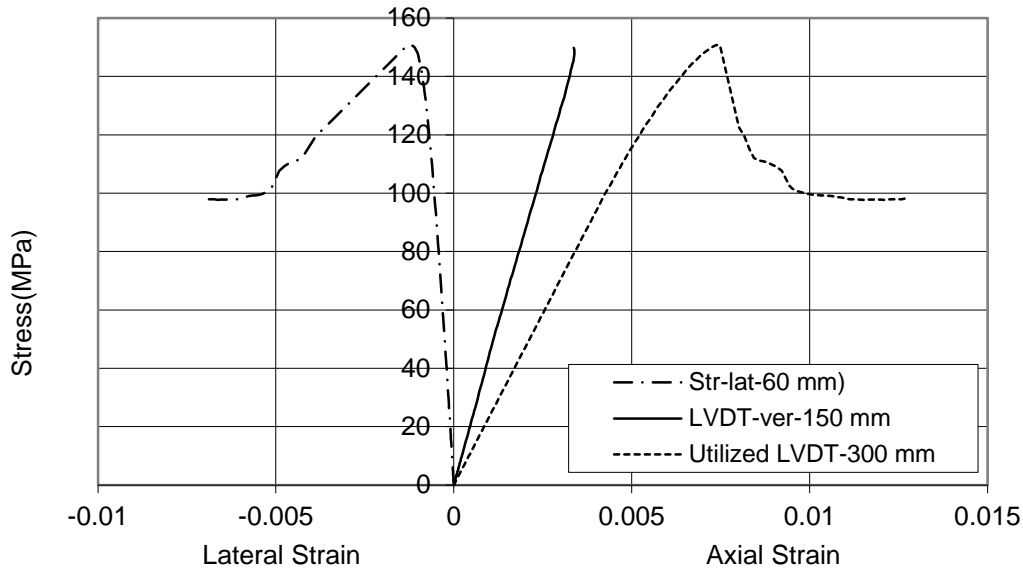


Figure 4.23: Stress - Strain Relationship for CC-C-2-7

A value of axial strain was observed as approximately 0.003. Also two Stress values, read by along middle and all surfaces LVDTs are close to each other at about 150.8 MPa at 195th day compressive. Approximately, at a lateral strain of 0.001 cementitious composite crushes under a stress of about 150.8 MPa as seen on figure. Maximum load reached during the test was 2664 kN. Enhancement ratios are 1.46 for stress and 1.021. A comparison for specimens that confined by 2 plies of CFRP can be seen on Figure 24.

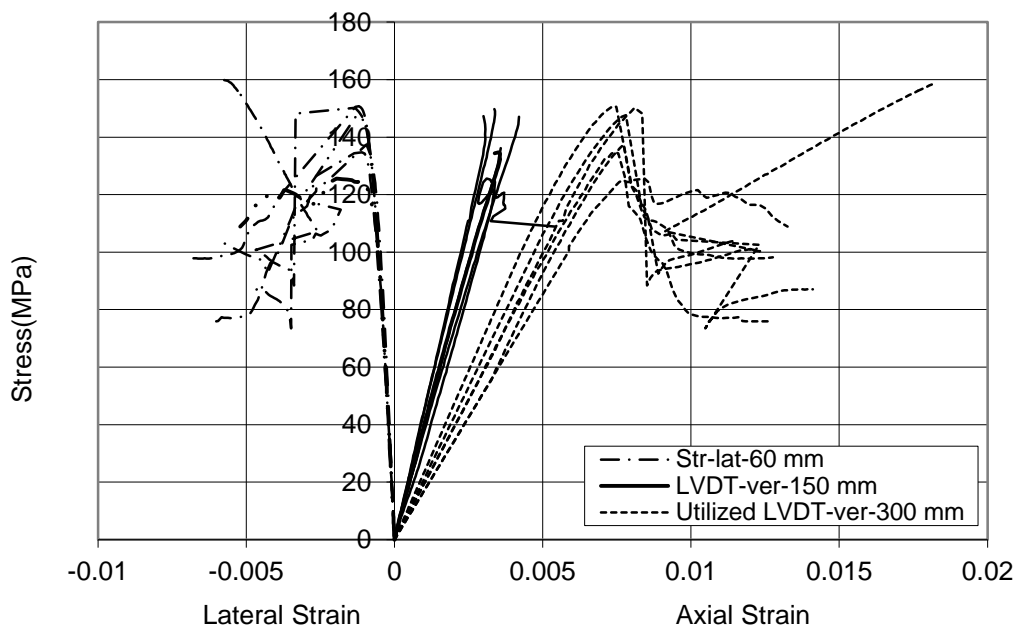


Figure 4.24: A Comparison for Specimens that Confined by 2 Plies of CFRP



Figure 4.25: CC-C-2-1



Figure 4.26: CC-C-2-2



Figure 4.27: CC-C-2-3



Figure 4.28: CC-C-2-4



Figure 4.29: CC-C-2-5



Figure 4.30: CC-C-2-6



Figure 4.31: CC-C-2-7

4.3.3 Circular specimens confined by 4 plies of CFRP

CC-C-4-1

This specimen was confined by 4 plies of CFRP. After the test, observed failure behavior is as seen on Figure 4.36. Rupture of FRP was seen along the surface both laterally and vertically. End zones retrofit were both occurred by 3cm width and two plies of CFRP sheets with an overlapping of 15cm. A value of axial strain was observed as approximately 0.005 at about 149.3 MPa at 90th day/compressive. Specimen reached a peak axial load of 2638 kN and then concrete crush was observed. FRP kept on load carrying until a strain of 0.006. Stress -Strain relationships are on Figure 4.33. Enhancement ratios were 1.463 for stress and 1.424 for strain.

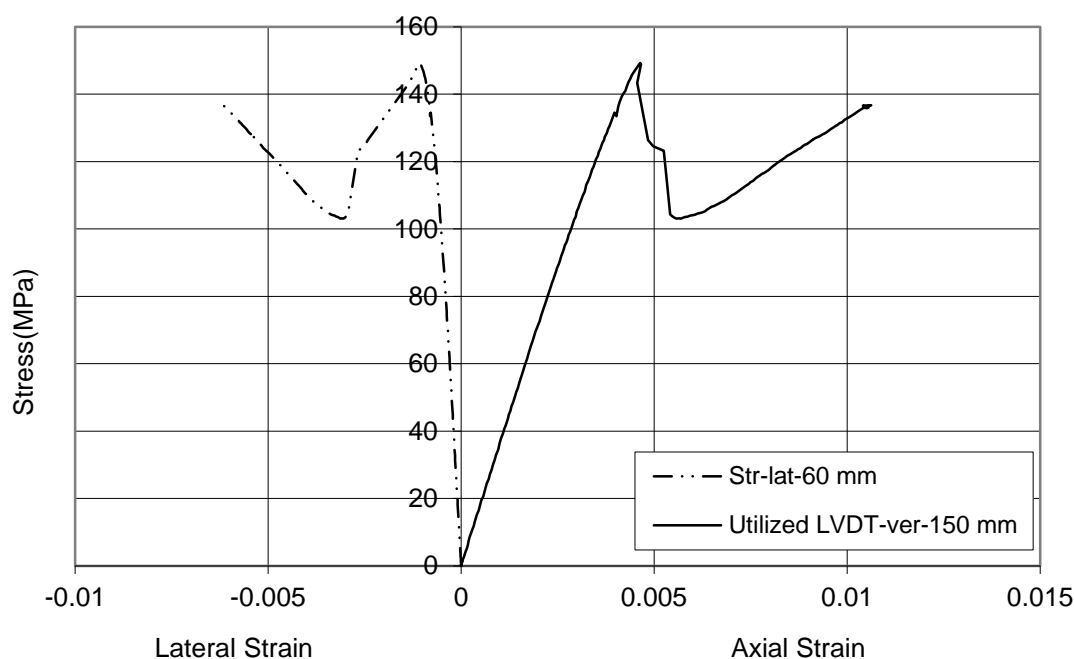


Figure 4.32: Stress - Strain relationship for C-CC-4-1

CC-C-4-2

This specimen was confined by 4 plies of CFRP. Test was carried out after 195 days of casting the composite. After the test, observed failure behavior is as seen on Figure 4.37. End zone retrofits were both occurred by 5cm width and 7 Plies of CFRP sheets with an overlapping of 15cm. Retrofit ruptured during the test.

A value of axial strain was observed as approximately 0.011. Also 2 Stress values, read by along middle and all surfaces LVDTs are close to each other at about 172.4 MPa at 195th day/compressive. Strain gauges did not work so we could not obtain lateral strains for this specimen.

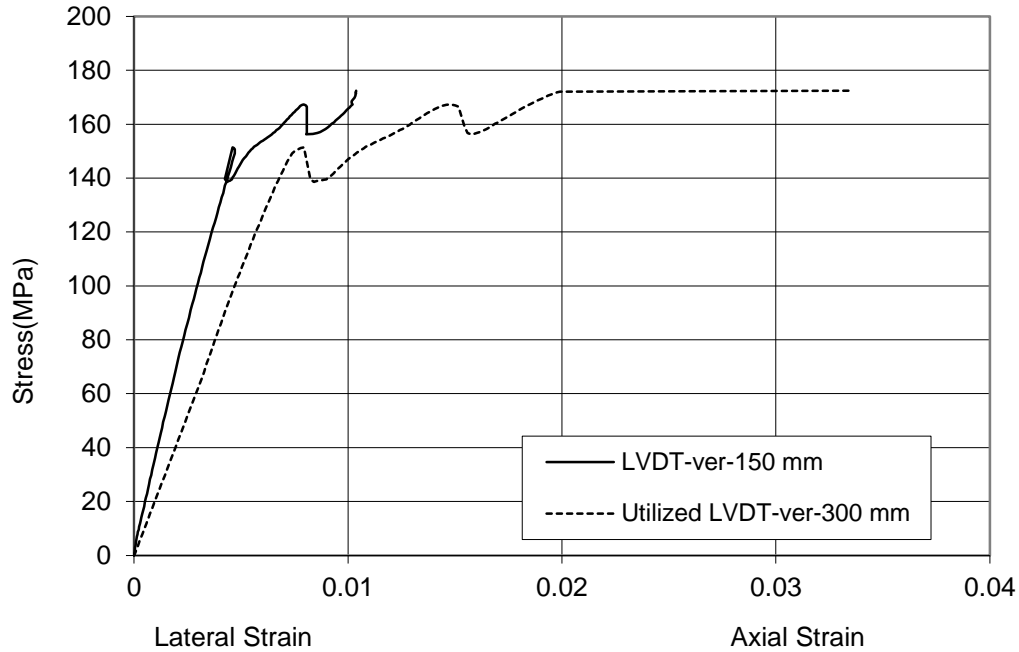


Figure 4.33: Stress - Strain relationship for CC-C-4-2

CC-C-4-3

This specimen was confined by 4 plies of CFRP. Test was carried out after 195 days of casting the composite. After the test, observed failure behavior is as seen on Figure 4.38. Rupture of FRP was seen along the surface both laterally and vertically. End zones retrofits were both occurred by 5 cm width and 7 plies of CFRP sheets with an overlapping of 15cm. Retrofit ruptured during the test. A value of axial strain was observed as approximately 0.005. We have two LVDTs to measure the axial strain along 300 mm gage length over the height of specimen similarly. Also two Stress values, read by along middle and all surfaces LVDTs are close to each other at about 155.7 MPa at 195th day / compressive.

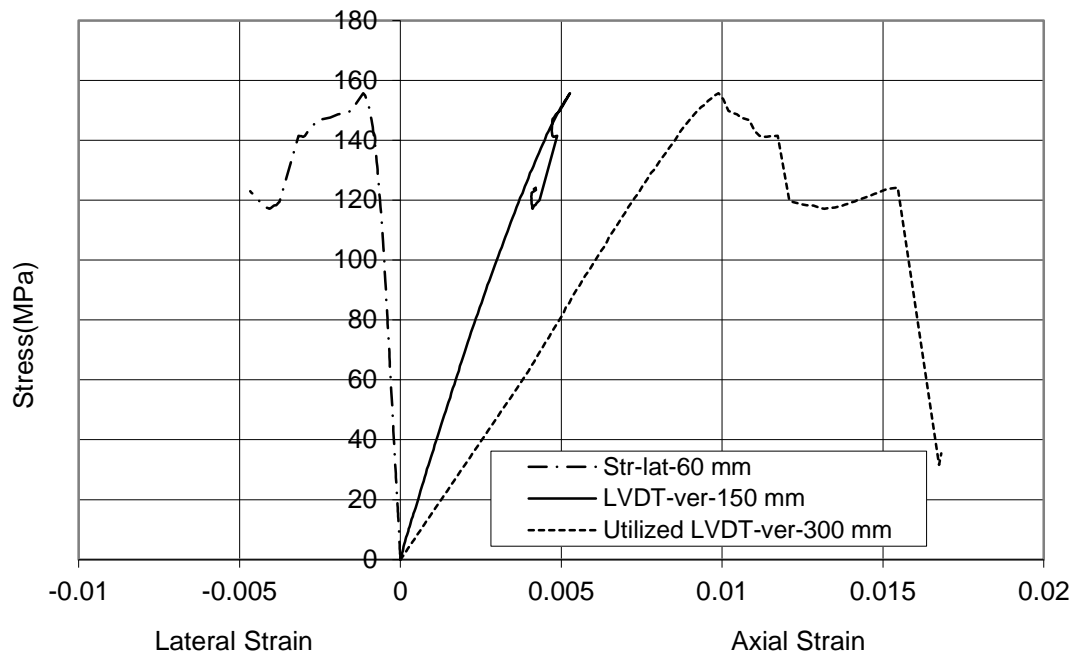


Figure 4.34: Stress - Strain relationship for CC-C-4-3

Approximately, at a lateral strain of 0.001 cementitious composite crushes under a stress of about 155.7 MPa as seen on figure. Maximum load reached during the test was 2751 kN. Stress enhancement ratio is 1.511 and strain is 1.606. A comparison for the specimens that confined by 4 plies of CFRP can be seen on Figure 35.

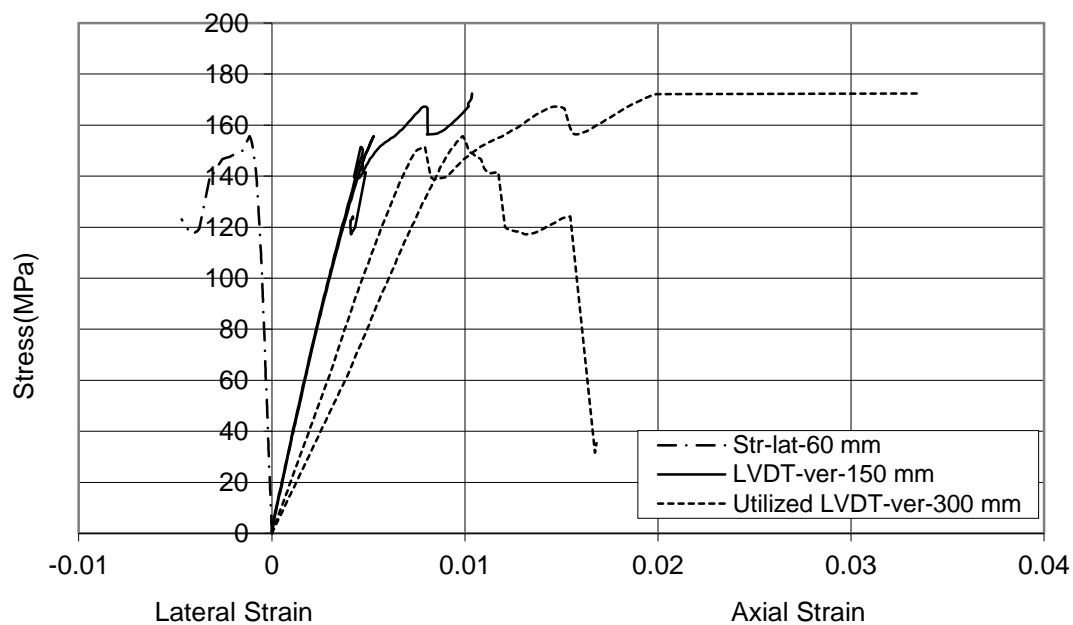


Figure 4.35: A Comparison for the Specimens that Confined by 4 Plies of CFRP



Figure 4.36: CC-C-4-1

Figure 4.37: CC-C-4-2

Figure 4.38: CC-C-4-3

4.3.4 Circular specimens confined by 6 plies of CFRP

CC-C-6-1

This specimen was confined by 6 plies of CFRP. Test was carried out after 225 days of casting the composite. After the test, observed failure behavior is as seen on Figure 43. Rupture of FRP was seen along the surface both laterally and vertically. End zone retrofits were both occurred by 5cm width and 9Plies of CFRP sheets with an overlapping of 15cm. Retrofit ruptured during the test. A value of axial strain was observed as approximately 0.007. Also two stress values, read by along middle and all surfaces LVDTs are close to each other at about 160.1 MPa at 225th day / compressive. Approximately, at a lateral strain of 0.006 cementitious composite crushes under a stress of about 160.1 MPa as seen on Figure 39. Maximum load reached during the test was 2829 kN. Since strain gauges did not work enhancement ratios could not be obtained for this specimen.

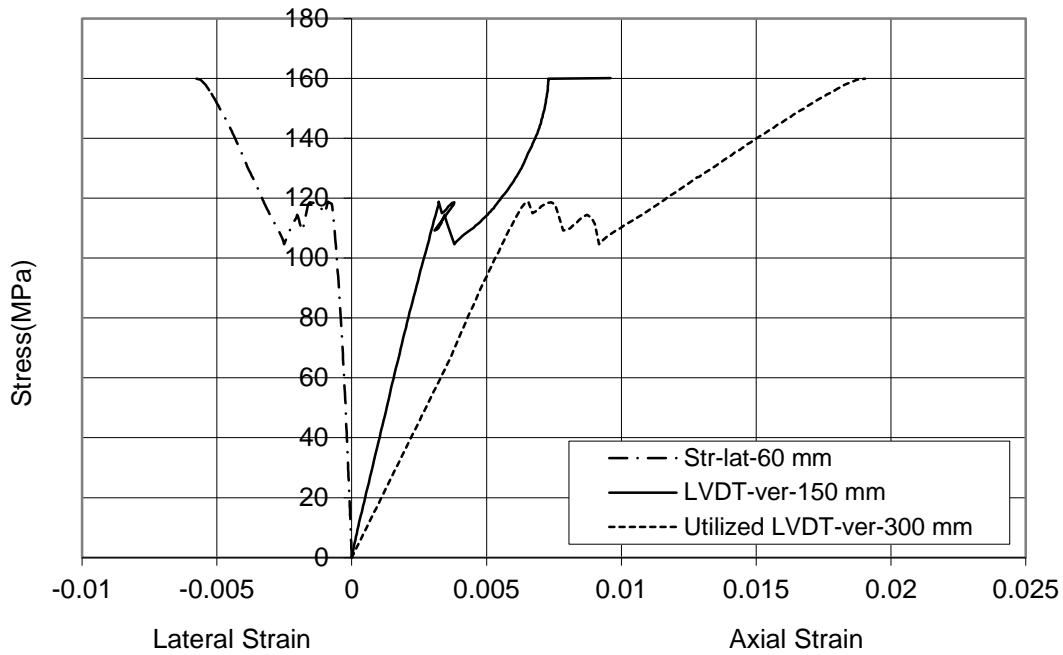


Figure 4.39: Stress - Strain relationship for CC-C-6-1

CC-C-6-2

This specimen was confined by 6 plies of CFRP. Test was carried out after 225 days of casting the composite. After the test, observed failure behavior is as seen on Figure 4.44. Rupture of FRP was seen along the surface both laterally and vertically. Retrofits were both occurred by 5cm width and 9 plies of CFRP sheets with an overlapping of 15 cm. Retrofit ruptured during the test. A value of axial strain was observed as approximately 0.004. We have two LVDTs to measure the axial strain along 300 mm gage length over the height of specimen similarly. Also two stress values, read by along middle and all surfaces LVDTs are close to each other at about 158.6 MPa at 225th day / compressive. Approximately, at a lateral strain of 0.0025 cementitious composite crushes under a stress of about 158.6 MPa as seen on Figure 41. Maximum load reached during the test was 2803 kN. There are 2 strain gauges to measure the lateral strains over all surfaces of the specimen. Lateral strain seen on figure is the average of those 2 strain gauges. Stress enhancement ratios for stress and strain are 1.539 and 1.181.

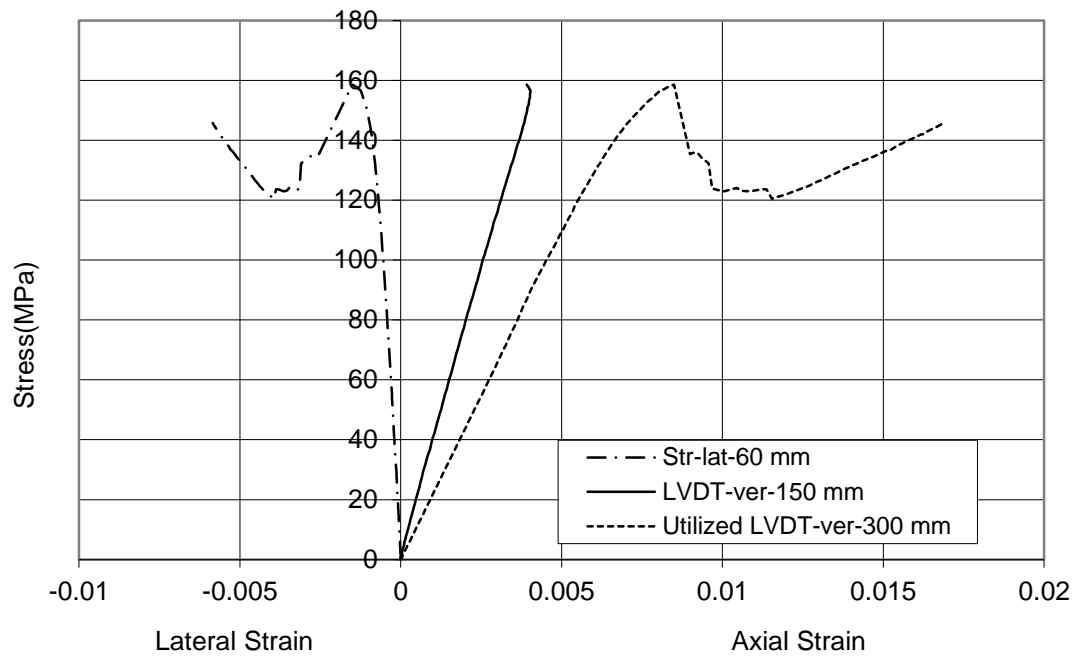


Figure 4.40: Stress - Strain relationship for CC-C-6-2

CC-C-6-3

After the test, observed failure behavior is as seen on Figure 4.45. Rupture of FRP was seen along the surface both laterally and vertically.

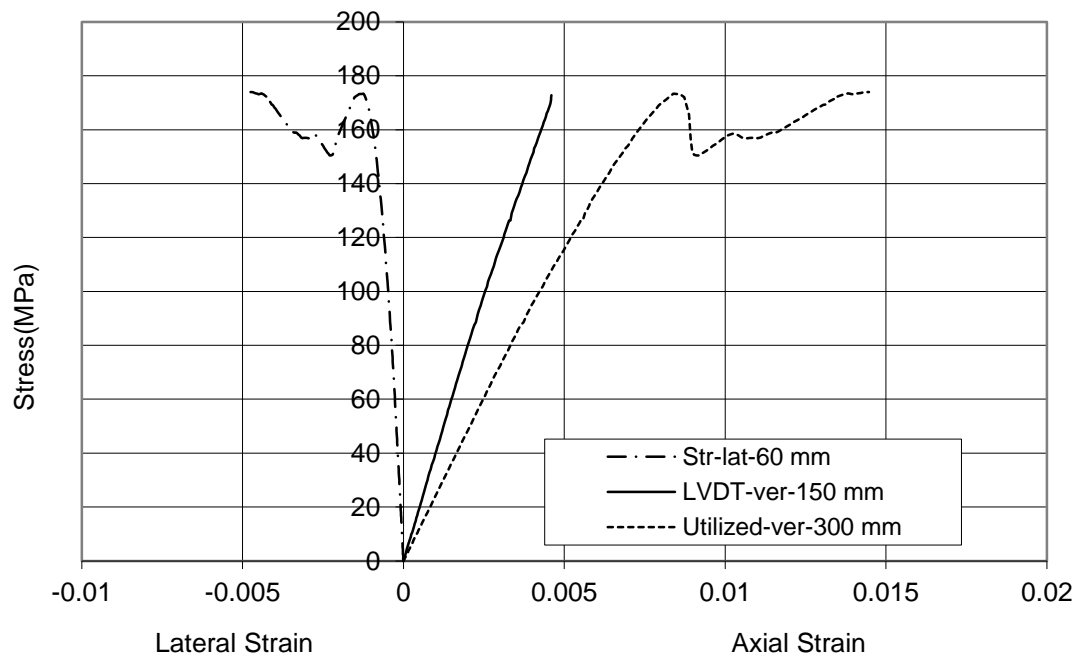


Figure 4.41: Stress - Strain relationship for CC-C-6-3

A value of strain was observed as approximately 0.004. Also two Stress values, read by along middle and all surfaces LVDTs are close to each other at about 179 MPa at 225th day / compressive. Approximately, at a lateral strain of 0.001 cementitious composite crushes under a stress of about 179 MPa as seen on figure. Maximum load reached during the test was 3158 kN. There are 2 strain gauges to measure the lateral strains over all surfaces of the specimen. Enhancement ratios are 1.73 and 1.394. A comparison for the specimens that confined by 6 plies of CFRP can be seen on Figure 4.42.

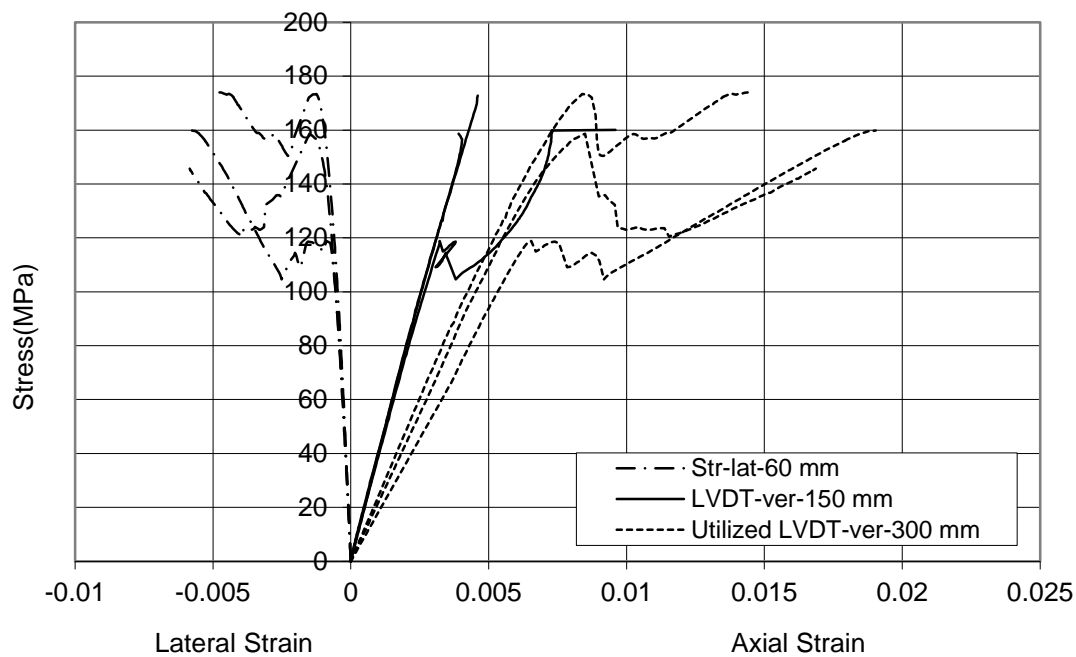


Figure 4.42: A Comparison for the Specimens that Confined by 6 Plies of CFRP



Figure 4.43: CC-C-6-1



Figure 4.44: CC-C-6-2



Figure 4.45: CC-C-6-3

4.3.5 Circular specimens confined by 8 plies of CFRP

CC-C-8-1

This specimen was confined by eight plies of CFRP. Test was carried out after 150 days of casting the composite. After the test, observed failure behavior is as seen on Figure 4.51. Rupture of FRP was seen along the surface both laterally and vertically. Retrofits were both occurred by 5 cm width and 11 plies of CFRP sheets with an overlapping of 15 cm.

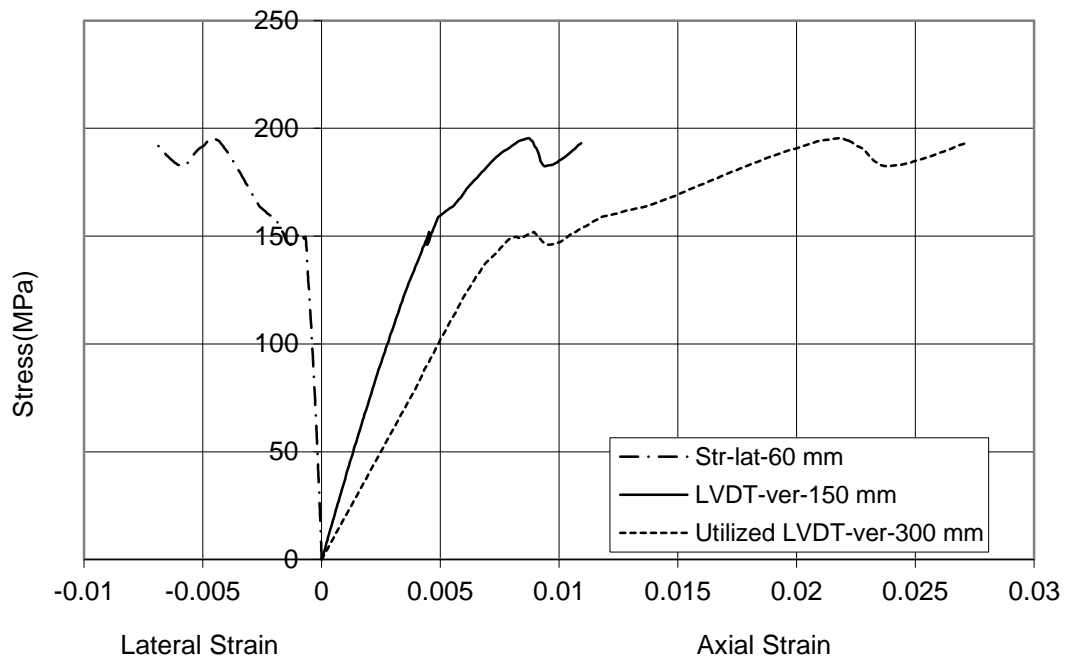


Figure 4.46: Stress - Strain relationship for CC-C-8-1

A value of axial strain was observed as approximately 0.010. Also two stress values, read by along middle and all surfaces LVDTs are close to each other at about 195.4 MPa at 150th day / compressive. Approximately, at a lateral strain of 0.005 cementitious composite crushes under a stress of about 195 MPa. Maximum load reached during the test was 3453 kN. There are two strain gauges to measure the lateral strains over all surfaces of the specimen. Lateral strain seen on figure is the average of those 2 strain gauges. Enhancement ratios are 1.893 and 3.03.

C-CC--17

This specimen was confined by 8 plies of CFRP. Test was carried out after 195 days of casting the composite. After the test, observed failure behavior is as seen on Figure 4.52. At the first peak of the curve test set up was out of order and no damage was observed on the specimen. A value of strain was observed as approximately 0.005. Also two stress values, read by along middle and all surfaces LVDTs are close to each other at about 146.5 MPa at 195th day / compressive. Approximately, at a lateral strain of 0.002 cementitious composite crushes under a stress of about 146.5 MPa. Maximum load reached during the test was 2589 kN. Enhancement ratios are 1.422 and 1.394 for stress and for strain. Since some instrumentation problems, it will not be a part of average.

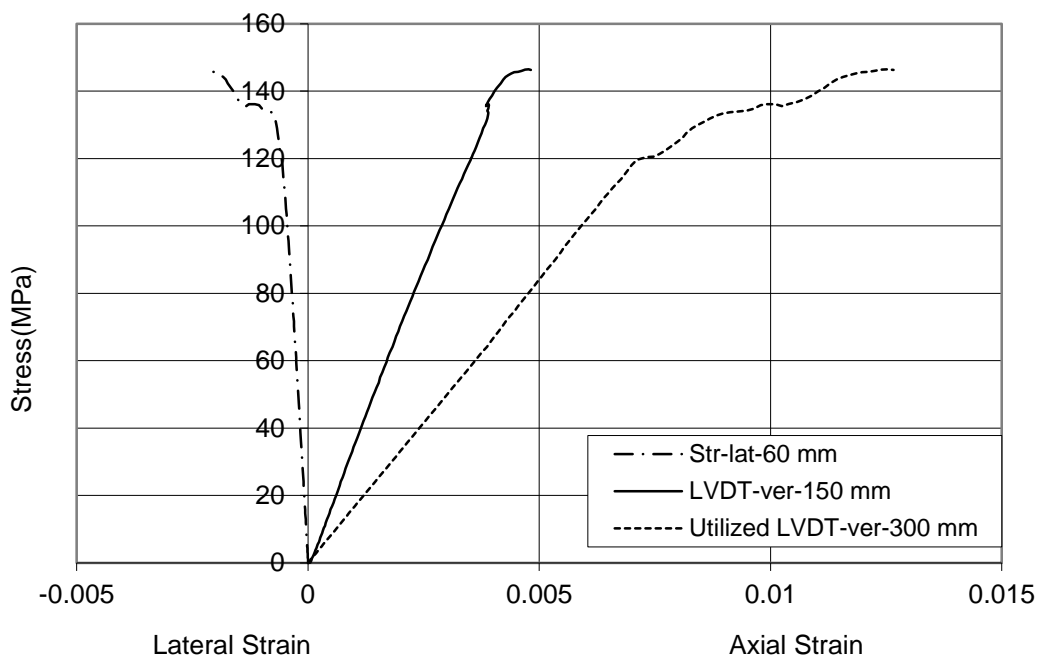


Figure 4.47: Stress - Strain relationship for CC-C-8-2

CC-C-8-3

This specimen was confined by 8 plies of CFRP. Test was carried out after 195 days of casting the composite. After the test, observed failure behavior is as seen on Figure 4.53. Rupture of FRP was seen along the surface vertically. Retrofits were both occurred by 5 cm width and 11 plies of CFRP sheets with an overlapping of 15 cm.

A value of strain was observed as approximately 0.007. Also 2 stress values, read by along middle and all surfaces LVDTs are close to each other at about 175.9 MPa at 195th day / compressive.

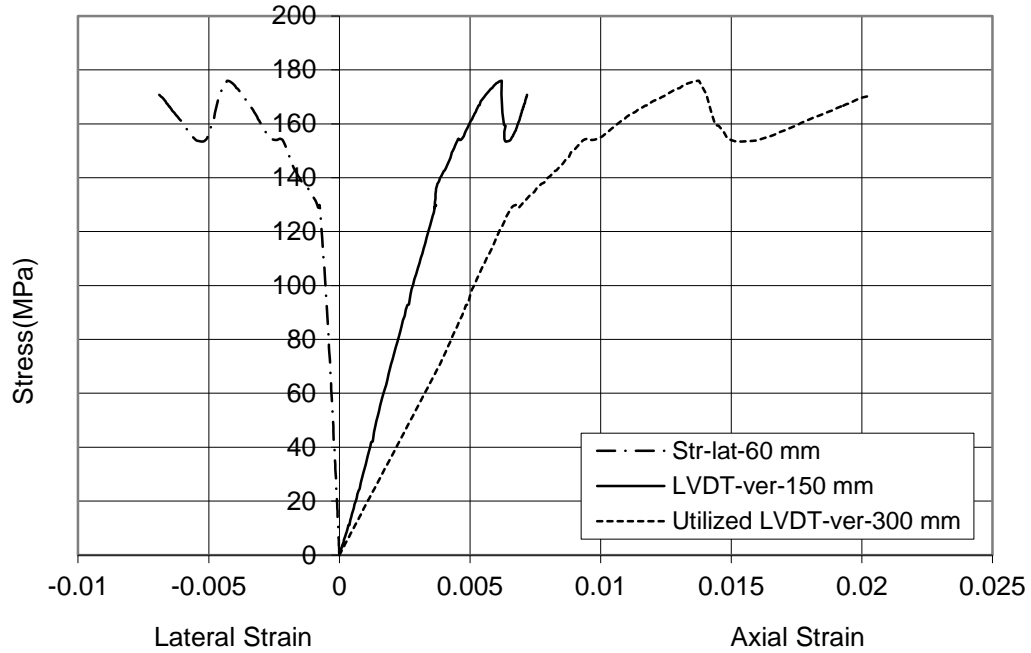


Figure 4.48: Stress - Strain relationship for CC-C-8-3

Approximately, at a lateral strain of 0.005 cementitious composite crushes under a stress of about 175.9 MPa. Maximum load reached during the test was 3109 kN, There are two strain gauges to measure the lateral strains over all surfaces of the specimen. Lateral strain seen on figure is the average of those 2 strain gauges. Enhancement ratios are 1.707 and 2.182.

CC-C-8-4

This specimen was confined by 8 plies of CFRP. Test was carried out after 195 days of casting the composite. After the test, observed failure behavior is as seen on Figure 4.54. Rupture of FRP was seen along the surface both laterally and vertically. A value of axial strain was observed as approximately 0.005. Also two Stress values, read by along middle and all surfaces LVDTs are close to each other at about 180.6 MPa at 195th day / compressive.

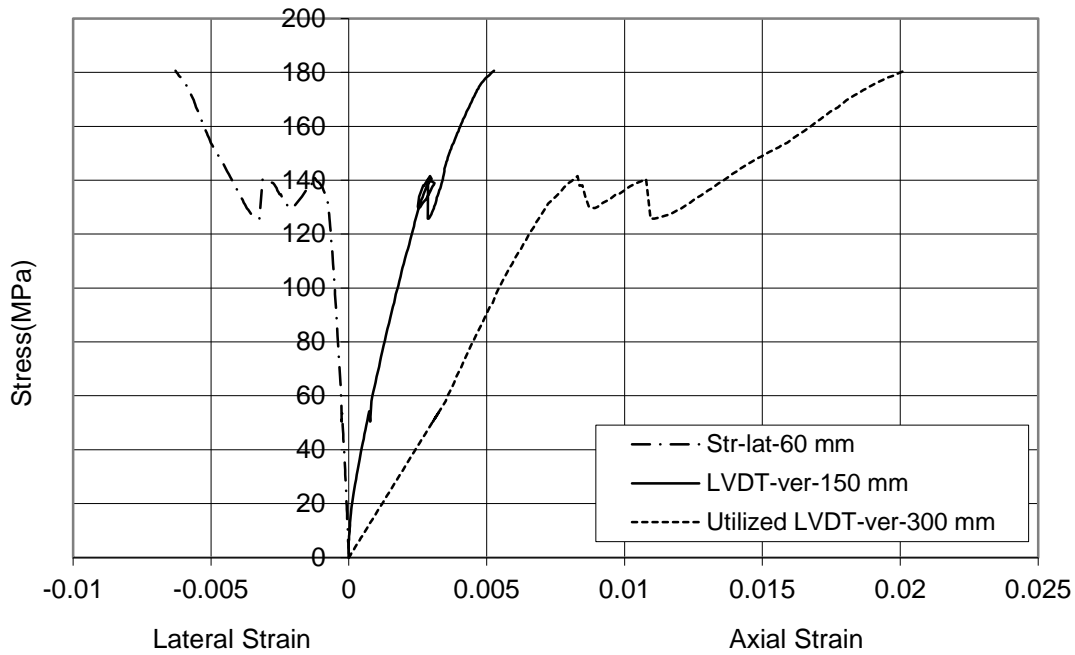


Figure 4.49: Stress - Strain Relationship for CC-C-8-4

Approximately, at a lateral strain of 0.006 cementitious composite crushes under a stress of about 180.6 MPa as seen on figure. Maximum load reached during the test was 3192 kN. Enhancement ratios are 1.753 and 1.575. A comparison for the specimens that confined by 8 plies of CFRP can be seen on Figure 50.

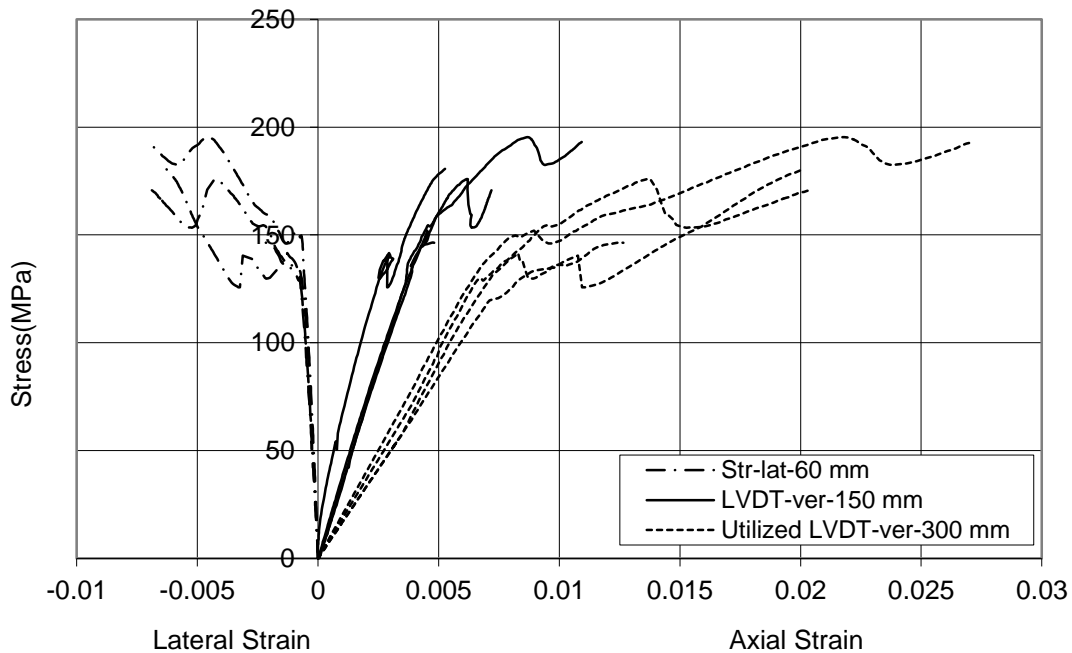


Figure 4.50: A Comparison for the Specimens that Confined by 8 Plies of CFRP



Figure 4.51: CC-C-8-1



Figure 4.52: CC-C-8-2



Figure 4.53: CC-C-8-3



Figure 4.54: CC-C-8-4

4.3.6 Circular specimens confined by 10 plies of CFRP

CC-C-10-1

This specimen was confined by 10 plies of CFRP. After the test, observed failure behavior is as seen on Figure 60. There could not observed damage on the specimen body. A value of axial strain was observed as approximately 0.005. Also two stress values, read by along middle and all surfaces LVDTs are close to each other at a stress about 163.7 MPa at 120th day / compressive. Specimen did not reach to the load carrying capacity.

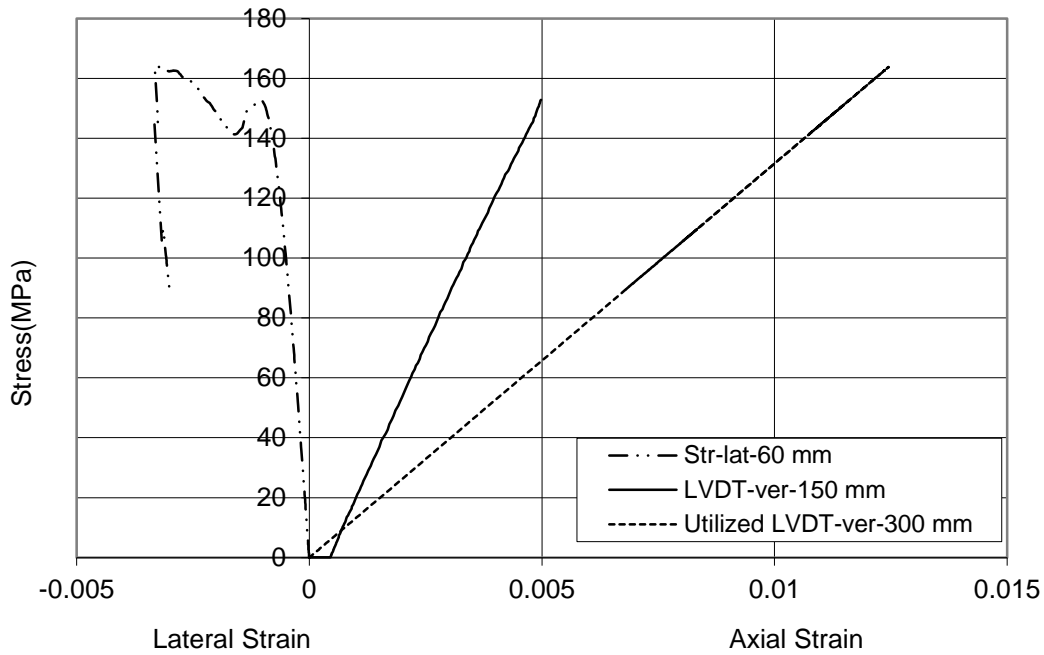


Figure 4.55: Stress - Strain relationship for C-CC-10-1

Approximately, at a lateral strain of 0.0032 cementitious composite crushes under a stress of about 163.7 MPa as seen on figure. Maximum load reached during the test was 2894 kN. There are two strain gauges to measure the lateral strains over all surfaces of the specimen. Enhancement ratios are 1.589 and 1.4848.

CC-C-10-2

This specimen was confined by 10 plies of CFRP. Test was carried out after 120 days of casting the composite. After the test, observed failure behavior is as seen on Figure 61. Rupture of FRP was seen along the body vertically.

A value of strain was observed as approximately 0.012. Also two stress values, read by along middle and all surfaces LVDTs are close to each other at about 232 MPa at 120th day / compressive. Approximately, at a lateral strain of 0.0061 cementitious composite crushes under a stress of about 232 MPa as seen on figure. Maximum load reached during the test was 4103 kN. Enhancement ratios are 2.12 and 3.63.

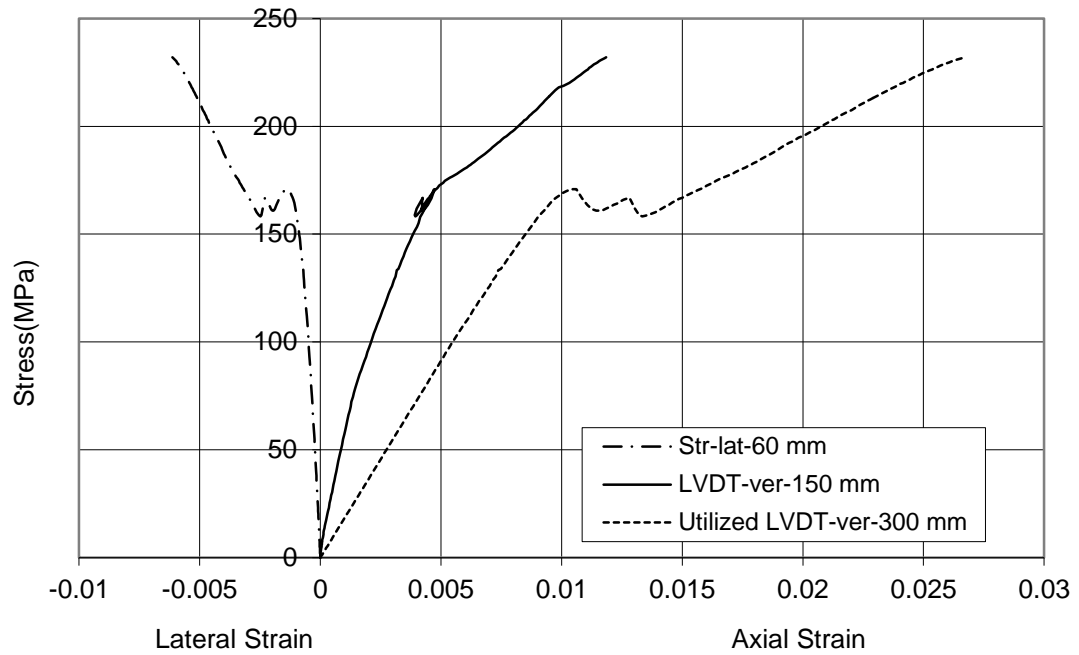


Figure 4.56: Stress - Axial Strain relationship for CC-C-10-2

CC-C-10-3

This specimen was confined by 10 plies of CFRP. Test was carried out after 150 days of casting the composite. After the test, observed failure behavior is as seen on Figure 4.62.

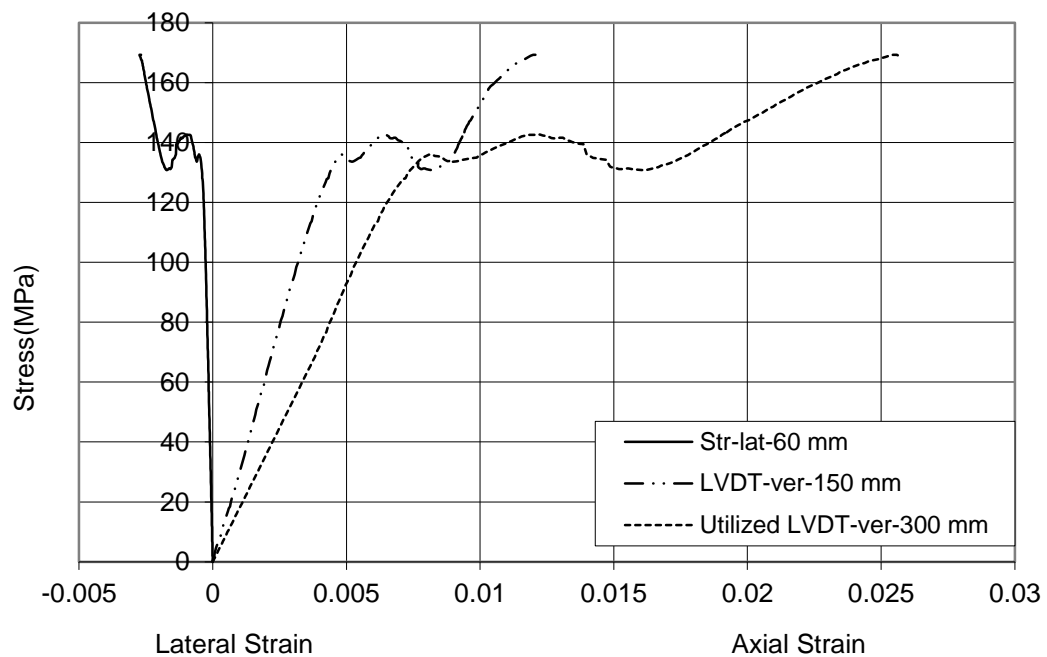


Figure 4.57: Stress - Strain relationship for CC-C-10-3

A value of strain was observed as approximately 0.012. Also two Stress values, read by along middle and all surfaces LVDTs are close to each other at about 169 MPa at 150th day / compressive. Approximately, at a lateral strain of 0.0028 cementitious composite crushes under a stress of about 169 MPa as seen on figure. Maximum load reached during the test was 2979 kN. Enhancement ratios are 1.641 and 3.636.

CC-C-10-4

This specimen was confined by 10 plies of CFRP. Test was carried out after 150 days of casting the composite. After the test, observed failure behavior is as seen on Figure 63. Rupture of FRP was seen along the body vertically and retrofits were both occurred by 5cm width and 13 plies of CFRP sheets with an overlapping of 15cm.

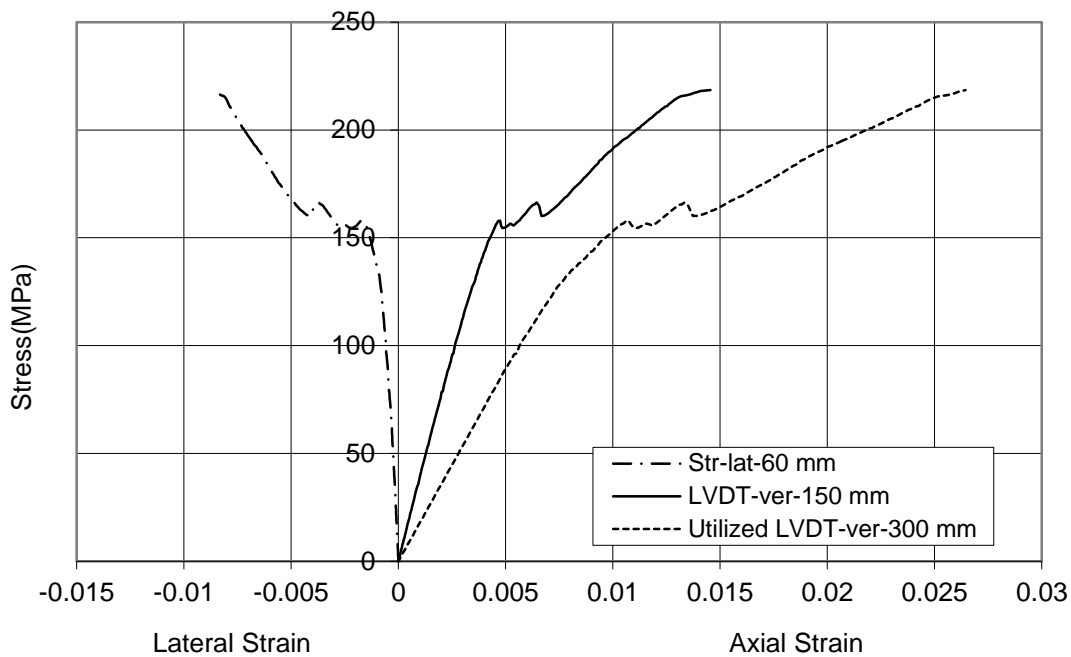


Figure 4.58: Stress - Strain relationship for CC-C-10-4

A value of strain was observed as approximately 0.015. Also two Stress values, read by along middle and all surfaces LVDTs are close to each other at about 218.5 MPa at 150th day / compressive. Approximately, at a lateral strain of 0.009 cementitious composite crushes under a stress of about 218.5 MPa as seen on figure. Maximum load reached during the test was 3862 kN. Enhancement ratios are 2.121 and 4.545. A comparison for the specimens that confined by 10 plies of CFRP can be seen on Figure 59. Test results for circular cross sections are summarized on Table 4.5.

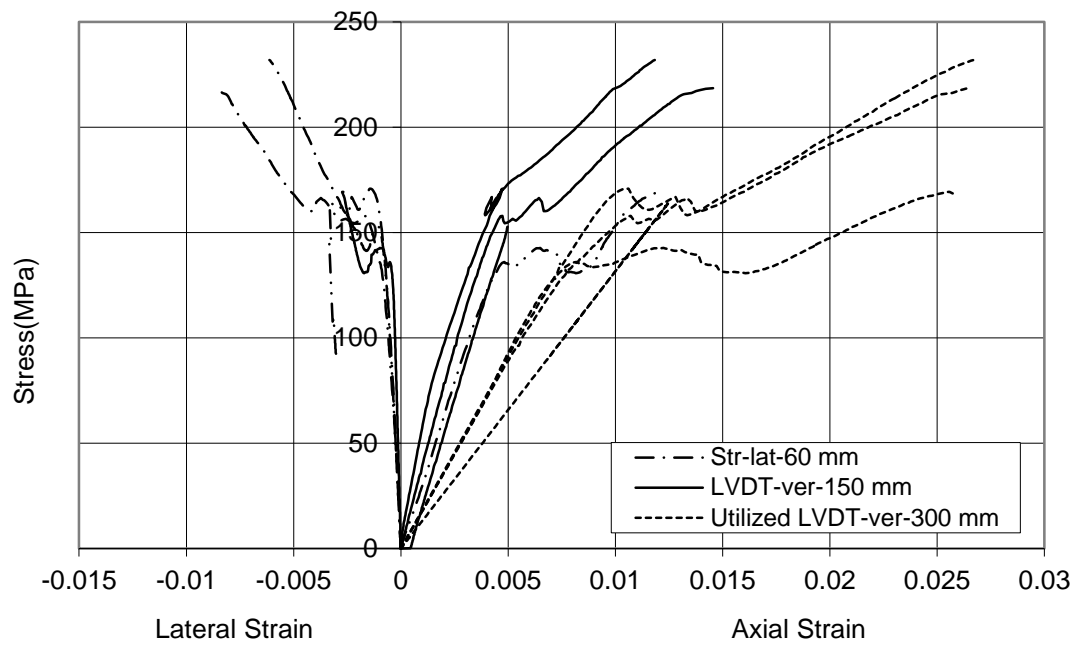


Figure 4.59: A Comparison for the Specimens that Confined by 10 Plies of CFRP



Figure 4.60: CC-C-10-1



Figure 4.61: CC-C-10-2



Figure 4.62: CC-C-10-3



Figure 4.63: CC-C-10-4

All test results for circular cross section specimens can be seen on Table 4.5. ϵ_{co} is the axial strain for the unconfined specimen at 150 mm gage length. All strain values were obtained by LVDTs at the same gage length. Specimens have two peak stress levels. ϵ_{cc-1} is the first axial strain for the first peak stress level and ϵ_{cc-2} is the second one. Two deformabilities for a specimen can be defined as the ratio of axial strain at first peak to unconfined axial strain and another for second peak to unconfined similarly. $\epsilon_{cc-1}/\epsilon_{co}$ refers to first definition and $\epsilon_{cc-2}/\epsilon_{co}$ refers to second one. These values can be called as strain enhancement ratio. Average values of those can be seen near the terms. f'_{cc} is the maximum stress during the test for confined composites and f'_{co} is for unconfined. Ratio for these two terms refers to axial stress enhancement ratio.

Table 4.5: Experimental Test Results for Circular Specimens

Shape	Name	f'_{co} (MPa)	ϵ_{co}	f'_{cc} (MPa)	ϵ_{cc-1}	ϵ_{cc-2}	ϵ_{hrup}	ϵ_{fu}	f'_{cc}/f'_{co}	$\epsilon_{cc-1}/\epsilon_{co}$	$\epsilon_{cc-2}/\epsilon_{co}$	$Av(\epsilon_{cc-1}/\epsilon_{co})$	$Av(\epsilon_{cc-2}/\epsilon_{co})$
Circular-0	CC-C-0-4	103.2	0.0025	0.0025	0.0025	0.0025	*	0.018	1	1	1	1	1
	CC-C-0-5	96.65	0.0047	0.0047	0.0047	0.0047	0.006	0.018	1	1	1		
	CC-C-0-6	108.1	0.0033	0.0033	0.0033	0.0029	*	0.018	1	1	1		
Circular-2	CC-C-2-1*	103	0.0033	116	0.0032	0.0032	0.008	0.018	1.13	0.97	0.97	1.19	1.16
	CC-C-2-2	103	0.0033	125.6	0.0051	0.0054	0.005	0.018	1.22	1.55	1.64		
	CC-C-2-3	103	0.0033	134.7	0.0041	0.0035	0.006	0.018	1.31	1.24	1.06		
	CC-C-2-4	103	0.0033	137.4	0.0036	0.0036	0.005	0.018	1.33	1.09	1.09		
	CC-C-2-5	103	0.0033	147.6	0.0042	0.0042	0.006	0.018	1.43	1.27	1.27		
	CC-C-2-6	103	0.0033	160.1	0.0031	0.003	0.006	0.018	1.55	0.94	0.91		
	CC-C-2-7	103	0.0033	150.8	0.0034	0.0033	0.007	0.018	1.46	1.03	1.00		
Circular-4	CC-C-4-1	103	0.0033	149.3	0.0047	0.0046	0.006	0.018	1.45	1.42	1.39	1.52	1.50
	CC-C-4-2*	103	0.0033	172.4	0.0104	0.0103	*	0.018	1.67	3.15	3.12		
	CC-C-4-3	103	0.0033	155.7	0.0053	0.0053	0.005	0.018	1.51	1.61	1.61		
Circular-6	CC-C-6-1	103	0.0033	160.1	0.0096	0.0096	0.006	0.018	1.55	2.91	2.91	1.84	1.84
	CC-C-6-2	103	0.0033	158.6	0.0039	0.004	0.006	0.018	1.54	1.18	1.21		
	CC-C-6-3	103	0.0033	179	0.0047	0.0046	0.005	0.018	1.74	1.42	1.39		
Circular-8	CC-C-8-1	103	0.0033	195.4	0.008	0.0108	0.0087	0.018	1.90	2.42	3.27	1.97	2.35
	CC-C-8-2*	103	0.0033	146.5	0.005	0.0048	0.002	0.018	1.42	1.52	1.45		
	CC-C-8-3	103	0.0033	175.9	0.0062	0.0072	0.007	0.018	1.71	1.88	2.18		
	CC-C-8-4	103	0.0033	180.6	0.0053	0.0053	0.007	0.018	1.75	1.61	1.61		
Circular-10	CC-C-10-1*	103	0.0033	163.7	0.005	0.005	0.033	0.018	1.59	1.52	1.52	3.94	3.89
	CC-C-10-2	103	0.0033	232	0.012	0.012	0.012	0.018	2.25	3.64	3.64		
	CC-C-10-3	103	0.0033	169	0.012	0.012	0.012	0.018	1.64	3.64	3.64		
	CC-C-10-4	103	0.0033	218.5	0.015	0.0145	0.015	0.018	2.12	4.55	4.39		

** indicates specimens that experienced problems with instrumentation

Lateral and axial stress and strain increments, due to the FRP layer thickness are summarized below on Figure 4.64. Each specimen, that were used at the table is the one of the specimens that has the same FRP layer and refers to the general behavior of that specimen type.

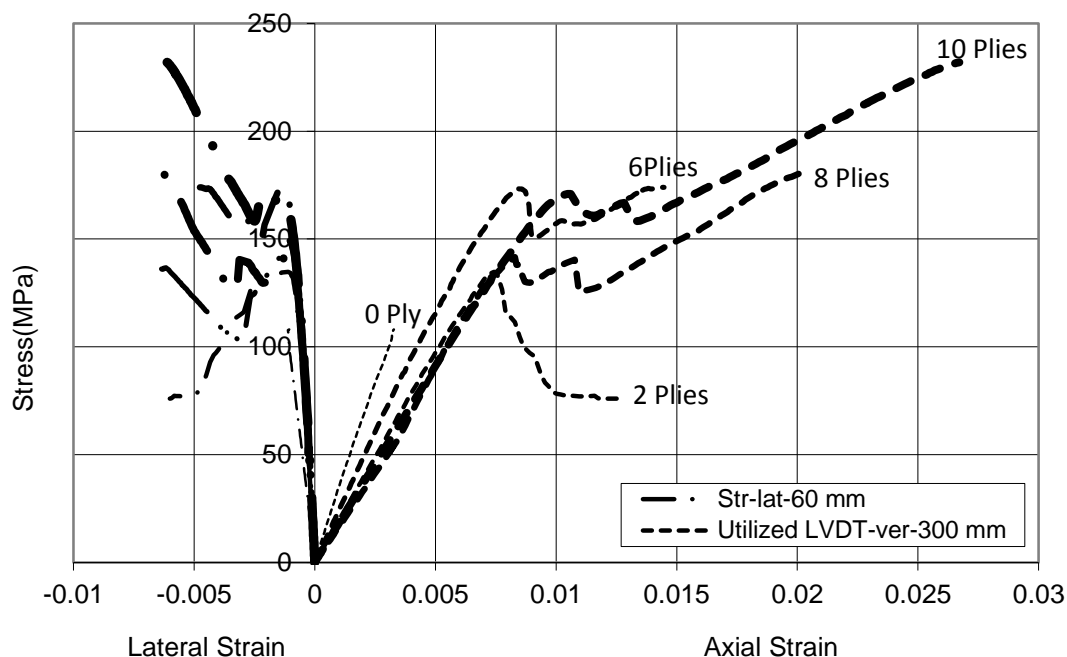


Figure 4.64: Lateral and Axial Stress and Strain Increments, Due to the FRP Layer

4.4 Test Results for Non-circular Members

Prepared specimens were tested on an Instron Test Machine with the capacity of 5000 kN as seen on previous chapter on Figure 4.1. The software Bluehill 2 performed loading steps of machine. All the datas were taken from the surface of the specimens by strain gauges and transducers. Lateral and vertical strains and the loads defiant these strains were measured. Strain gauges were used four for square specimens except CC-S-0-1 and CC-S-0-2. These two unconfined specimens have two strain gauges for each surface and 8 totally. Two of these are perpendicular to each other on each surface. CDP-25 refers to 25 mm measurement capacity of transducer (LVDT) to measure the axial strain. LVDTs were used two for along all height of specimens and four for middle of four surfaces of specimens. Test set-up is summarized below on Figure 4.65.

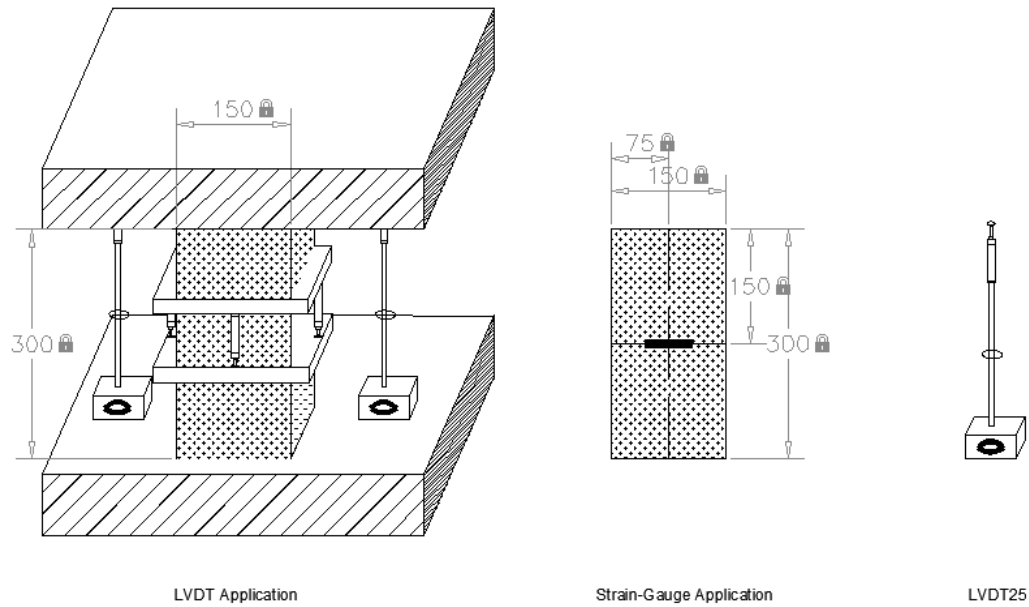


Figure 4.65: Test set-up for square specimens

There are 19 square cross-sectional specimens to perform. All specimens have the same sizes as 150*150*300 mm. Loading rate during the test was 0,6 mm/min for confined specimens and 0,4 mm/min for unconfined with respect to TS EN 12390-3. A pre-load applied before test to consider either the space between cap of specimen and test machine or the crush of the cap under test start and calculated as 125 kN. Axial compressive stress, obtained from the reference specimens' tests is summarized average as below;

$$f_c = \frac{102.22 + 110.62}{2} = 106.44 \cong 106.4 \text{ MPa}$$

All confinements are lateral and the load applied during tests is monotonic. Retrofitted specimens have quarter circle shaped rounding on the corners with a diameter of 25 mm. Stress-Lateral Strain and Stress-Axial Strain relationships after tests are mentioned and photos are over the graphics. There is a comparison at the end with the unconfined and confined specimens. Stress, lateral and axial strains are the parameters. Average stress and strain enhancements subjected to CFRP confinement thickness are summarized as a result at the end of the part.

Details of the specimens are mentioned on a chart below;

Table 4.6: Details of the Square Specimens

Specimen Code	Number of CFRP Sheet Plies
CC-S-0-1	0
CC-S-0-2	0
CC-S-0-3	0
CC-S-0-4	0
CC-S-2-1	2
CC-S-2-2	2
CC-S-2-3	2
CC-S-8-1	8
CC-S-8-2	8
CC-S-8-3	8
CC-S-8-4	8
CC-S-10-1	10
CC-S-10-2	10
CC-S-10-3	10
CC-S-10-4	10

4.4.1 Unconfined Non-circular Specimens

CC-S-0-1

This specimen is an unconfined reference specimen. After the test, observed failure behavior is as seen on Figure 71. On all surfaces of the specimen, totally the same failure was observed. Some concrete pieces spilled before crush and longitudinal cracks occurred after the test. Four LVDTs we have and this branch represents average values of these. As seen on the figure, due to the rotating of the LVDT's, gage length transducers' axial strains, obtained from test after was approximately 0.0033.

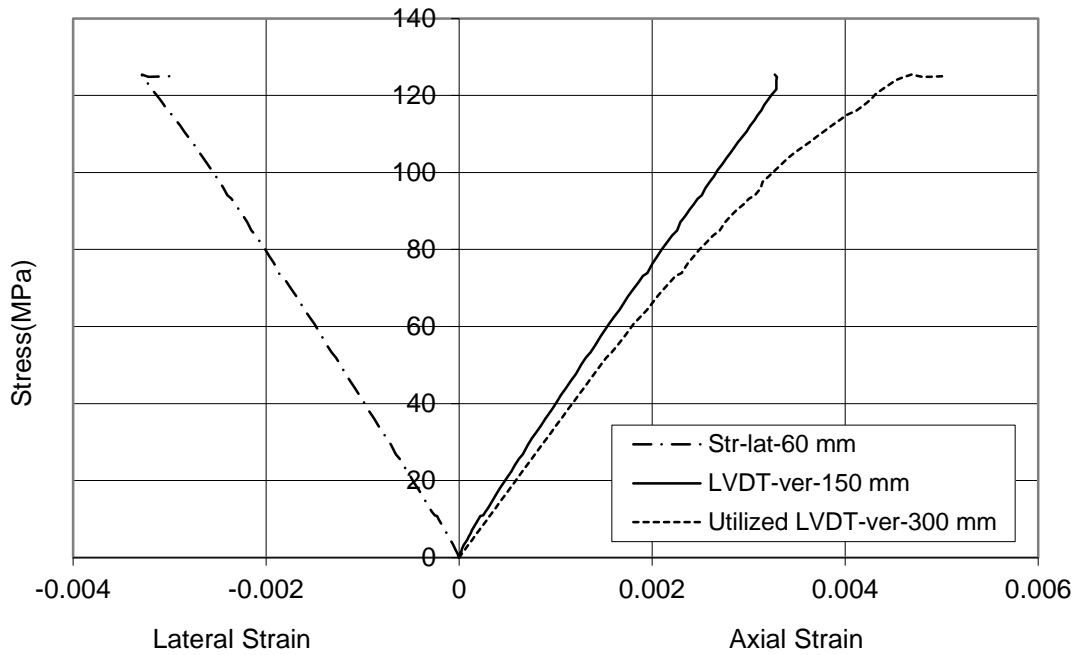


Figure 4.66: Stress - Strain Relationship for CC-S-0-1

We have 2 LVDTs to measure the axial strain along 320 mm gage length over the height of specimen similarly. A value of approximately 0.005 was observed from these. Also 2 stress values, read by along middle and all surfaces LVDTs are close to each other at about 125 MPa at 226th day / compressive. Approximately, at a lateral strain of 0.0032 cementitious composite crushes under a stress of about 125 MPa as seen on figure. Maximum load reached during the test was 2822 kN. There are eight strain gauges to measure the lateral strains over all surfaces of the specimen. Lateral strain seen on figure is the average of these eight strain gauges.

CC-S-0-2

This specimen is an unconfined reference specimen. After the test, observed failure behavior is as seen on Figure 72. On all surfaces of the specimen, totally the same failure was observed. Some concrete pieces spilled before crush and longitudinal cracks occurred after the test. The failure was concentrated at the bottom of the specimen. Hooked up steel fibers could be seen clearly with almost homogeneous directions of them.

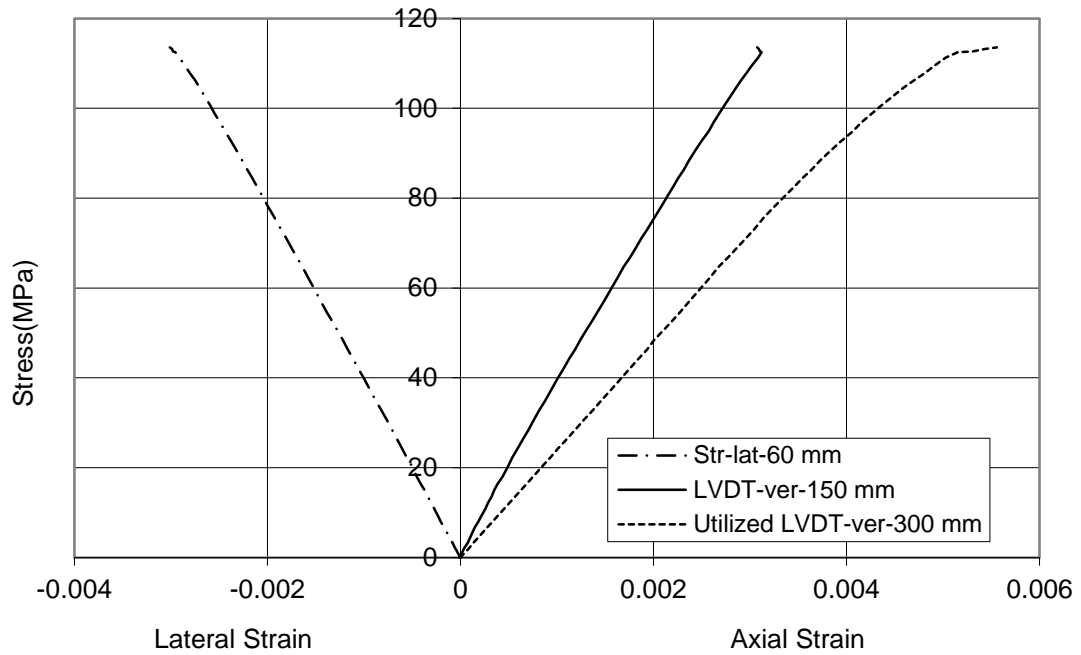


Figure 4.67: Stress - Strain Relationship for CC-S-0-2

Four LVDTs we have and this branch represents average values of these. As seen on the figure, axial strain after test is approximately 0.003. We have two LVDTs to measure the axial strain along 311 mm gage length over the height of specimen similarly. A value of approximately 0.0055 was observed from these. Also 2 stress values, read by along middle and all surfaces LVDTs are close to each other at about 113 MPa at 228th day / compressive. Approximately, at a lateral strain of 0.003 cementitious composite crushes under a stress of about 113 MPa as seen on figure. Maximum load reached during the test was 2555 kN. There are eight strain gauges to measure the lateral strains over all surfaces of the specimen. Lateral strain seen on figure is the average of these eight strain gauges.

CC-S-0-3

This specimen is an unconfined reference specimen. After the test, observed failure behavior is as seen on Figure 73. On all surfaces of the specimen, totally the same failure was observed. Some concrete pieces spilled before crush and longitudinal cracks occurred after the test. The failure was concentrated at the middle of the specimen.

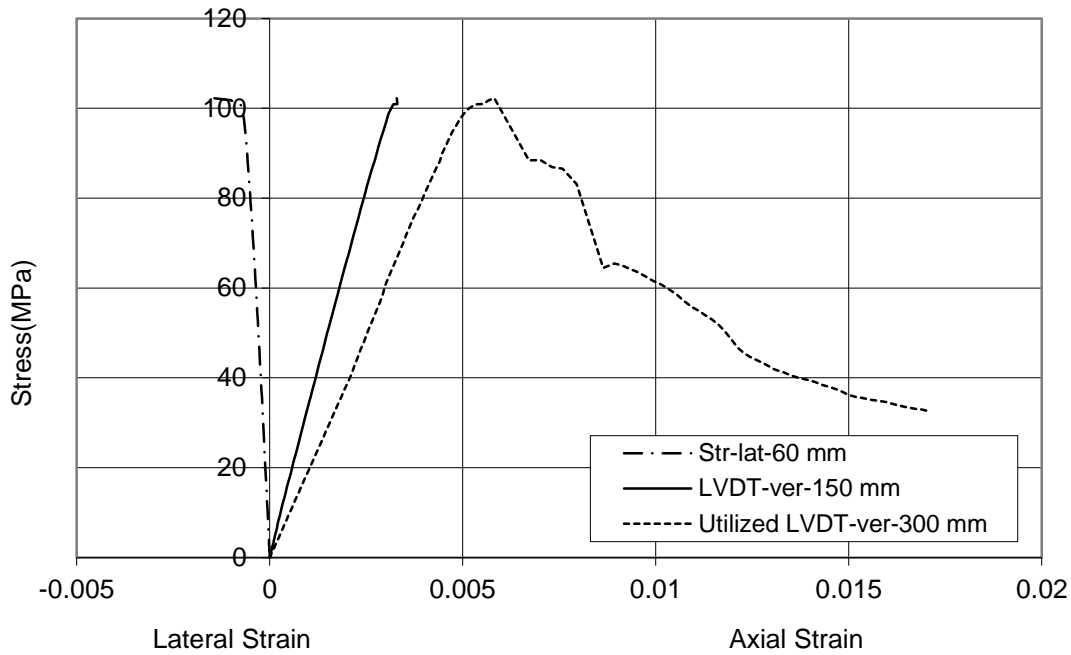


Figure 4.68: Stress - Strain Relationship for CC-S-0-3

We have two LVDTs to measure the axial strain along 307 mm gage length over the height of specimen similarly. A value of axial strain was observed as approximately 0.003. Also two Stress values, read by along middle and all surfaces LVDTs are close to each other at about 102 MPa at 304th day / compressive. Approximately, at a lateral strain of 0.0014 cementitious composite crushes under a stress of about 102 MPa as seen on figure. Maximum load reached during the test was 2300 kN. There are four strain gauges to measure the lateral strains over all surfaces of the specimen. Lateral strain seen on figure is the average of these four strain gauges. It can be told that after a lateral strain of 0.0014 strain gauge values are not carefully considered.

CC-S-0-4

This specimen is an unconfined reference specimen. After the test, observed failure behavior is as seen on Figure 74. On all surfaces of the specimen, totally the same failure was observed. Some concrete pieces spilled before crush and longitudinal cracks occurred after the test. The failure was concentrated at the bottom of the specimen.

We have two LVDTs to measure the axial strain along 305 mm gage length over the height of specimen similarly. A value of axial strain was observed as approximately 0.0033. Also 2 stress values, read by along middle and all surfaces LVDTs are close to each other at about 110 MPa at 304th day/compressive. Approximately, at a lateral

strain of 0.0013 cementitious composite crushes under a stress of about 110 MPa as seen on figure. Maximum load reached during the test was 2489 kN. There are four strain gauges to measure the lateral strains over all surfaces of the specimen. Lateral strain seen on figure is the average of these four strain gauges. It can be told that after a lateral strain of 0.0013 strain gauge values are not carefully considered.

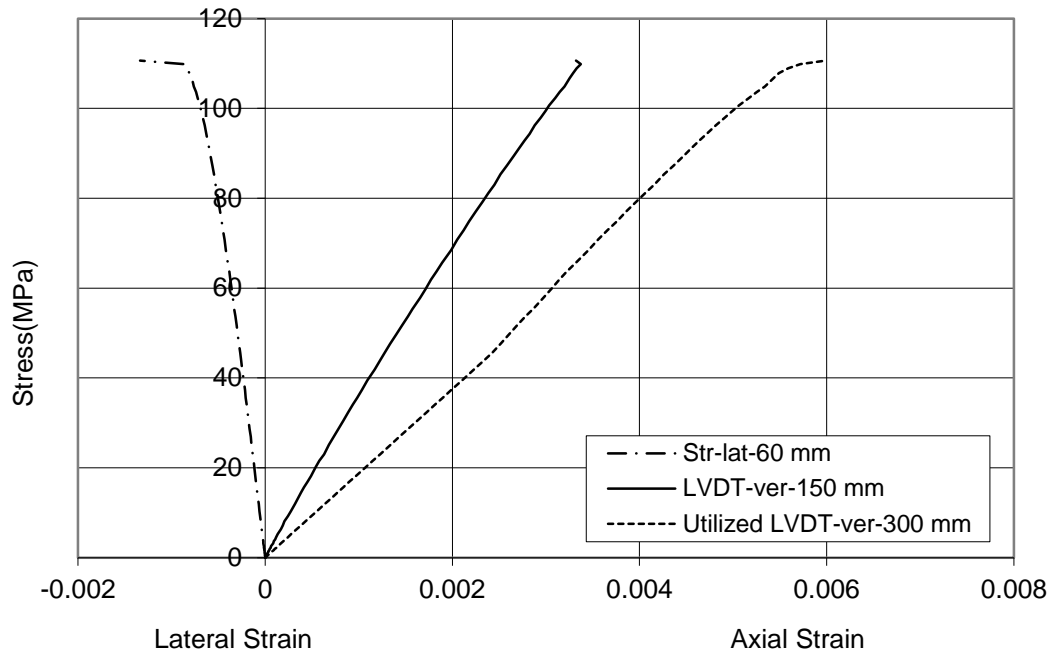


Figure 4.69: Stress - Strain Relationship for CC-S-0-4

A comparison for the unconfined specimens can be seen on Figure 70.

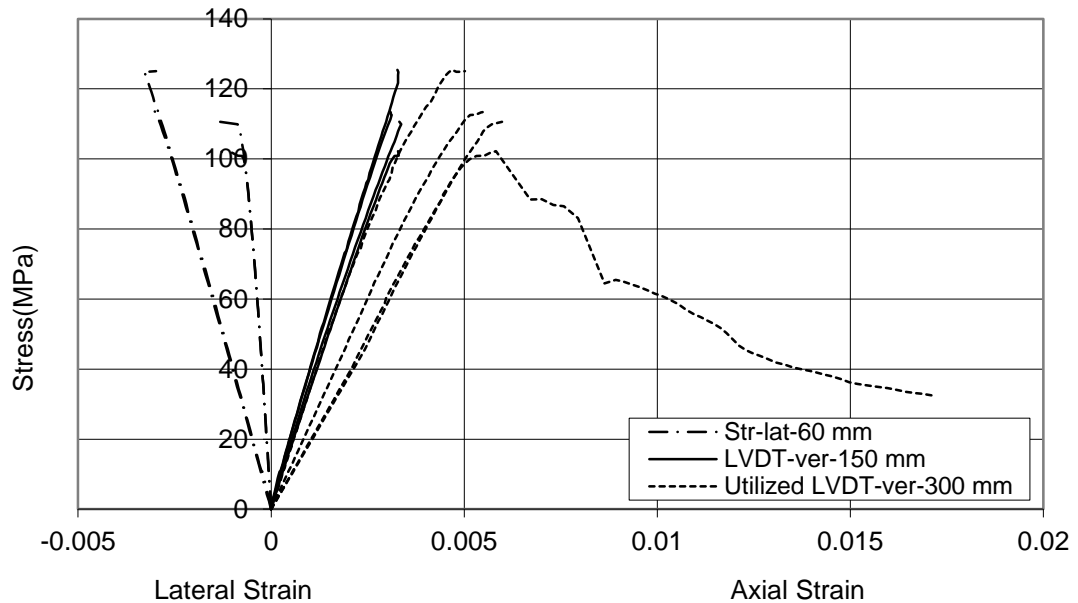


Figure 4.70: A Comparison for the Unconfined Square Specimens



Figure 4.71: CC-S-0-1



Figure 4.72: CC-S-0-2



Figure 4.73: CC-S-0-3



Figure 4.74: CC-S-0-4

4.4.2 Specimens Confined by 2 Plies of CFRP

CC-S-2-1

This specimen was confined by two plies of CFRP. Test was carried out after 60 days of casting the composite. After the test, observed failure behavior is as seen on Figure 79. Rupture of FRP was seen both on the corner of C and D edges and along the D surface laterally. End zone retrofits were both occurred by 5 cm width and two plies of CFRP sheets with an overlapping of 15 cm.

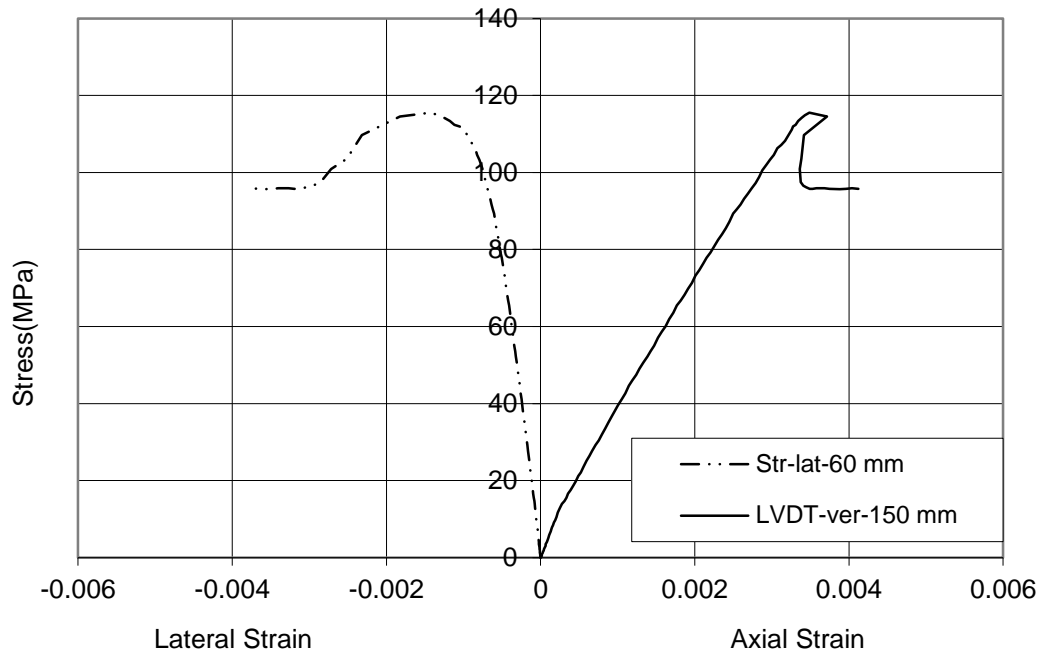


Figure 4.75: Stress - Strain Relationship for CC-S-2-1

A value of axial strain was observed as approximately 0.004 and a compressive axial stress of 117 MPa was reached.

Approximately, at a lateral strain of 0.001 cementitious composite crushes under a stress of about 117 MPa as seen on figure. Maximum load reached during the test was 2635 kN. There are four strain gauges to measure the lateral strains over all surfaces of the specimen. Lateral strain seen on figure is the average of those four strain gauges. Enhancements after confining externally are neglected on evaluation since the problems during instrumentation.

CC-S-2-2

This specimen was confined by two plies of CFRP. Test was carried out after 304 days of casting the composite. After the test, observed failure behavior is as seen on Figure 80. Rupture of FRP was seen both near to the corner of C and D edges and along the D surface laterally. Retrofits were both occurred by 3.5 cm width and 5 plies of CFRP sheets with an overlapping of 15 cm.

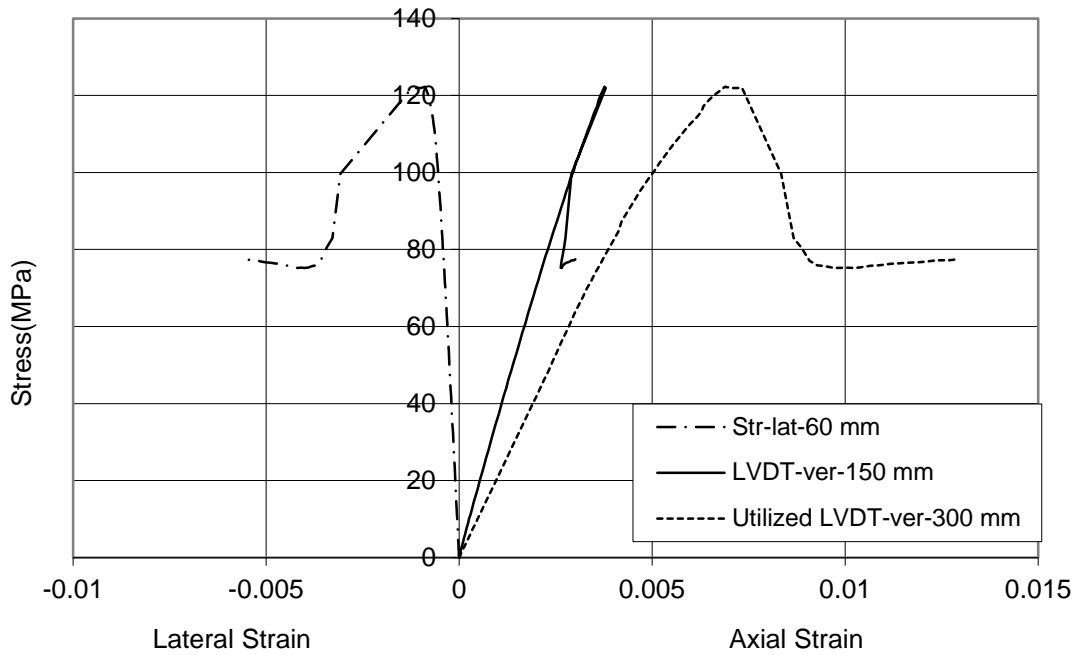


Figure 4.76: Stress - Strain Relationship for CC-S-2-2

We have two LVDTs to measure the axial strain along 310 mm gage length over the height of specimen similarly. Under ultimate stress, ultimate axial strain for 150 mm gage length was about 0.0037 and for 310 mm gage length 0.013. Also 2 Stress values, read by along middle and all height LVDTs are close to each other at about 122 MPa at 304th day/compressive. Approximately, at an ultimate lateral strain of 0.0008 cementitious composite crushed under a maximum compressive stress of about 122 MPa as seen on figure. Maximum load reached during the test was 2752 kN. There are totally four strain gauges to measure the lateral strains over all surfaces of the specimen. They are applied one to each surface. Lateral strain seen on figure is the average of those four strain gauges. Enhancements are 1.147/1.152 for stress/strain.

CC-S-2-3

This specimen was confined by two plies of CFRP. Test was carried out after 304 days of casting the composite. After the test, observed failure behavior is as seen on Figure 81. Rupture of FRP was the failure mode and damage was vertical on C surface of the specimen. End zone retrofits were both occurred by 3.5cm width and 5 plies of CFRP sheets with an overlapping of 15cm.

Under an ultimate stress of 121.8 MPa, ultimate axial strain for 150 mm gage length was about 0.0037 and for 310 mm gage length 0.013. In addition, two Stress values, read by along middle and all height LVDTs are close to each other at about 122.8 MPa at 304th day / compressive. Approximately, at an ultimate lateral strain of 0.012 cementitious composite crushed under a maximum compressive stress of about 121.8 MPa as seen on figure.

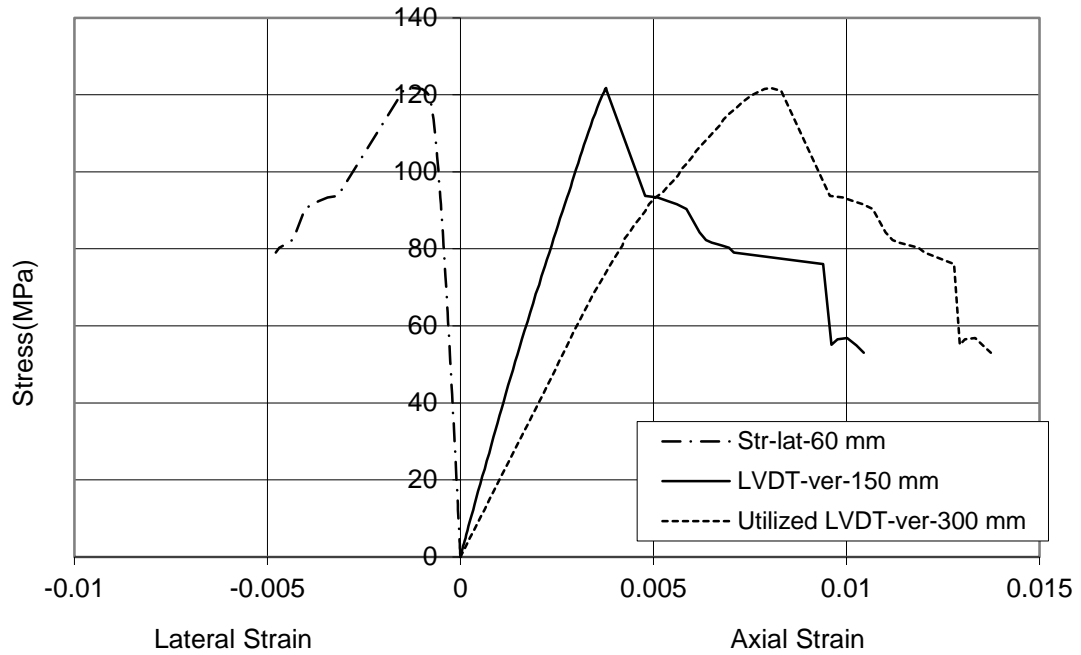


Figure 4.77: Stress - Strain Relationship for CC-S-2-3

Maximum load reached during the test was 2740 kN. There are totally four strain gauges to measure the lateral strains over all surfaces of the specimen. They are applied one to each surface. Lateral strain seen on figure is the average of those four strain gauges. Enhancements are 1.154/1.152 for stress/strain. A comparison for the specimens that confined by 2 plies of CFRP can be seen on Figure 78.

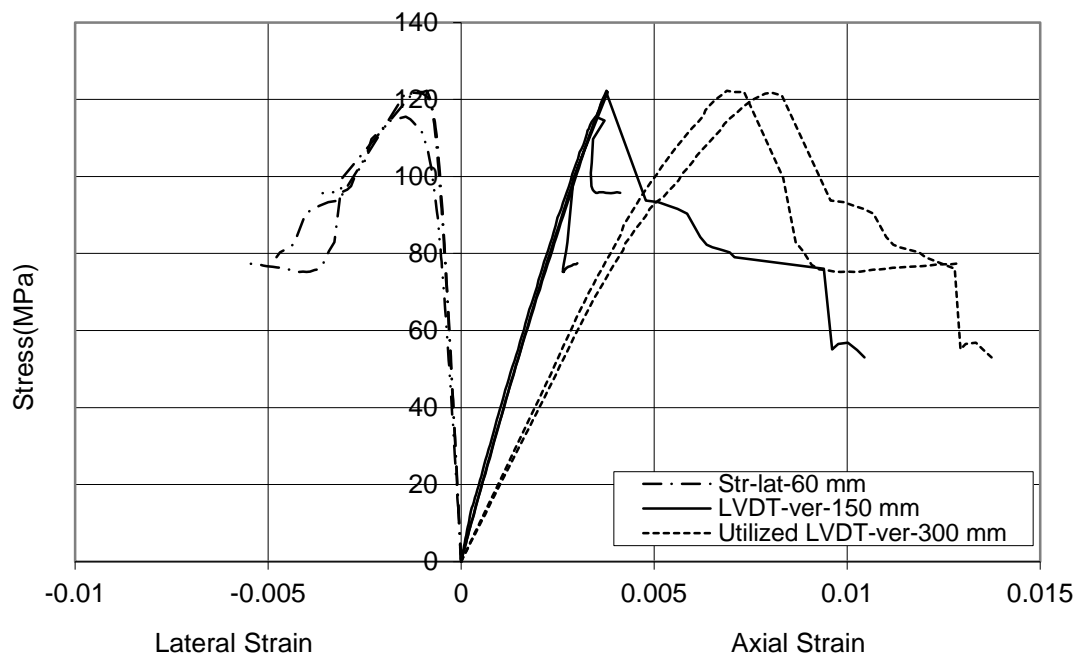


Figure 4.78: A Comparison for the Specimens that Confined by 2 Plies of CFRP



Figure 4.79: CC-S-2-1



Figure 4.80: CC-S-2-2



Figure 4.81: CC-S-2-3

4.4.3 Specimens Confined by 8 Plies of CFRP

CC-S-8-1

This specimen was confined by 8 plies of CFRP. Test was carried out after 270 days of casting the composite. After the test, observed failure behavior is as seen on Figure 87. Rupture of FRP was the failure mode and damage was vertical on surface of the specimen on the corner.

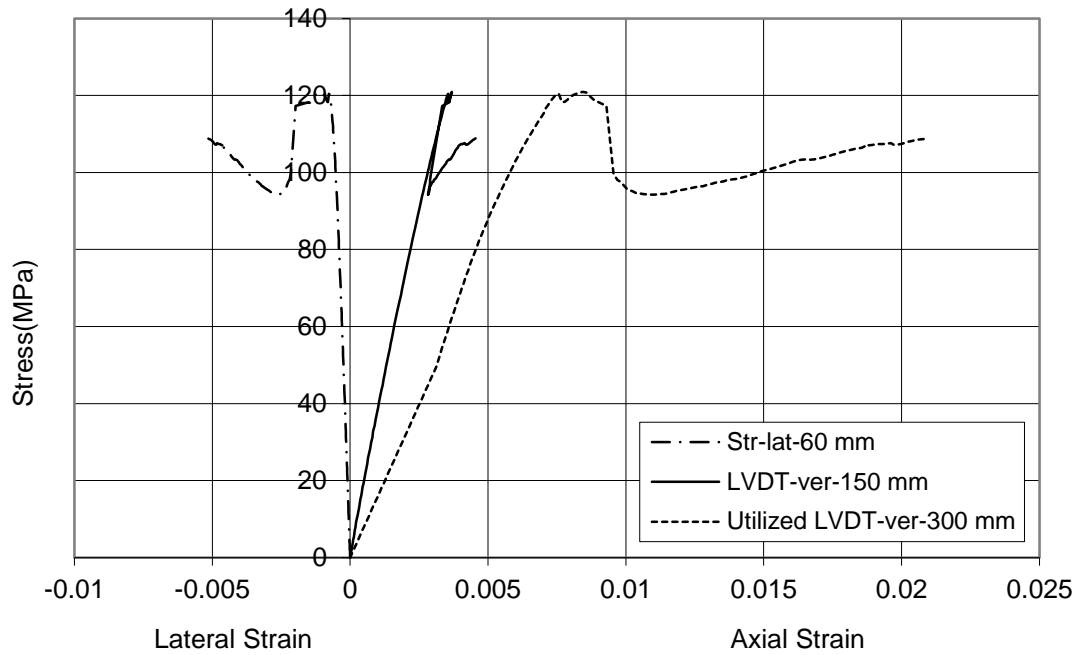


Figure 4.82: Stress - Strain Relationship for CC-S-8-1

Under an ultimate stress of 120.9 MPa, axial strain for 150 mm gage length was about 0.004 and for 319 mm gage length 0.006. Approximately, at an ultimate lateral strain of 0.001 cementitious composite crushed under a maximum compressive stress of about 120.9 MPa as seen on figure. Maximum load reached during the test was 2711 kN. There are totally four strain gauges to measure the lateral strains over all surfaces of the specimen. They are applied one to each surface. Lateral strain seen on figure is the average of those four strain gauges. Enhancements are 1.136/1.121 for stress/strain.

CC-S-8-2

This specimen was confined by eight plies of CFRP. Test was carried out after 270 days of casting the composite. After the test, observed failure behavior is as seen on Figure 88. Rupture of FRP was the failure mode and damage was vertical on surface of the specimen on the corner.

Under ultimate stress of 130.5MPa, axial strain for 150 mm gage length was about 0.004 and for 308 mm gage length 0.021. In addition, two stress values, read by

along middle and all height LVDTs are close to each other at about 130.5 MPa at 270th day/compressive.

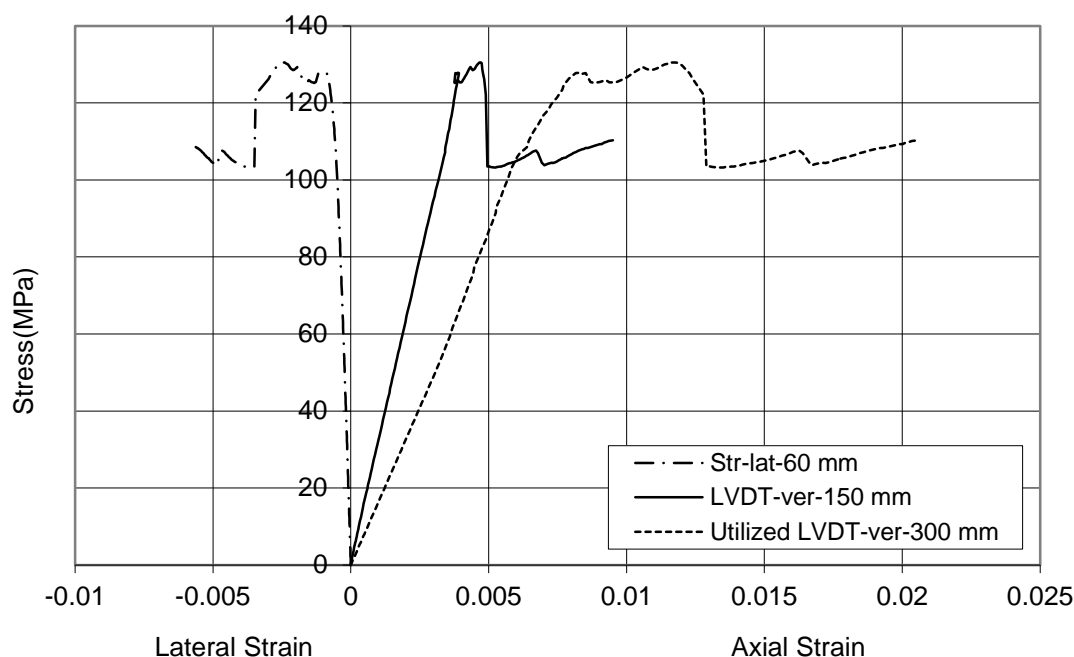


Figure 4.83: Stress - Strain relationship for CC-S-8-2

Approximately, at an ultimate lateral strain of 0.0025 cementitious composite crushed under a maximum compressive stress of about 130.5 MPa as seen on figure. Maximum load reached during the test was 2937 kN. There are totally four strain gauges to measure the lateral strains over all surfaces of the specimen. They are applied one to each surface. Lateral strain seen on figure is the average of those four strain gauges. Enhancements are 1.227/1.424 stress-strain.

CC-S-8-3

After the test, observed failure behavior is as seen on Figure 89. Rupture of FRP was the failure mode and damage was vertical on surface of the specimen on the corner. Under an ultimate stress of 138.3 MPa, axial strain for 150 mm gage length was about 0.004 and for 314 mm gage length 0.022. Approximately, at an ultimate lateral strain of 0.0008 cementitious composite crushed under a maximum compressive stress of about 138.3 MPa as seen on figure. Maximum load reached during the test was 3111 kN. There are totally 4 strain gauges to measure the lateral strains over all surfaces of the specimen. Enhancements are 1.300/1.424 stress/strain.

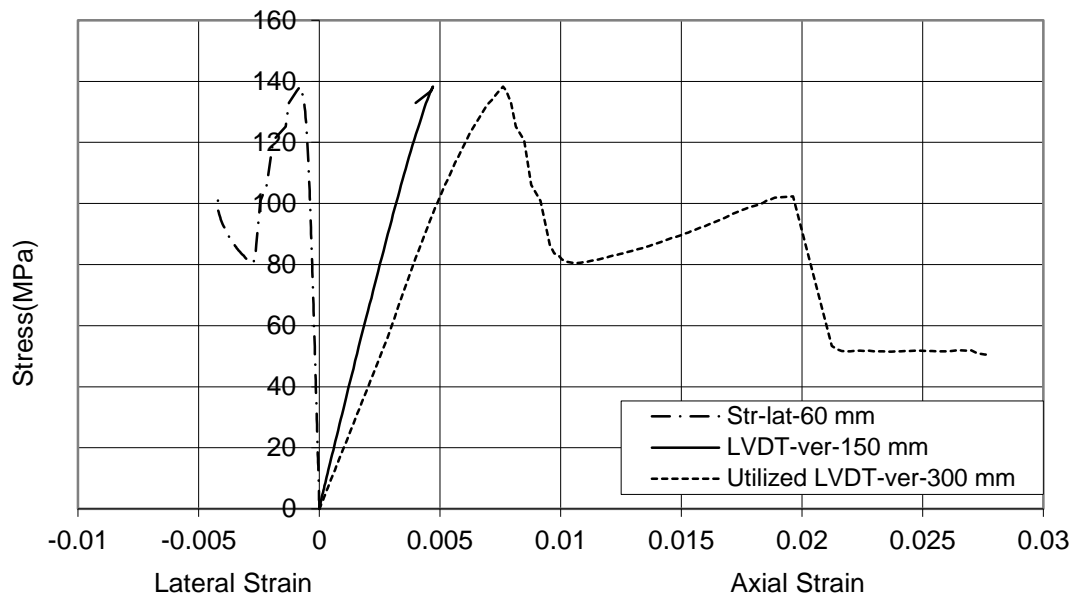


Figure 4.84: Stress - Strain Relationship for CC-S-8-3

CC-S-8-4

This specimen was confined by 8 plies of CFRP. Test was carried out after 270 days of casting the composite. After the test, observed failure behavior is as seen on Figure 90. Rupture of FRP was the failure mode and damage was vertical on surface of the specimen on the corner.

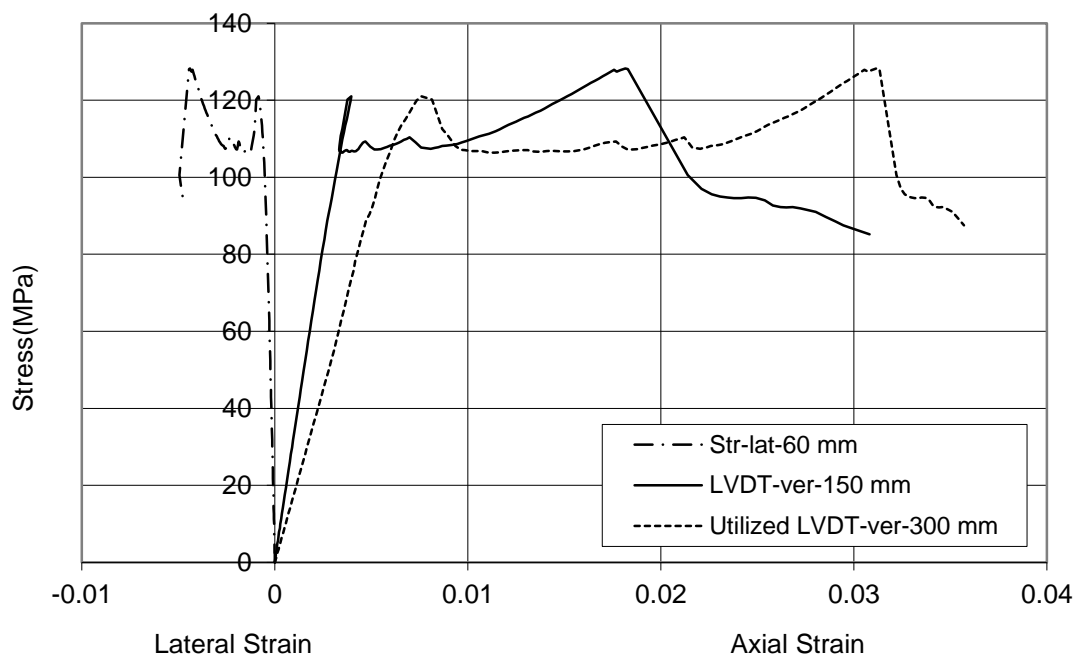


Figure 4.85: Stress - Strain Relationship for CC-S-8-4

Under ultimate stress of 128.2 MPa, an ultimate axial strain for 150 mm gage length was about 0.018. Approximately, at an ultimate lateral strain of 0.004 cementitious composite crushed under a maximum compressive stress of about 128.2 MPa as seen on figure. Maximum load reached during the test was 2885 kN. There are totally 4 strain gauges to measure the lateral strains over all surfaces of the specimen. They are applied one to each surface. Lateral strain seen on figure is the average of those four strain gauges. Enhancements are 1.205/1000 stress/strain. A comparison for the specimens that confined by 8 plies of CFRP can be seen on Figure 86.

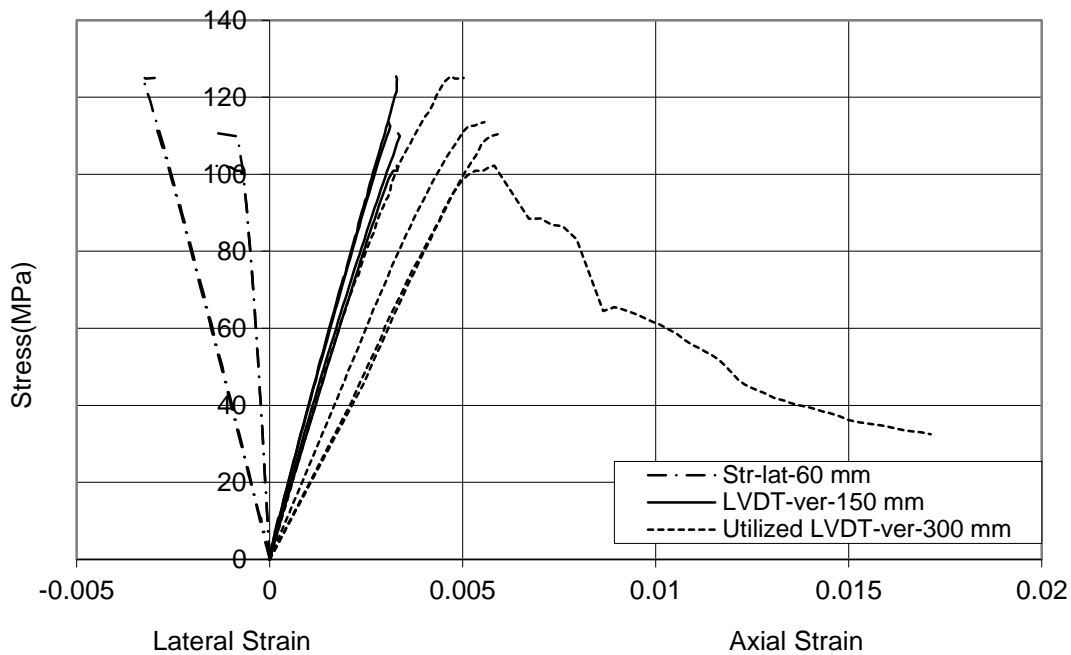


Figure 4.86: A Comparison for the Specimens that Confined by 8 Plies of CFRP



Figure 4.87: CC-S-8-1



Figure 4.88: CC-S-8-2



Figure 4.89: CC-S-8-3



Figure 4.90: CC-S-8-4

4.4.4 Specimens Confined by 10 Plies of CFRP

CC-S-10-1

This specimen was confined by 10 plies of CFRP. Test was carried out after 230 days of casting the composite. After the test, observed failure behavior is as seen on Figure 96. Rupture of FRP was the failure mode and damage was vertical on surface of the specimen on the corner. End zones retrofits were both occurred by 3,5 cm width and 5 plies of CFRP sheets with an overlapping of 15 cm.

Under an ultimate stress of 137.6 MPa, an ultimate axial strain for 150 mm gage length was about 0.005 and for 311 mm gage length 0.032. A brittle behavior was observed after the peak stress. Approximately, at an ultimate lateral strain of 0.007 cementitious composite crushed under a maximum compressive stress of about 137.6 MPa as seen on figure. Maximum load reached during the test was 3096 kN. There are totally 4 strain gauges to measure the lateral strains over all surfaces of the specimen. They are applied one to each surface. Lateral strain seen on figure is the average of those 4 strain gauges. Enhancements ratios after confining are 1.293/1.636 stress/strain.

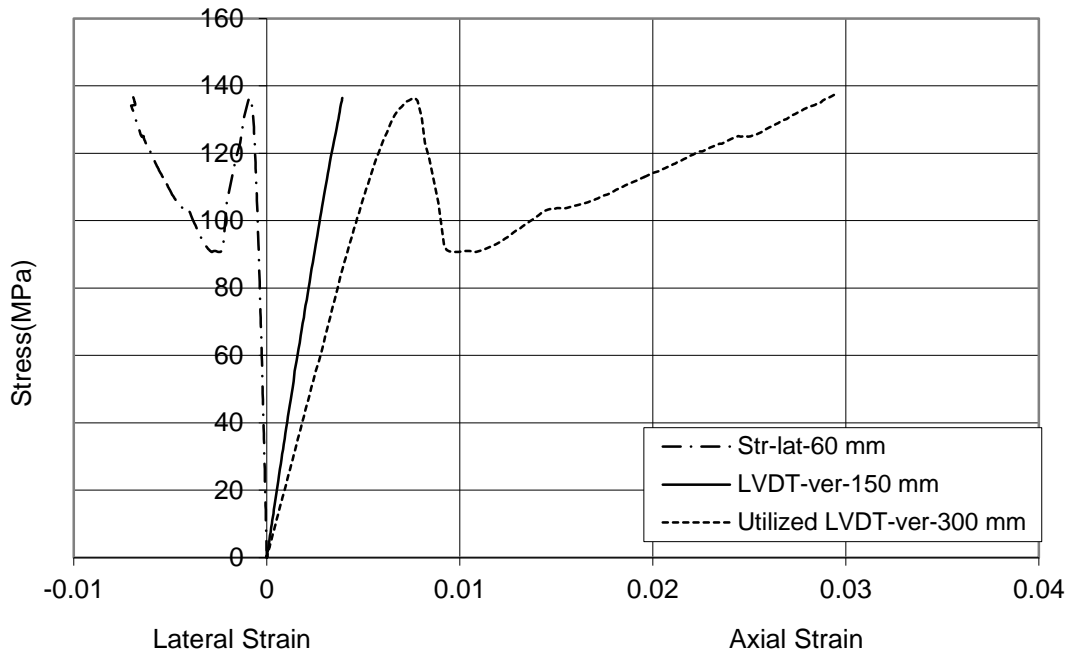


Figure 4.91: Stress - Strain Relationship for CC-S-10-1

CC-S-10-2

After the test, observed failure behavior is as seen on Figure 97. Rupture of FRP was the failure mode and damage was vertical on surface of the specimen on the corner. End zones retrofits were both occurred by 3.5 cm width and 5 Plies of CFRP sheets with an overlapping of 15 cm. End zones retrofit ruptured.

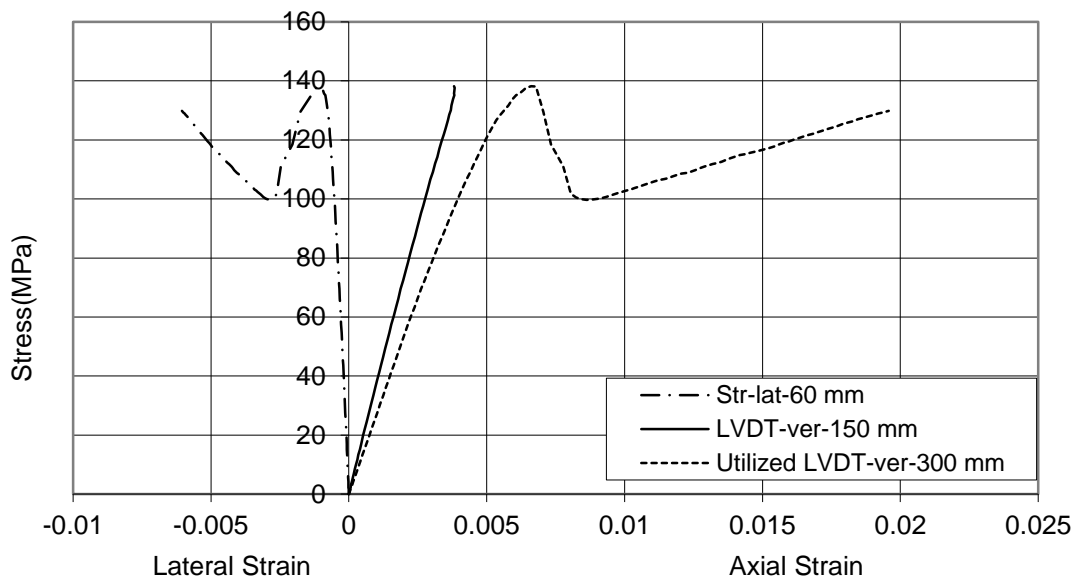


Figure 4.92: Stress - Strain Relationship for CC-S-10-2

Under ultimate stress of 138.1MPa, an ultimate axial strain for 150 mm gage length was about 0.004 and for 308 mm gage length 0.02. Approximately, at an ultimate lateral strain of 0.001 cementitious composite crushed under a maximum compressive stress of about 138.1 MPa as seen on figure. Maximum load reached during the test was 3108 kN. Enhancement ratios are 1.298/1.152 stress/strain.

CC-S-10-3

This specimen was confined by 10 plies of CFRP. Test was carried out after 230 days of casting the composite. After the test, observed failure behavior is as seen on Figure 98. Rupture of FRP was the failure mode and damage was vertical on surface of the specimen on the corner.

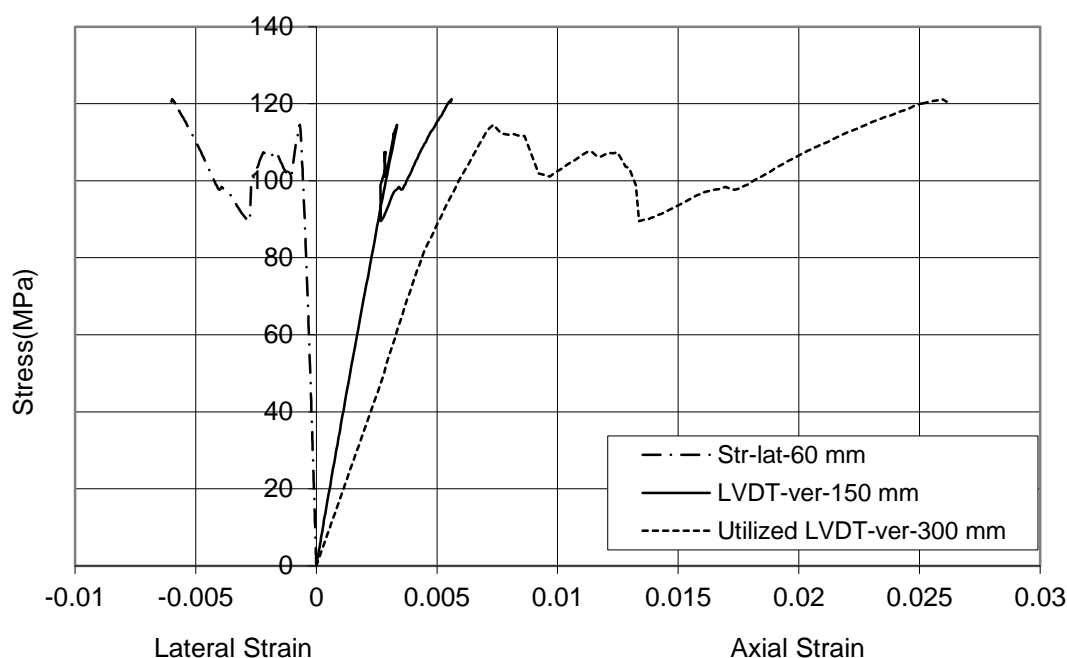


Figure 4.93: Stress - Strain Relationship for CC-S-10-3

Under an ultimate stress of 121.2 MPa, an axial strain for 150 mm gage length was about 0.006 and for 311 mm gage length 0.026. Approximately, at an ultimate lateral strain of 0.006 cementitious composite crushed under a maximum compressive stress of about 121.2 MPa as seen on figure. Maximum load reached during the test was 2727 kN. There are totally four strain gauges to measure the lateral strains over all surfaces of the specimen. They are applied one to each surface. Lateral strain seen on figure is the average of those four strain gauges. Enhancement ratios are 1.139/1.697. stress/ strain.

CC-S-10-4

After the test, observed failure behavior is as seen on Figure 99. Rupture of FRP was the failure mode and damage was vertical on surface of the specimen on the corner.

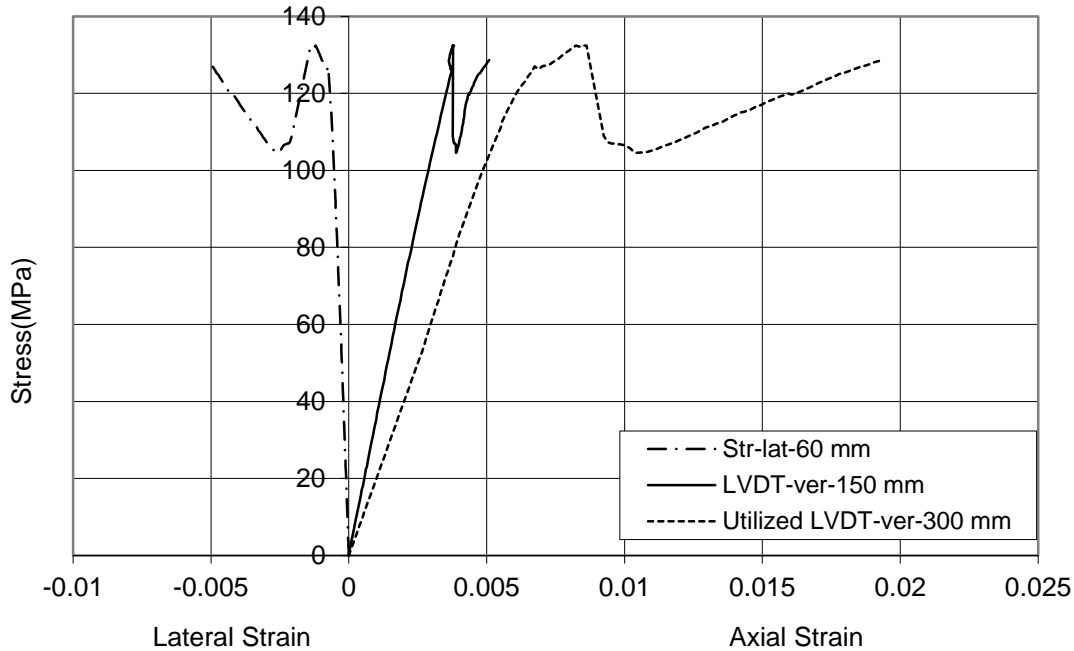


Figure 4.94: Stress - Strain Relationship for CC-S-10-4

Ultimate axial strain for 150 mm gage length was about 0.004 and for 310 mm gage length 0.02. Approximately, at an ultimate lateral strain of 0.001 cementitious composite crushed under a maximum compressive stress of about 132.4 MPa as seen on figure. Maximum load reached during the test was 2979 kN. There are totally 4 strain gauges to measure the lateral strains over all surfaces of the specimen. They are applied one to each surface. Lateral strain seen on figure is the average of those four strain gauges. Enhancement ratios are 1.244/1.152 stress/strain. A comparison for the specimens that confined by 10 plies of CFRP can be seen on Figure 95 . All test results for non-circular cross sectional specimens can be seen on Table 4.7.

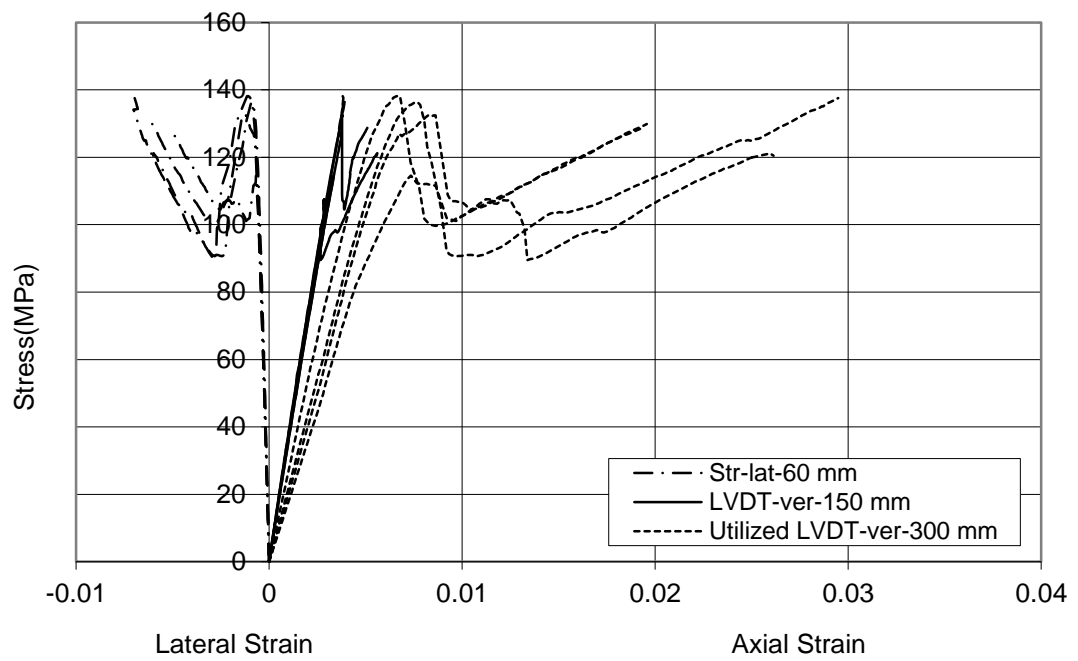


Figure 4.95: A Comparison for the Specimens that Confined by 10 Plies of CFRP



Figure 4.96: CC-S-10-1



Figure 4.97: CC-S-10-2



Figure 4.98: CC-S-10-3



Figure 4.99: CC-S-10-4

All test results for square cross section specimens can be seen on Table 4.7. ϵ_{co} is the axial strain for the unconfined specimen at 150 mm gage length. All strain values were obtained by LVDTs at the same gage length. Specimens have two peak stress levels. ϵ_{cc-1} is the first axial strain for the first peak stress level and ϵ_{cc-2} is the second one. Two deformabilities for a specimen can be defined as the ratio of axial strain at first peak to unconfined axial strain and another for second peak to unconfined similarly. $\epsilon_{cc-1}/\epsilon_{co}$ refers to first definition and $\epsilon_{cc-2}/\epsilon_{co}$ refers to second one. These values can be called as strain enhancement ratio. Average values of those can be seen near the terms. f'_{cc} is the maximum stress during the test for confined composites and f'_{co} is for unconfined. Ratio for these two terms refers to axial stress enhancement ratio.

Table 4.7: Experimental Test Results for Square Cross Section Specimens

Shape	Name	f'_{co} (MPa)	ϵ_{co}	f'_{cc} (MPa)	ϵ_{cc-1}	ϵ_{cc-2}	ϵ_{hrup}	ϵ_{fu}	f'_{cc}/f'_{co}	$\epsilon_{cc-1}/\epsilon_{co}$	$\epsilon_{cc-2}/\epsilon_{co}$	$Av(\epsilon_{cc-1}/\epsilon_{co})$	$Av(\epsilon_{cc-2}/\epsilon_{co})$
square-0	CC-S-0-3	102.2	0.0033	102.2	0.0033	0.0033	x	0.018	1.00	1	1	1	1
	CC-S-0-4	110.6	0.0033	110.6	0.0033	0.0033	x	0.018	1.00	1	1		
square-2	CC-S-2-1	106.4	0.0033	117	0.0037	0.0041	0.003	0.018	1.10	1.12	1.24	1.14	1.20
	CC-S-2-2	106.4	0.0033	122	0.0038	0.0038	0.005	0.018	1.15	1.15	1.15		
	CC-S-2-3*	106.4	0.0033	122.8	0.0038	0.01	0.004	0.018	1.15	1.15	3.03		
square-8	CC-S-8-1	106.4	0.0033	120.9	0.0037	0.0046	0.005	0.018	1.14	1.12	1.39	1.27	1.41
	CC-S-8-2*	106.4	0.0033	130.5	0.0038	0.0095	0.006	0.018	1.23	1.15	2.88		
	CC-S-8-3	106.4	0.0033	138.3	0.0047	0.0047	0.004	0.018	1.30	1.42	1.42		
	CC-S-8-4*	106.4	0.0033	128.2	0.0033	0.0310	0.005	0.018	1.20	1.00	9.39		
square-10	CC-S-10-1	106.4	0.0033	137.6	0.0039	0.0054	0.007	0.018	1.29	1.18	1.64	1.12	1.52
	CC-S-10-2	106.4	0.0033	138.1	0.0038	0.0041	0.007	0.018	1.30	1.15	1.24		
	CC-S-10-3	106.4	0.0033	121.2	0.0033	0.0056	0.007	0.018	1.14	1.00	1.70		
	CC-S-10-4	106.4	0.0033	132.4	0.0038	0.0050	0.005	0.018	1.24	1.15	1.52		

* indicates specimens that experienced problems either with loading or instrumentation

Lateral and axial stress and strain increments due to the CFRP thickness are summarized below on Figure 100. Enhancement ratios for all specimens are summarized on Table 4.8.

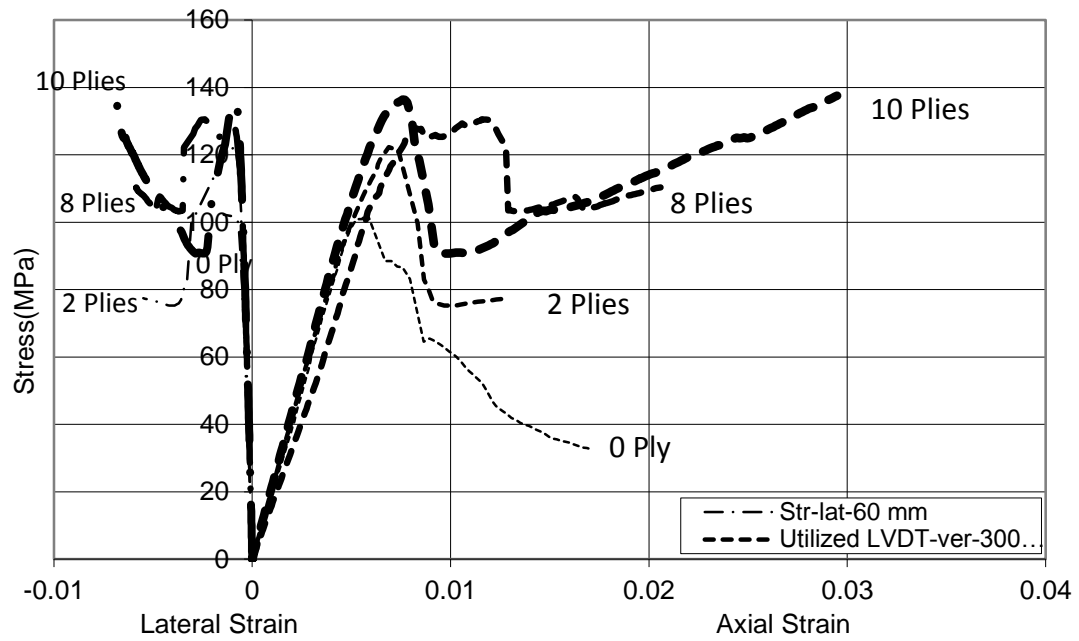


Figure 100: Lateral and Axial Stress and Strain Increments Due to the CFRP Thickness

Table 4.8: After-test Enhancement Ratios for all Specimens

	Confined by 2 plies of CFRP		Confined by 4 plies of CFRP		Confined by 6 plies of CFRP		Confined by 8 plies of CFRP		Confined by 10 plies of CFRP	
	Average Strength Enhancement(%)	Average Strain Enhancement(%)	Average Strength Enhancement(%)	Average Strain Enhancement(%)	Average Strength Enhancement(%)	Average Strain Enhancement(%)	Average Strength Enhancement(%)	Average Strain Enhancement(%)	Average Strength Enhancement(%)	Average Strain Enhancement(%)
Circular	38.544	18.687	48.058	51.515	61.068	83.838	78.608	96.970	100.48	293.93
Square	15.038	15.152	x	x	x	x	22.086	32.323	24.36	40.90

5. ANALYTICAL WORK

Two of CFRP confined concrete Stress – Strain Models were investigated and compared with experimental work in this chapter. Lam and Teng (2003) and Ilki et al. (2004) used for comparison. All of the models have different equations to obtain the strength and strain enhancement ratios. For circular and non-circular cross sections, charts are summarized for circular on Table 5.1 and for square shaped Table 5.2.

Table 5.1: Experimental and Analytical Comparison for Circular Specimens

Circular Cross Section Specimens			EXPERIMENTAL		ANALYTICAL			
			Experimental		Lam and Teng (2003)		Ilki (2004)	
Specimen	nf	fco'	fcc'/fco'	Ecc/Eco	fcc'/fco'	Ecc/Eco	fcc'/fco'	Ecc/Eco
CC-C-0-4	0	103	X	X	X	X	X	X
CC-C-0-5	0	103	X	X	X	X	X	X
CC-C-0-6	0	103	X	X	X	X	X	X
CC-C-2-1	2	103	1.13	0.97	1.36	4.54	1.21	8.21
CC-C-2-2	2	103	1.22	1.55	1.36	4.54	1.21	8.21
CC-C-2-3	2	103	1.31	1.24	1.36	4.54	1.21	8.21
CC-C-2-4	2	103	1.33	1.09	1.36	4.54	1.21	8.21
CC-C-2-5	2	103	1.43	1.27	1.36	4.54	1.21	8.21
CC-C-2-6	2	103	1.55	0.94	1.36	4.54	1.21	8.21
CC-C-2-7	2	103	1.46	1.03	1.36	4.54	1.21	8.21
CC-C-4-1	4	103	1.45	1.42	1.72	7.32	1.48	11.20
CC-C-4-2	4	103	1.67	3.15	1.72	7.32	1.48	11.20
CC-C-4-3	4	103	1.51	1.61	1.72	7.32	1.48	11.20
CC-C-6-1	6	103	1.55	2.91	2.08	10.11	1.78	13.49
CC-C-6-2	6	103	1.54	1.18	2.08	10.11	1.78	13.49
CC-C-6-3	6	103	1.74	1.42	2.08	10.11	1.78	13.49
CC-C-8-1*	8	103	1.90	2.42	2.45	12.90	2.09	15.42
CC-C-8-2	8	103	1.42	1.52	2.45	12.90	2.09	15.42
CC-C-8-3	8	103	1.71	1.88	2.45	12.90	2.09	15.42
CC-C-8-4	8	103	1.75	1.61	2.45	12.90	2.09	15.42
CC-C-10-1	10	103	1.59	1.52	2.81	15.68	2.43	17.12
CC-C-10-2	10	103	2.25	3.64	2.81	15.68	2.43	17.12
CC-C-10-3	10	103	1.64	3.64	2.81	15.68	2.43	17.12
CC-C-10-4	10	103	2.12	4.55	2.81	15.68	2.43	17.12

* indicates specimens that experienced problems either with loading or instrumentation

Table 5.2: Experimental and Analytical Comparison for Non - circular Specimens

Non-circular Cross Section Specimens				Experimental		Lam and Teng(2003)		Ilki et al.(2004)	
Specimen	nf	fco'	Eco	fcc'/fco'	Ecc/Eco	fcc'/fco'	Ecc/Eco	fcc'/fco'	Ecc/Eco
CC-S-0-3	0	106.4	0.0033	X	X	X	X	X	X
CC-S-0-4	0	106.4	0.0033	X	X	X	X	X	X
CC-S-2-1	2	106.4	0.0033	1.10	1.12	1.17	2.81	1.12	6.83
CC-S-2-2	2	106.4	0.0033	1.15	1.15	1.17	2.81	1.12	6.83
CC-S-2-3	2	106.4	0.0033	1.15	1.15	1.17	2.81	1.12	6.83
CC-S-8-1	8	106.4	0.0033	1.14	1.12	1.69	5.99	1.66	12.67
CC-S-8-2	8	106.4	0.0033	1.23	1.42	1.69	5.99	1.66	12.67
CC-S-8-3	8	106.4	0.0033	1.30	1.42	1.69	5.99	1.66	12.67
CC-S-8-4	8	106.4	0.0033	1.20	1.00	1.69	5.99	1.66	12.67
CC-S-10-1	10	106.4	0.0033	1.29	1.64	1.86	7.05	1.86	14.04
CC-S-10-2	10	106.4	0.0033	1.30	1.15	1.86	7.05	1.86	14.04
CC-S-10-3	10	106.4	0.0033	1.14	1.70	1.86	7.05	1.86	14.04
CC-S-10-3	10	106.4	0.0033	1.24	1.15	1.86	7.05	1.86	14.04

After analytical work, it is clear that there is an obvious need to develop an effective stress-strain model for HPFRCCs that can predict ultimate strain and stress under axial loads.

6. CONCLUSION AND RECOMMANDATIONS

The goal of the study is to research if FRP is not only available for low or medium strength concretes, but also it is effective for high performance cement-based composites or not.

Comparison of two different commercially available carbon fiber sheets showed that their contributions to the strength and ductility of HPFRCCs are similar.

When jacketed with CFRP sheets, the compressive strength and axial deformation capacity of HPFRCC specimens are enhanced remarkably.

Like the case of low and medium strength concrete, external jacketing with CFRP sheets is more effective for specimens with circular sections in terms of both strength and ductility.

Confinement efficiency is highly dependent on the sufficiency of the FRP sheets when sufficient amount of FRP is used both for specimens with circular and non-circular cross-sections, exhibit a strain-hardening behavior leading to significantly higher energy dissipation.

After externally confining, obvious increments on the energy dissipation capacities of the specimens were obtained. This increment is a result of rehabilitation on the strain and stress tolerably.

Cross-section shape has a serious effect on the behavior of jacketed specimens. Since the lateral confining pressure is uniform on circular cross-sectional specimens, these specimens have a better behavior than non circular in terms of both strength and deformability.

Existing stress-strain models for the stress - strain behavior of FRP confined concrete are defective on predicting the ultimate stress and strain when applied to HPFRCCs. Especially none of the assessed models is able to provide sufficient accuracy in predicting the ultimate deformations.

Enhancement on deformability is much remarkable than the enhancement on the axial strength.

Majority of the models overestimated both the strength and strain capacity enhancement ratios.

There is an obvious need to develop an effective stress strain model for HPFRCCs that can precisely predict ultimate stress and strain

REFERENCES

- [1] **Biryukovich KL, Biryukovich YuL, Biryukovich DL.** 1964. Glass-fiber-reinforced cement. Kiev: Budivelnik; 1964 [CERA Translation, 1965, No. 12].
- [2] **Brandt AM.** 1995. Cement-based composites: materials, mechanical properties and performance. London: E&FN Spon; 1995. p. 470.
- [3] **Betterman LR, Ouyang C, Shah SP.** 1995. Fiber-matrix interaction in microfiber reinforced matrix. *Adv Cem Bas Mat* 1995;2:52–61.
- [4] **Ilki, A. Peker, O. Karamuk, E. Demir, C. and Kumbasar, N.** 2008. FRP retrofit of low and medium strength circular and rectangular reinforced concrete columns, *Journal of Materials in Civil Engineering*, 2, 1-20. 2008.
- [5] **Ilki, A. and Kumbasar, N.** 2003. Compressive Behavior of carbon fiber composite jacketed concrete with circular and non-circular crosssections, *Journal of Earthquake Engineering*, 3, 381-406 2003.
- [6] **Majumdar AJ, Ryder JR.** 1968. Glass fiber reinforcement of cement products. *Glass Technol* 1968;9(3):78–84.
- [7] **Naaman AE.** 2003. Strain hardening and deflection hardening fiber reinforced cement composites. In: Reinhardt HW, Naaman AE, editors. Proceedings of the international RILEM workshop ‘High performance fiber reinforced cement composites’ HPFRCC4, Ann Arbor; 2003. p. 95–113.
- [8] **Naaman AE.** 1997. High performance fiber reinforced cement composites. Concrete structures for the future, IABSE Symposium, Paris, France, September, 1997
- [9] **Naaman AE, Reinhardt HW** 1996. Characterization of high performance fiber reinforced cement composites. In: Naaman AE, Reinhardt HW (eds) High performance fiber reinforced cement composites: HPFRCC 2. Proceedings of 2nd international workshop on HPFRCC, Chapter 41. RILEM, No. 31, E. & FN Spon, London, pp 1–24 1996
- [10] **Naaman AE, Reinhardt HW** 2006. Proposed classification of HPFRC composites based on their tensile response. *Materials and Structures, RILEM* 39(5):547–555 pp 371–376 2006
- [11] **Romualdi JP, Batson GB.** 1963. Mechanics of crack arrest in concrete. *J Eng Mech Div ASCE Proc* 1963;89(EM3):147–68.

- [12] **Romualdi JP, Mandel JA.** 1964. Tensile strength of concrete affected by uniformly distributed and closely spaced short lengths of wire reinforcement. *J ACI* 657–70.
- [13] **Sujivorakul C, Naaman AE.** 2003. Modeling bond components of deformed steel fibers in FRC composites. In: Reinhardt HW, Naaman AE, editors. Proceedings of the international RILEM workshop ‘High performance fiber reinforced cement composites’ HPFRCC4, Ann Arbor; p. 35–48.
- [14] **Lam, L. and Teng, J.G.,** 2003. Design-oriented stress-strain model for FRP confined concrete in rectangular columns, *Journal of Reinforced Plastics and Composites*, **13**, 1149-1186.
- [15] **Samaan, M., Mirmiran, A. and Shahawy, M.,** 1998. Model of concrete confined by fiber composites, *Journal of Structural Engineering*, **9**, 1025-1031.
- [16] **Ilki, A., Kumbasar, N. and Koc, V.,** 2004. Low strength concrete members externally confined with FRP sheets, *Structural Engineering and Mechanics*, **2**, 167-194.
- [17] **Rousakis, T.C., Karabinis, A.I. and Kiouisis, P.D.,** 2007. FRP-confined concrete members: axial compression experiments and plasticity modelling, *Engineering Structures*, **29**, 1343-1353.
- [18] **Campione, G. and Miraglia, N.,** 2003. Strength and strain capacities of concrete compression members reinforced with FRP, *Cement and Concrete Composites*, **25**, 31-41.
- [19] **Rochette, P. and Labossiere, P.,** 2000. Axial testing of rectangular column models confined with composites, *Journal of Composites for Construction*, **3**, 129-136.
- [20] **Shahawy, M., Mirmiran, A. and Beitelman, T.,** 2000. Tests and modelling of carbon-wrapped concrete columns, *Composites: Part B*, **31**, 471-480.
- [21] **Silva, M.A.G. and Rodrigues, C.C.,** 2006. Size and relative stiffness effects on compressive failure of concrete columns wrapped with glass FRP, *Journal of Materials in Civil Engineering*, **3**, 334-342.159
- [22] **Lam, L. and Teng, J.G.,** 2002. Strength models for fiber-reinforced plastic confined concrete, *Journal of Structural Engineering*, **5**, 612-623.
- [23] **Turkish Design Code,** 2007, Ankara
- [24] **ACI 318-08 Building Code Requirements for Structural Concrete and Commentary,** 2007. *American Concrete Institute*, Farmington Hills.
- [25] **Ahmad, S.H.,** 1981. Properties of confined concrete under static and dynamic loads, *PhD Thesis*, Univ. of Illinois, Chicago Circle, Chicago.

[26] **Wang, Y.C. and Restrepo, J.I.**, 2001. Investigation of concentrically loaded reinforced concrete columns confined with glass fiber-reinforced polymer jackets, *ACI Structural Journal*, **3**, 377-385.

[27] **Hassan, M. and Chaallal, O.**, 2007. Fiber-reinforced polymer confined rectangular columns: assessment of models and design guidelines, *ACI Structural Journal*, **6**, 693-702.

[28] **TS EN 12390-3**, Concrete test code

[29] **Fukayama, H and Sugano S.**, 2000. Japanese seismic rehabilitation of concrete buildings after the Hyogoken-Nanbu Earthquake, *Cement and Concrete Composites*, Volume 22, Issue 1, 1 February 2000, Pages 59–79

[30] **Fardis Michael N.; Khalili Homayoun H.** 1982, *Magazine of Concrete Research*, Volume 34, Issue 121, 01 December 1982 , pages 191 –202 , ISSN: 0024-9831, E-ISSN: 1751-763X

CURRICULUM VITAE

Name Surname: Ugur DEMIR

Place and Date of Birth: Kars / 1982

Address: Yeni Mah. Sehit Yakup Kulaksiz Sok.19/25 Bahcekoy-Sariyer

E-Mail: udemir@itu.edu.tr

B.Sc.: Kocaeli University